ALZHEIMER **PET**HOLOGY

The studies described in this thesis were carried out at the Alzheimer Center VUmc and Department of Radiology & Nuclear Medicine, embedded in the neurodegeneration research program of the Neuroscience Campus Amsterdam. Part of this research was performed within the framework of CTMM, the Center for Translational Molecular Medicine (www.ctmm.nl), project LeARN. The Alzheimercenter Vumc is supported by Innovatiefonds Ziektekostenverzekeraars and by unrestricted grants to the Stichting Vumc Fonds from:

AEGON Nederland NV, Ars Donandi Kas Bank Welzijnsfonds, Heer en Mw Capitain, Heineken Nederland NV, Nationale Nederlanden, Janssen Cilag NV, Gebroeders Boeschen, Genootschap Steun Alzheimercentrum, Kroonenberg Groep, KLM Royal Dutch Airlines, KPMG/Plexus, Marcel Boekhoorn, Nutricia Nederland, Onvergetelijke vrienden Alzheimercentrum, RABO Bank Amsterdam, SNS Reaal, Soroptimisten Bussum e.o, Stichting ITON, Stichting De Merel, Stichting ZABAWAS, Stichting Alzheimer Nederland, Stichting Dioraphte, Stichting Mooiste Contact Fonds KPN, Stichting Buytentwist, Twentse Kabel Holding, Ton Aan de Stegge, van Leeuwen-Rietberg stichting, and many kind individual donors!

ISBN: 978-94-6108-430-9

Printing: Gildeprint drukkerijen

Layout: Rik Ossenkoppele & Robbert-Coen Koreman

Cover design: Robbert-Coen Koreman, Fieke Ossenkoppele & Lenie Ossenkoppele.

Publication of this thesis has been accomplished with gratefully acknowledged financial support, provided by Internationale Stichting Alzheimer Onderzoek, Alzheimer Nederland, Pfizer, Nutricia advanced medical nutrition, and CTMM LeARN.

VRIJE UNIVERSITEIT

Alzheimer PEThology

ACADEMISCH PROEFSCHRIFT

ter verkrijging van de graad Doctor aan
de Vrije Universiteit Amsterdam,
op gezag van de rector magnificus
prof.dr. L.M. Bouter,
in het openbaar te verdedigen
ten overstaan van de promotiecommissie
van de Faculteit der Geneeskunde
op woensdag 8 mei 2013 om 13.45 uur
in de aula van de universiteit,
De Boelelaan 1105

door

Rik Ossenkoppele

geboren te Uithoorn

promotoren:	prof.dr. Ph. Scheltens
	prof.dr. A.A. Lammertsma
copromotoren:	dr. B.N.M. van Berckel
	dr. W.M. van der Flier

“Life is what happens to you,
while you’re busy making other plans”

John Lennon (1940-1980)

CONTENTS

Chapter 1

General introduction

Aims

Thesis outline

GENERAL INTRODUCTION

Until recently, confirmation of Alzheimer's disease (AD) pathology was only possible at post-mortem examination of the brain or with a brain biopsy. The development of positron emission tomography (PET) tracers to detect amyloid plaque deposition *in vivo*, like Pittsburgh compound-B (PIB), caused a major paradigm shift in diagnostic thinking and contributes to the general understanding of neurodegenerative disorders. Several biomarkers, including [^{11}C]PIB and [^{18}F]fluorodeoxyglucose (FDG) PET, are now incorporated in diagnostic criteria for the diagnosis of dementia and the concept of "preclinical" or "presymptomatic" AD has been revised. This thesis focuses on the relationships between amyloid deposition, glucose metabolism and cognition in a spectrum encompassing presymptomatic AD, prodromal AD and AD dementia.

Alzheimer's disease

AD is a progressive neurodegenerative disorder that affects approximately 250.000 people in the Netherlands and 35 million individuals worldwide [1]. Despite extensive research, AD is currently incurable and without a major breakthrough the number of patients will possibly exceed 115 million by 2050. AD places a large burden on caregivers and is the single most costly disease in the Netherlands. The growing socio-economic impact of AD on society demands scientific progress towards an efficient treatment of the disease.

Patients with AD usually present with episodic memory impairment, followed by progressive decline in language, visuo-spatial and executive functions. In early-onset AD (disease onset before the age of 65), however, approximately 30% initially shows non-memory deficits [2-5]. This may hinder diagnostic decision making, as there is substantial phenotypical overlap with other forms of dementia in young patients. Another factor that has impact on the clinical manifestation of AD is apolipoprotein E (APOE) genotype [6,7]. The mechanisms underlying clinical heterogeneity are currently not well understood [8].
Regardless of the clinical presentation, at least two cognitive domains should be affected in addition to interference with activities of daily living (ADL) to fulfill diagnostic criteria for AD [9]. These criteria were recently revised and now take into account biomarker

findings such as [^{11}C]PIB and [^{18}F]FDG PET and structural MRI to establish the likelihood of the clinical diagnosis [10].

The clinical stage of dementia is preceded by a prodromal phase, often referred to as mild cognitive impairment (MCI). MCI patients have significant cognitive deficits but do not experience ADL interference [11]. The annual rate of progression from MCI to AD is 10-15% [12]. Not all MCI patients convert to AD, as in some cases depression, stress or a non-AD type of dementia may explain their condition. In the prospect of disease-modifying treatment it is important to identify patients who are in the prodromal stage of AD. To facilitate an earlier diagnosis of AD, research criteria were proposed that incorporate biomarker findings to establish a diagnosis of "prodromal AD" or "MCI due to AD" in MCI patients [13,14]. It still has to be determined, however, whether abnormal biomarkers are indeed indicative of clinical progression in MCI patients.

At an even earlier stage, advances in neuroimaging and other biomarkers were translated into remodeling the concept "preclinical" or "asymptomatic" AD for research purposes [15]. The major risk factors for AD, age and APOE genotype [16-18], are strongly associated with greater AD pathology in cognitively normal elderly [19-22]. Emerging data in these individuals suggest that presence of AD pathology is associated with functional and structural brain changes in a pattern consistent with observations in MCI and AD patients [23-33]. This has led to the notion that cognitively normal individuals with cerebral amyloidosis are at risk for AD. Additional signs of neurodegeneration (e.g. increased CSF-tau, glucose hypometabolism or brain atrophy in AD specific regions) or subtle cognitive deficits increase the likelihood of rapid emergence of cognitive symptoms and clinical decline within several years [15]. An intriguing and still unresolved question related to this topic is how some elderly are capable of withstanding extensive AD pathology in their brain and preserve, at least temporarily, normal cognitive function.

The neuropathological cascade of Alzheimer's disease

The neuropathological characteristics underlying AD are extracellular senile plaques consisting of amyloid-β (Aβ) and intracellular neurofibrillary tangles consisting of hyperphosphorylated tau. Aβ is a peptide that is produced by cleavage of the larger protein Aβ precursor protein (APP) by β- or γ-secretase [34]. Amyloid plaque depositions

are widely distributed throughout the cortex with relative sparing of the medial temporal lobe [35]. It is thought that neurofibrillary tangle formation starts in the medial temporal lobe and spreads into adjacent inferior temporal cortex and to other neocortical areas in advanced stages [36].

In search for the pathogenesis of AD, the "amyloid cascade hypothesis" was postulated in which Aβ starts to accumulate approximately 15 years before the clinical symptoms of AD emerge [21,37-40]. Aβ supposedly initiates a cascade of neuropathological events such as formation of neurofibrillary tangles and neuroinflammation. This, in turn, may lead to loss of synaptic function that causes the cognitive deterioration ultimately resulting in dementia. In general, Aβ is considered to be a key player in the etiology of AD, whereas tangle pathology may be more closely related to cognitive performance and disease progression [41]. Not much is known about temporal changes in amyloid plaque deposition and tangle formation *in vivo* along the spectrum of AD.

Positron emission tomography

PET enables *in vivo* visualization and quantification of physiological and pathophysiological processes using positron emitting radionuclides [42,43]. Using PET, the time course of radioligand uptake in tissue can be measured accurately. Subsequently, these measurements can be translated into quantitative values of specific (patho)physiological parameters (e.g. blood flow, glucose metabolism or specific binding to a receptor site) using appropriate tracer kinetic models [44].

[^{18}F]FDG

[^{18}F]FDG PET is a validated tool for the differential diagnosis of dementia and provides a measure of metabolic activity of the brain at rest [45]. [^{18}F]FDG PET can be used to identify patterns of glucose metabolism that characterize several neurodegenerative diseases [46,47]. For example, AD patients typically show a pattern of glucose hypometabolism in the posterior cingulate and bilateral temporo-parietal regions [48]. [^{18}F]FDG PET does not directly measure pathology, but the extent of metabolic impairment predicts cognitive decline and is closely related to disease severity [49,50].

In vivo imaging of AD pathology: [^{11}C]PIB and [^{18}F]FDDNP

In the past it was thought that the definitive diagnosis of AD could only be established after death using post-mortem neuropathological examination. The introduction of two radiotracers capable of imaging AD pathology *in vivo* therefore had a major impact on the field. In 2002, the first clinical PET study using [^{18}F]FDDNP confirmed its unique feature to bind with high affinity to both amyloid plaques and neurofibrillary tangles [51]. The first PET study in human using [^{11}C]PIB, designed to image the amount and distribution of fibrillary amyloid plaque deposits, followed shortly thereafter [52]. Both tracers discriminate between healthy controls and AD patients [53-55]. In a head-to-head comparison, [^{11}C]PIB appeared to be the better diagnostic marker due to higher specific binding, feasibility for visual assessment of its parametric images and sharper contrast between controls and MCI and AD patients [54,56]. [^{18}F]FDDNP, however, showed highest binding in tangle-enriched medial temporal lobe structures, and correlated with tau levels in cerebrospinal fluid and with episodic memory performance [54,57,58]. Given the strong relationship between tangle pathology and clinical status, it may be hypothesized that [^{18}F]FDDNP is a suitable PET tracer for monitoring the time-course of AD.

Clinical application of [^{11}C]PIB and [^{18}F]FDG PET

Imaging studies indicated that both [^{11}C]PIB and [^{18}F]FDG PET have great promise as diagnostic tools in a memory clinic. [^{18}F]FDG is the more established PET tracer with high sensitivity (94%) for diagnosing AD [59]. Specificity is lower (73%), however, as other neurodegenerative diseases can induce a decrease in glucose metabolism resembling the pattern seen in AD [46,47]. Furthermore, reading [^{18}F]FDG images requires a well trained eye, and even then only moderate interrater reliability is accomplished [56,60]. Probing the underlying neuropathological substrate using [^{11}C]PIB helps to discriminate AD patients from cognitively normal elderly and is a strong predictor of progression of MCI to AD [52,54,61-63]. In addition, visual assessment of parametric [^{11}C]PIB images is straightforward and shows high agreement between readers [56,60]. Presence of comorbid pathologies, as seen in frontotemporal and vascular dementia, and in dementia with Lewy bodies may, however, decrease diagnostic accuracy in demented patients [64-67]. To date, diagnostic performance of [^{18}F]FDG and particularly [^{11}C]PIB has never been thoroughly investigated in a memory clinic population encompassing a wide variety of cognitive and behavioural symptoms.

AIMS

The general aim of this thesis was to gain more insight in the role of amyloid pathology in Alzheimer's disease by exploring its relationships with glucose metabolism and cognition. To this end, [^{11}C]PIB and [^{18}F]FDG PET were used to image and quantify amyloid deposition and metabolic activity, respectively.

Specific aims

1. To describe temporal change in [^{11}C]PIB and [^{18}F]FDDNP binding and in [^{18}F]FDG uptake.
2. To investigate the inter-relationships between amyloid burden, glucose metabolism and cognition in cognitively normal elderly.
3. To explore distributions of amyloid pathology and glucose metabolism according to age-at-onset and APOE genotype in order to find plausible mechanisms that underlie clinical heterogeneity in AD.
4. To determine the additional value of [^{11}C]PIB and [^{18}F]FDG PET in the diagnostic work-up in a memory clinic.

OUTLINE OF THE THESIS

Chapter 2 focuses on longitudinal imaging of Alzheimer pathology. In **chapter 2.1** several models for analyzing repeat [^{11}C]PIB scans are evaluated using both clinical data and simulations. **Chapter 2.2** describes longitudinal changes of [^{11}C]PIB and [^{18}F]FDDNP binding, together with [^{18}F]FDG uptake, in controls and in MCI and AD patients.

In **chapter 3** the relationships between amyloid plaque deposition, metabolic activity and cognition are investigated in cognitively normal elderly using [^{11}C]PIB and [^{18}F]FDG PET and neuropsychological testing.

Chapter 4 presents [^{11}C]PIB and [^{18}F]FDG data obtained in AD patients to study mechanisms that underlie clinical heterogeneity according to age-at-onset (**chapter 4.1**) and APOE ε4 genotype (**chapter 4.2**).

In **Chapter 5** the application of molecular imaging in a clinical setting is investigated. **Chapter 5.1** describes the diagnostic performance of [^{11}C]PIB and [^{18}F]FDG PET in a memory clinic population, encompassing patients with a wide variety of cognitive and behavioral deficits. **Chapter 5.2** discusses the potential of [^{11}C]PIB PET to predict future progression of MCI patients.

In **chapter 6** the main findings of this thesis are summarized followed by a general discussion and recommendations for future research.

REFERENCES

1. Alzheimer's Association. 2012 Alzheimer's disease facts and figures. Alzheimers Dement 2012;8(2):131-68.
2. Koss E, Edland S, Fillenbaum G, et al. Clinical and neuropsychological differences between patients with earlier and later onset of Alzheimer's disease: A CERAD analysis, part XII. Neurology 1996;46(1):136-41.
3. Stopford CL, Snowden JS, Thompson JC, et al. Variability in cognitive presentation of Alzheimer's disease. Cortex 2008;44(2):185-95.
4. Koedam EL, Lauffer V, van der Vlies AE, et al. Early-versus late-onset Alzheimer's disease: More than age alone. J Alzheimers Dis 2010;19(4):1401-8.
5. Smits LL, Pijnenburg YA, Koedam EL, et al. Early onset Alzheimer's disease is associated with a distinct neuropsychological profile. J Alzheimers Dis 2012;30(1):101-8.
6. Schott JM, Ridha BH, Crutch SJ, et al. Apolipoprotein e genotype modifies the phenotype of Alzheimer disease. Arch Neurol 2006, Jan;63(1):155-6.
7. van der Vlies AE, Pijnenburg YA, Koene T, et al. Cognitive impairment in Alzheimer's disease is modified by APOE genotype. Dement Geriatr Cogn Disord 2007;24(2):98-103.
8. van der Flier WM, Pijnenburg Y, Fox NC, et al. Early-onset versus late-onset Alzheimer's disease: The case of the missing APOE ε4 allele. Lancet Neurol 2011;10(3):280-8.
9. McKhann G, Drachman D, Folstein M, et al. Clinical diagnosis of Alzheimer's disease: Report of the NINCDS-ADRDA work group under the auspices of department of health and human services task force on Alzheimer's disease. Neurology 1984;34(7):939-44.
10. McKhann GM, Knopman DS, Chertkow H, et al. The diagnosis of dementia due to Alzheimer's disease: Recommendations from the national institute on aging-Alzheimer's association workgroups on diagnostic guidelines for Alzheimer's disease. Alzheimers Dement 2011;7(3):263-9.
11. Petersen RC, Smith GE, Waring SC, et al. Mild cognitive impairment: Clinical characterization and outcome. Arch Neurol 1999;56(3):303-8.
12. DeCarli C. Mild cognitive impairment: Prevalence, prognosis, aetiology, and treatment. Lancet Neurol 2003;2(1):15-21.
13. Dubois B, Feldman HH, Jacova C, et al. Research criteria for the diagnosis of Alzheimer's disease: Revising the NINCDS-ADRDA criteria. Lancet Neurol 2007;6(8):734-46.
14. Albert MS, DeKosky ST, Dickson D, et al. The diagnosis of mild cognitive impairment due to Alzheimer's disease: Recommendations from the national institute on aging-Alzheimer's association workgroups on diagnostic guidelines for Alzheimer's disease. Alzheimers Dement 2011;7(3):270-9.
15. Sperling RA, Aisen PS, Beckett LA, et al. Toward defining the preclinical stages of Alzheimer's disease: Recommendations from the national institute on aging-Alzheimer's association workgroups on diagnostic guidelines for Alzheimer's disease. Alzheimers Dement 2011;7(3):280-92.
16. Cummings JL. Alzheimer's disease. N Engl J Med 2004;351(1):56-67.
17. Poirier J, Davignon J, Bouthillier D, et al. Apolipoprotein E polymorphism and Alzheimer's disease. Lancet 1993;342(8873):697-9.
18. Corder EH, Saunders AM, Strittmatter WJ, et al. Gene dose of apolipoprotein E type 4 allele and the risk of Alzheimer's disease in late onset families. Science 1993;261(5123):921-3.
19. Price JL, Morris JC. Tangles and plaques in nondemented aging and "preclinical" Alzheimer's disease. Ann Neurol 1999;45(3):358-68.
20. Reiman EM, Chen K, Liu X, et al. Fibrillar amyloid-beta burden in cognitively normal people at 3 levels of genetic risk for Alzheimer's disease. Proc Natl Acad Sci USA 2009;106(16):6820-5.
21. Rowe CC, Ellis KA, Rimajova M, et al. Amyloid imaging results from the Australian imaging, biomarkers and lifestyle (AIBL) study of aging. Neurobiol Aging 2010;31(8):1275-83.
22. Fleisher AS, Chen K, Liu X, et al. Apolipoprotein E ε4 and age effects on florbetapir positron emission tomography in healthy aging and Alzheimer disease. Neurobiol Aging 2012[Epub ahead of print].

23. Cabeza R, Anderson ND, Locantore JK, et al. Aging gracefully: Compensatory brain activity in high-performing older adults. Neuroimage 2002;17(3):1394-402.
24. Rosen AC, Prull MW, O'Hara R, et al. Variable effects of aging on frontal lobe contributions to memory. Neuroreport 2002;13(18):2425-8.
25. Park DC, Reuter-Lorenz P. The adaptive brain: Aging and neurocognitive scaffolding. Annu Rev Psychol 2009;60:173-96.
26. Mormino EC, Brandel MG, Madison CM, et al. Aβ deposition in aging is associated with increases in brain activation during successful memory encoding. Cereb Cortex 2012;22(8):1813-23.
27. Bookheimer SY, Strojwas MH, Cohen MS, Set al. Patterns of brain activation in people at risk for Alzheimer's disease. N Engl J Med 2000;343(7):450-6.
28. Filippini N, MacIntosh BJ, Hough MG, et al. Distinct patterns of brain activity in young carriers of the apoe-epsilon4 allele. Proc Natl Acad Sci U S A 2009;106(17):7209-14.
29. Dickerson BC, Bakkour A, Salat DH, et al. The cortical signature of Alzheimer's disease: Regionally specific cortical thinning relates to symptom severity in very mild to mild AD dementia and is detectable in asymptomatic amyloid-positive individuals. Cereb Cortex 2009;19(3):497-510.
30. Mormino EC, Kluth JT, Madison CM, et al. Episodic memory loss is related to hippocampal-mediated beta-amyloid deposition in elderly subjects. Brain 2009;132(Pt 5):1310-23.
31. Oh H, Mormino EC, Madison C, Hayenga A, et al. B-Amyloid affects frontal and posterior brain networks in normal aging. Neuroimage 2011;54(3):1887-95.
32. Chételat G, Villemagne VL, Bourgeat P, et al. Relationship between atrophy and beta-amyloid deposition in Alzheimer disease. Ann Neurol 2010;67(3):317-24.
33. Becker JA, Hedden T, Carmasin J, et al. Amyloid-β associated cortical thinning in clinically normal elderly. Ann Neurol 2011;69(6):1032-42.
34. Haass C, Selkoe DJ. Cellular processing of beta-amyloid precursor protein and the genesis of amyloid beta-peptide. Cell 1993;75(6):1039-42.
35. Braak H, Braak E. Neuropathological staging of Alzheimer-related changes. Acta Neuropathology 1991;82:239-59.
36. Braak H, Braak E. Staging of Alzheimer's disease related neurofibrillary changes. Neurobiol Aging 1995;16:271-8.
37. Hardy JA, Higgins GA. Alzheimer's disease: The amyloid cascade hypothesis. Science 1992;256(5054):184-5.
38. Hardy J, Selkoe DJ. The amyloid hypothesis of Alzheimer's disease: Progress and problems on the road to therapeutics. Science 2002;297(5580):353-6.
39. Jack CR, Knopman DS, Jagust WJ, et al. Hypothetical model of dynamic biomarkers of the Alzheimer's pathological cascade. Lancet Neurol 2010;9(1):119-28.
40. Bateman RJ, Xiong C, Benzinger TL, et al. Clinical and biomarker changes in dominantly inherited Alzheimer's disease. N Engl J Med 2012;367(9):795-804.
41. Bierer LM, Hof PR, Purohit DP, et al. Neocortical neurofibrillary tangles correlate with dementia severity in Alzheimer's disease. Arch Neurol 1995;52(1):81-8.
42. Phelps ME. Positron emission tomography provides molecular imaging of biological processes. Proc Natl Acad Sci USA 2000;97(16):9226-33.
43. Lammertsma AA. Radioligand studies: Imaging and quantitative analysis. Eur Neuropsychopharmacol 2002;12(6):513-6.
44. Gunn RN, Gunn SR, Cunningham VJ. Positron emission tomography compartmental models. J Cereb Blood Flow Metab 2001;21(6):635-52.
45. Bohnen N, Djang D, Herholz K, et al. Effectiveness and safety of ^{18}F-FDG PET in the evaluation of dementia: Review of the recent literature. J Nucl Med 2012;53(1):59-71.
46. Ishii K, Sakamoto S, Sasaki M, et al. Cerebral glucose metabolism in patients with frontotemporal dementia. J Nucl Med 1998;39(11):1875-8.
47. Ishii K, Imamura T, Sasaki Met al. Regional cerebral glucose metabolism in dementia with lewy bodies and Alzheimer's disease. Neurology 1998;51(1):125-30.
48. Minoshima S, Giordani B, Berent S, et al. Metabolic reduction in the posterior cingulate cortex in very early Alzheimer's disease. Ann Neurol 1997;42(1):85-94.

49. Alexander GE, Chen K, Pietrini P, et al. Longitudinal PET evaluation of cerebral metabolic decline in dementia: A potential outcome measure in Alzheimer's disease treatment studies. Am J Psychiatry 2002;159(5):738-45.
50. Chételat G, Desgranges B, de la Sayette V, et al. Mild cognitive impairment: Can FDG-PET predict who is to rapidly convert to Alzheimer's disease? Neurology 2003;60(8):1374-7.
51. Shoghi-Jadid K, Small GW, Agdeppa ED, et al. Localization of neurofibrillary tangles and beta-amyloid plaques in the brains of living patients with Alzheimer disease. Am J Geriatr Psychiatry 2002;10(1):24-35.
52. Klunk WE, Engler H, Nordberg A, et al. Imaging brain amyloid in Alzheimer's disease with Pittsburgh compound-B. Ann Neurol 2004;55(3):306-19.
53. Small GW, Kepe V, Ercoli LM, et al. PET of brain amyloid and tau in mild cognitive impairment. N Engl J Med 2006;355(25):2652-63.
54. Tolboom N, Yaqub M, van der Flier WM, et al. Detection of Alzheimer pathology in vivo using both ^{11}C-PIB and ^{18}F-FDDNP PET. J Nucl Med 2009;50(2):191-7.
55. Shin J, Lee S, Kim SJ, et al. Voxel-based analysis of Alzheimer's disease PET imaging using a triplet of radiotracers: PIB, FDDNP, and FDG. Neuroimage 2010;52(2):488-96.
56. Tolboom N, van der Flier WM, Boverhoff J, et al. Molecular imaging in the diagnosis of Alzheimer's disease: Visual assessment of [^{11}C]PIB and [^{18}F]FDDNP PET images. J Neurol Neurosurg Psychiatry 2010;81(8):882-4.
57. Tolboom N, van der Flier WM, Yaqub M, et al. Relationship of cerebrospinal fluid markers to ^{11}C-PIB and ^{18}F-FDDNP binding. J Nucl Med 2009;50(9):1464-70.
58. Tolboom N, van der Flier WM, Yaqub M, et al. Differential association of [^{11}C]PIB and [^{18}F]FDDNP binding with cognitive impairment. Neurology 2009;73(24):2079-85.
59. Silverman DH, Small GW, Chang CY, et al. Positron emission tomography in evaluation of dementia: Regional brain metabolism and long-term outcome. JAMA 2001;286(17):2120-7.
60. Ng S, Villemagne VL, Berlangieri S, et al. Visual assessment versus quantitative assessment of ^{11}C-PIB PET and ^{18}F-FDG PET for detection of Alzheimer disease. J Nucl Med 2007;48(4):547-52.
61. Forsberg A, Engler H, Almkvist O, et al. PET imaging of amyloid deposition in patients with mild cognitive impairment. Neurobiol Aging 2008;29(10):1456-65.
62. Okello A, Koivunen J, Edison P, et al. Conversion of amyloid positive and negative MCI to AD over 3 years: An 11C-PIB PET study. Neurology 2009;73(10):754-60.
63. Koivunen J, Scheinin N, Virta JR, et al. Amyloid PET imaging in patients with mild cognitive impairment: A 2-year follow-up study. Neurology 2011;76(12):1085-90.
64. Engler H, Santillo A, Wang S, et al. In vivo amyloid imaging with PET in frontotemporal dementia. Eur J Nucl Med Mol Imaging 2008;35(1):100-6.
65. Rabinovici GD, Rosen HJ, Alkalay A, et al. Amyloid vs FDG-PET in the differential diagnosis of AD and FTLD. Neurology 2011;77(23):2034-42.
66. Lee JH, Kim SH, Kim GH, et al. Identification of pure subcortical vascular dementia using 11c-pittsburgh compound B. Neurology 2011;77(1):18-25.
67. Gomperts SN, Rentz DM, Moran E, et al. Imaging amyloid deposition in lewy body diseases. Neurology 2008;71(12):903-10.

Chapter 2

Longitudinal imaging of Alzheimer pathology

Chapter 2.1

Longitudinal Amyloid Imaging Using [^{11}C]PIB: Methodological Considerations

Journal of Nuclear Medicine [in press]

Bart N.M. van Berckel, Rik Ossenkoppele, Nelleke Tolboom, Maqsood Yaqub,
Jessica C. Foster-Dingley, Albert D. Windhorst, Philip Scheltens,
Adriaan A. Lammertsma & Ronald Boellaard

ABSTRACT

Introduction

Several methods are in use for analysing [^{11}C]PIB data. The objective of this study was to identify the method of choice for measuring longitudinal changes in specific [^{11}C]PIB binding.

Methods

Dynamic 90 minutes [^{11}C]PIB baseline and follow-up scans (interval 30±5 months) were performed in seven Alzheimer's disease (AD) patients, eleven patients with mild cognitive impairment (MCI) and eleven healthy controls. Parametric images were generated using reference parametric mapping (RPM2), reference Logan and standardized uptake volume ratios (SUVr), the latter for intervals between 60-90 ($SUVr_{60\text{-}90}$) and 40-60 ($SUVr_{40\text{-}60}$) minutes post injection. In all analyses cerebellar grey matter was used as reference region. A global cortical volume of interest was defined using a probability map based template. Percentage change between baseline and follow-up was derived for all analytical methods.

Results

$SUVr_{60\text{-}90}$ and $SUVr_{40\text{-}60}$ values overestimated binding with 13% and 10%, respectively, compared with RPM2. Reference Logan values were on average 6% lower than RPM2. Both SUVr measures showed high inter-subject variability. Over time, R1, the delivery of tracer to the cortex relative to that to the cerebellum, decreased in AD patients ($p<0.05$), but not in MCI patients and controls. Simulations showed that SUVr but not RPM2 and reference Logan were highly dependent on uptake period and that changes in SUVr over time were sensitive to changes in flow.

Conclusions

To reliably assess amyloid binding over time, for example in drug intervention studies, it is essential to use fully quantitative methods for data acquisition and analysis.

INTRODUCTION

Neuropathologically, Alzheimer's disease (AD) is characterized by the presence of senile plaques that consist mainly of amyloid-β (Aβ) [1]. Amyloid burden can be measured *in vivo* using positron emission tomography (PET) and the ligand N-methyl[^{11}C]2-4(4'-methylaminophenyl)-6-hydroxy-benzothiazole ([^{11}C]PIB) [2]. Previous studies using [^{11}C]PIB have shown high diagnostic accuracy for the detection of AD [2,3]. Longitudinal studies, however, have provided inconsistent findings with either no [4-6] or modest [7-9] changes in [^{11}C]PIB binding over time in AD patients. Apart from other methodological considerations, one possible explanation for these inconsistent results could be the method used to quantify specific [^{11}C]PIB binding.

In a previous study, receptor parametric mapping (RPM2, a basis function implementation of the simplified reference tissue model) [10] was identified as the best parametric method for analysing [^{11}C]PIB data [11]. Compared with other methods, RPM2 was least sensitive to noise and it showed the highest contrast. The difference in quantitative performance between RPM2 and reference Logan [12] was small, but RPM2 showed slightly better image quality. SUVr (standardized uptake value (SUV) normalized to SUV of cerebellar grey matter), however, showed higher variability and poorer image quality.

In the majority of clinical [^{11}C]PIB studies, SUVr has been used as the measure of amyloid load. This is understandable as SUVr has numerous advantages, such as computational simplicity, shorter scan duration, and less vulnerability to patient movement. Nevertheless, this method is sensitive to differences in both wash-in and wash-out of the tracer between subjects [13]. Although SUVr may be acceptable for diagnostic purposes, e.g. "PIB positive" versus "PIB negative", more accurate quantification methods may be needed for longitudinal studies aimed to measure changes in [^{11}C]PIB binding over time.
Therefore, the aim of this longitudinal study was to compare the most frequently used methods for the analysis of [^{11}C]PIB scans (RPM2, reference Logan, SUVr) in relation to changes in binding over time.

MATERIALS AND METHODS

Subjects

Data of seven Alzheimer's disease (AD) patients, eleven patients with mild cognitive impairment (MCI) and eleven healthy controls were used [5]. All subjects underwent baseline and follow-up [^{11}C]PIB scans with an interval of 30±5 months (range 24-48). Subjects underwent [^{11}C]PIB scans within an interval of 2±1 (at baseline) and 1±1 (at follow-up) months of the clinical evaluation. Written informed consent was obtained from all subjects after a complete written and verbal description of the study. The study was approved by the Medical Ethics Review Committee of the VU University Medical Center.

PET

PET scans were performed on an ECAT EXACT HR+ scanner (Siemens/CTI, Knoxville, USA), equipped with a neuro-insert to reduce the contribution of scattered photons from outside the field of view of the scanner. This scanner enables the acquisition of 63 transaxial planes over a 15.5 cm axial field of view, thus allowing the whole brain to be imaged in one bed position. The properties of this scanner have been reported elsewhere [14]. All subjects received a venous cannula for tracer injection. First, a 10 minutes transmission scan was performed in 2D acquisition mode using three retractable rotating ^{68}Ge line sources. This scan was used to correct the subsequent emission scan for tissue attenuation. Next, a dynamic emission scan in 3D acquisition mode was started simultaneously with the intravenous injection of 351±82 (baseline) or 377±91 (follow-up) MBq [^{11}C]PIB, with specific activities of 41±22 and 88±40 GBq·μmol^{-1}, respectively. [^{11}C]PIB was injected using an infusion pump (Med-Rad, Beek, the Netherlands) at a rate of 0.8 mL·s^{-1}, followed by a flush of 42 mL saline at 2.0 ml·$^{s-1}$. The emission scan consisted of 23 frames with progressive increase in frame duration (1×15, 3×5, 3×10, 2×30, 3×60, 2×150, 2×300, 7×600 s) for a total scan duration of 90 minutes. Patient motion was restricted by the use of a head holder and monitored by checking the position of the head using laser beams.

MRI

All subjects underwent a structural MRI scan using a 1.5T Sonata scanner (Siemens Medical Solutions, Erlangen, Germany) at baseline and at follow-up (mean interval between PET and MRI was 2±1 and 1±1 months, respectively. The scan protocol included

a coronal T1-weighted 3D MPRAGE (magnetization prepared rapid acquisition gradient echo; slice thickness = 1.5 mm, 160 slices; matrix size = 256×256; voxel size = 1×1×1.5 mm^3; echo time = 3.97 ms; repetition time = 2700 ms; inversion time = 950 ms; flip angle = 8°), which was used for co-registration, segmentation and region of interest (ROI) definition.

Image and data analysis

All PET sinograms were corrected for dead time, tissue attenuation using the transmission scan, decay, scatter and randoms, and reconstructed using a standard filtered back projection algorithm and a Hanning filter with a cut-off at 0.5 times the Nyquist frequency. A zoom factor of 2 and a matrix size of 256×256×63 were used, resulting in a voxel size of 1.2×1.2×2.4 mm^3 and a spatial resolution of approximately 7 mm full-width at half-maximum at the centre of the field of view. MRI images were aligned to corresponding PET images using a mutual information algorithm. Data were further analysed using PVElab, a software package that uses a probability map based on 35 delineated ROIs that have been validated previously [15]. For the evaluation of the different analytical methods, a global cortical ROI was used. This was composed from the volume weighted average of orbital frontal, medial inferior frontal, superior frontal, parietal, superior temporal, medial inferior temporal, and enthorinal cortex, together with hippocampus and posterior cingulate.

Kinetic analysis

Data were analyzed on a voxel-by-voxel level using receptor parametric mapping (RPM2) [16,17], reference Logan [12] and standardized uptake value ratios (SUVr) [18]. Cerebellar grey matter was used as reference tissue because of its low levels of fibrillar amyloid in AD patients [19].

RPM2 is a “two-step” basis function implementation of the simplified reference tissue model [10], which was applied to the full 90 minutes dynamic PET data. The outcome measure BP_{ND} (non-displaceable binding potential) is a quantitative measure of specific binding. For RPM2 the dynamic scan was first processed using RPM/SRTM. This first step provided parametric images of R1, BP_{ND} and k2’. Next, the median value of k2’ was determined and subsequently fixed in the second run of RPM2 processing of the dynamic scan. Consequently, k2’ is fixed on an individual scan basis. The parametrically obtained

BP_{ND} reflects the concentration of specifically bound tracer relative to that of free and non-specifically bound tracer in tissue under equilibrium conditions. Furthermore, parametric maps of relative delivery (R_1), i.e. delivery of tracer to the cortex (K_1) relative to that to the cerebellum (K_1'), were also generated using RPM2. Reference Logan is based on integration of the differential model equations for target and reference regions. The outcome measure DVR (distribution volume ratio) represents the ratio of distribution volumes of cortex and cerebellum. For reference Logan we used the implementation published by Logan *et al.* [12]. In this implementation it is not required to fix k2' and DVR is derived directly as the slope of the linear part of the graphical plot. More information can be found in Yaqub *et al.* [11] where we described and evaluated the performance of the various parametric methods in detail. $SUVr_{60\text{-}90}$ and $SUVr_{40\text{-}60}$ are the ratios of tissue concentrations in cortex and cerebellum, measured in the time frame from 60 to 90 and from 40 to 60 minutes after injection, respectively. The global cortical ROI was projected onto the various parametric images. For the present comparison, results obtained using RPM2 were expressed as $BP_{ND}+1$, which corresponds to the outcome measures obtained using reference Logan and SUVr. Percentage changes over time within methods for all groups were calculated using: percentage change (%) = 100×(Follow-up value – Baseline value)/(Baseline value). Next, relative differences between methods for both baseline and follow-up conditions were calculated using: relative difference (%)=100×(Method A – Method B)/Method B).

Simulations

Simulations were performed to assess effects of flow variations on accuracy of [^{11}C]PIB binding parameters. Parameters, derived from clinical studies [21], were used in combination with a typical plasma input function. For the reference region the following parameters were used: blood volume fraction V_B=0.05, together with K_1=0.32 mL·cm^{-3}·min^{-1}, k_2=0.16 min^{-1}, k_3=0.025 min^{-1}, k_4=0.033 min^{-1}, BP_{ND}=0.76 (=k_3/k_4) and V_T=3.5 (=K_1/k_2·(1+k_3/k_4)). Parameters for a typical AD region were set at: V_B =0.05, K_1=0.32 mL·cm^{-3}·min^{-1}, k_2=0.16 min^{-1}, k_3=0.075 min^{-1}, k_4=0.033 min^{-1}, BP_{ND}=2.25 and V_T =6.5.

Flow changes were simulated by proportionally changing R_1, defined as the K_1 ratio between target and reference regions, whilst keeping the K_1/k_2 ratio constant. Note that in the simulation a change in flow is simulated by changing K_1 (and k_2), thereby assuming no change in first pass extraction. This simulation reflects a change in flow between

reference and cerebral AD regions (i.e. a heterogeneous flow change) at follow-up. R_1 was varied from 0.6 to 1.4. In addition, a second simulation was performed by keeping K_1' in the reference region constant and only changing K_1 in cerebral AD regions. K_1 in both cerebral AD and K_1' in cerebellar reference regions (and proportionally k_2, keeping K_1/k_2 constant) were varied from $K_1=K_1'=0.19$ to 0.48 $mL \cdot cm^{-3} \cdot min^{-1}$.

For all simulations SUVr were calculated for several uptake times and with several simulated flow variations. For comparison, $BP_{ND}+1$ (=DVR) was obtained using RPM2 and reference Logan applied to the entire simulated 90 minutes reference and cortical time activity curves. For all measures (i.e. SUVr, RPM2 and reference Logan based $BP_{ND}+1$), percent bias compared with 'true' or simulated DVR values were determined. In addition, percent change in all parameters as a result of both global and heterogeneous K_1 changes were calculated by comparing these values with 'true' or simulated $BP_{ND}+1$ (that was kept constant at follow-up).

Simulations were performed both with and without adding noise to the TAC, using a noise model according to Yaqub et al [22]**.** In case of noisy simulations, 100 TACs per simulation were generated. The average results from SUVr, RPM2 and Reference Logan then were evaluated to study effect of changes in R_1 and K_1. However, noisy simulations showed near identical results as those obtained without noise. Therefore, results from the simulations without noise will be reported, such that only flow or K_1 effects are illustrated.

Statistics

Demographic and clinical differences between groups were assessed using analysis of variance (ANOVA) with post-hoc LSD tests and age as covariate. At both baseline and follow-up, mean parameter values of [^{11}C]PIB binding for the different methods were compared using ANOVA with post-hoc LSD tests and age as covariate. Finally, group differences in R_1 values at baseline and follow-up were examined using ANOVA with adjustment for age. R_1 changes over time within groups were assessed using paired samples t-tests. Data are presented as mean ± SD, unless otherwise stated

RESULTS

Demographic and clinical characteristics of the three diagnostic groups are presented in Table 1. Groups did not differ with respect to age or mean interval between baseline and follow-up.

Table 1. Demographic characteristics according to diagnostic group

Variable	Diagnostic group			P value
	Controls (n=11)	MCI (n=11)	AD (n=7)	
Age at baseline, year	66±7	67±7	61±6	0.17
Age at follow up, year	69±7	70±7	64±6	0.18
Interval between scans (months	30±4	30±6	32±7	0.61
MMSE at baseline	29±1	28±2	26±2	≤0.001[a]
MMSE at follow up	29±1	26±3	22±5	<0.001[b]

MMSE = Mini-mental State Examination; MCI = mild cognitive impairment; AD = Alzheimer's disease.
ANOVA with post hoc LSD tests:
*AD<MCI, p=0.06; AD<Controls, p<0.001; MCI<Controls, p<0.05
**AD<MCI, p<0.05; AD<Controls, p<0.001; MCI<Controls, p<0.01

Baseline and follow-up binding measures

Significant differences in [^{11}C]PIB binding between groups, both at baseline and follow-up, were found with all methods (Table 2). For all subjects together, $SUVr_{60\text{-}90}$ values were on average 14 and 13% higher at baseline and follow-up, respectively, than corresponding (BP_{ND}+1) values obtained with RPM2. For $SUVr_{40\text{-}60}$, these overestimations were 9 and 10% at baseline and follow-up, respectively. Results were similar for the group of AD patients (Table 2). Reference Logan values were on average 6% lower than RPM2 values both at baseline and follow-up.

Longitudinal changes in binding measures

Percentage changes between baseline and follow-up differed between methods, especially in AD patients. While BP_{ND}+1 (RPM2), DVR (reference Logan) and $SUVr_{40\text{-}60}$ values were relatively stable (0±6, -1±5 and 0±6%, respectively), $SUVr_{60\text{-}90}$ values decreased with

4±8% in AD patients. Both SUVr measures showed larger variability than RMP2 values, especially at follow-up (Figure 1). Differences were less pronounced for MCI patients and controls (RPM2: 6±7, 2±3%; reference Logan: 5±6, 2±3%; $SUVr_{60-90}$: 8±9, 3±4%; $SURr_{40-60}$: 5±7, 6±6% for MCI and controls, respectively). Parametric images of an AD patient at both baseline and follow-up are presented in Figure 2 for all analytical models.

Table 2. Binding values of [^{11}C]PIB according to analytic method

	AD	MCI	Controls	All
RPM2 (BP_{ND}+1)				
Baseline	1.87±0.10	1.39±0.39	1.12±0.27	1.40±0.41
Follow-up	1.86±0.13	1.46±0.39	1.15±0.29	1.44±0.41
% change	-0.3±5.9	5.5±7.4[b]	1.9±3.2[c]	2.7±6.0[b]
Logan DVR				
Baseline	1.70±0.08	1.31±0.32	1.08±0.23	1.32±0.34
Follow-up	1.68±0.10	1.37±0.32	1.11±0.24	1.35±0.33
% change	-1.0±5.2	5.3±6.0[a]	2.1±3.5[b]	2.6±5.4[a]
$SUVr_{60-90}$				
Baseline	2.16±0.09	1.57±0.52	1.26±0.38	1.59±0.52
Follow-up	2.07±0.22	1.67±0.50	1.29±0.35	1.62±0.49
% change	-4.3±8.6	8.0±9.2[a]	2.6±4.2	2.9±8.7
$SUVr_{40-60}$				
Baseline	2.02±0.10	1.54±0.46	1.21±0.32	1.53±0.46
Follow-up	2.02±0.19	1.62±0.46	1.28±0.35	1.59±0.46
% change	0.1±6.4	5.5±7.4[b]	5.8±6.1[a]	4.3±6.9[a]

RPM2 = receptor parametric mapping; BP_{ND} = non-displaceable binding potential; DVR = distribution volume ratio; SUVr = standardized uptake ratio value; FU = follow-up.

Letters indicate the level of significance for percentage change and for differences between baseline and follow-up values: [a] $p<0.05$; [b] $p=0.06$; [c] $p=0.07$

Relative tracer delivery

At baseline, mean R_1 values of [^{11}C]PIB were 0.87±0.05 in patients with AD, 0.89±0.03 in MCI patients and 0.87±0.04 in controls. At follow-up, R_1 values were 0.83±0.06 in AD patients, 0.88±0.03 in MCI patients and 0.88±0.04 in controls (Figure 3). ANOVA adjusted

for age revealed no differences in R_1 between groups at baseline ($F(2,28)=0.65$, $p=0.59$). At follow-up, however, AD patients showed lower R1 values compared with MCI patients and controls at trend level ($F(2,28)=2.82$, $p=0.06$) (Figure 3). Paired samples t-test revealed a significant decrease in R_1 over time in AD patients ($t(6)=2.85$, $p<0.05$), whereas no changes in R_1 were found for MCI patients ($t(10)=1.73$, $p=0.12$) or controls ($t(10)=1.03$, $p=0.33$).

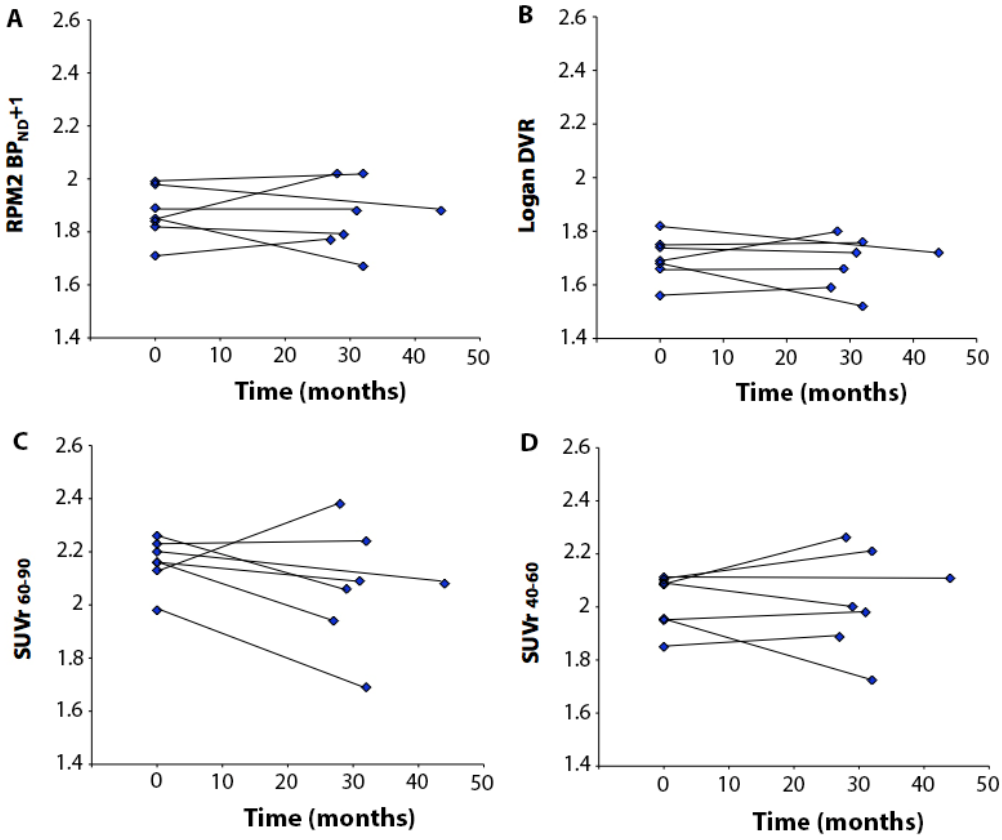

Figure 1: Global cortical binding of [^{11}C]PIB in AD patients using (A) RPM2, (B) reference Logan, (C) $SUVr_{60\text{-}90}$ and (D) $SUVr_{40\text{-}60}$.

Simulations

Simulations revealed that SUVr was dependent on uptake period (Figures 4A and 5A). In general, SUVr overestimated $BP_{ND}+1$ (=DVR) for all simulated K_1 variations from 60 minutes post injection onwards. Moreover, both changes in K_1 (global flow changes) and

R_1 (heterogeneous flow changes), as shown in Figures 4B and 5B, induced both positive and negative bias in SUVr changes when compared with reference (i.e. baseline) conditions (K1=0.32 mL·cm^{-3}·min^{-1}and R1=1, respectively). Bias and flow dependence of SUVr were larger than those of BP_{ND}+1 (RPM2) and DVR (reference Logan), while the latter 2 methods showed comparable results.

DISCUSSION

This study directly compared changes in [^{11}C]PIB binding parameters using four different analytical methods. It revealed marked differences between methods. Whilst both kinetic methods (RPM2 and reference Logan) showed relatively stable estimates of [^{11}C]PIB binding in AD patients over time, $SUVr_{60\text{-}90}$ demonstrated a decrease in [^{11}C]PIB uptake. Although this was not observed with $SUVr_{40\text{-}60}$, compared with the quantitative methods, both SUVr measures showed larger variability between subjects. This could be related to changes over time in relative tracer delivery (R1) to the region of interest, as this decreased over time in AD patients.

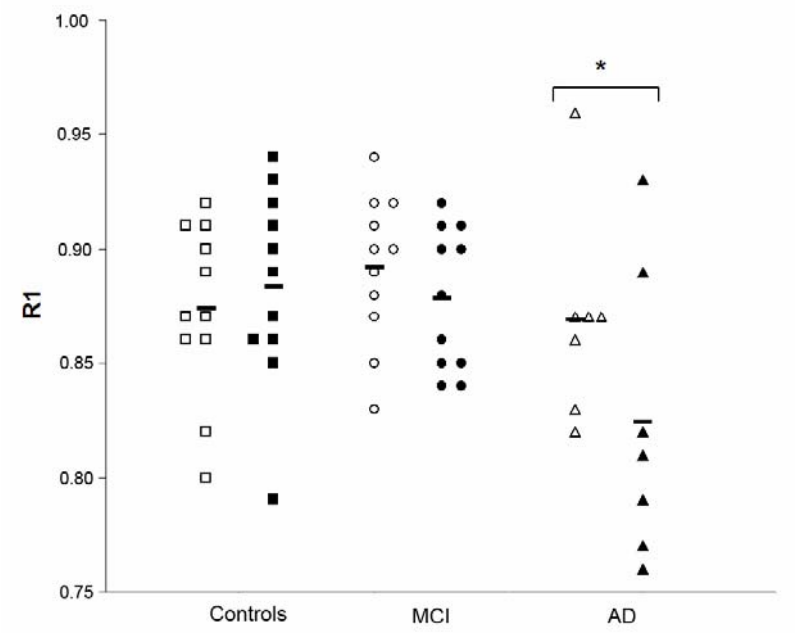

Figure 3: R_1 values at baseline and follow-up for AD patients, MCI patients and controls.
A significant decrease in R1 was found in the AD group only (* $p<0.05$).

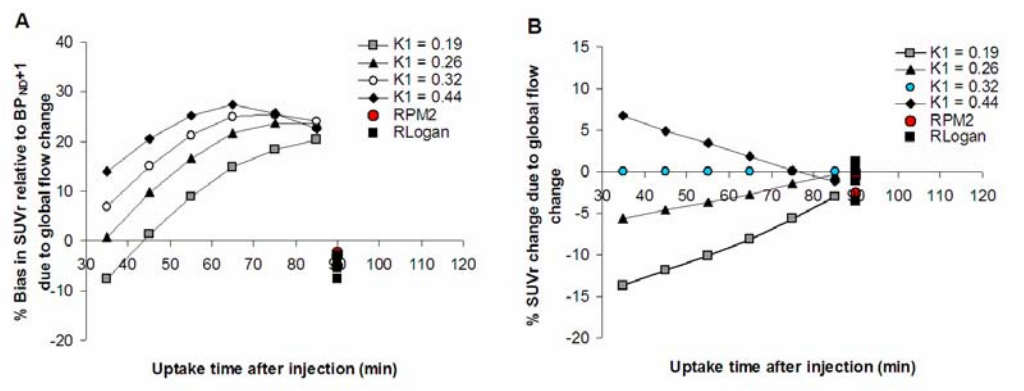

Figure 4: (A) Percentage bias in SUVr (relative to BP_{ND}+1) as function of time for various K_1 values with R_1=1 (i.e. K_1=K_1'). For comparison, BP_{ND}+1 obtained with RPM2 and reference Logan are indicated at 90 min p.i. (B) Percentage bias in change in SUVr (relative to change in BP_{ND}+1) as function of time for various follow-up K_1 values, a baseline K_1=0.32 mL·cm^{-3}·min^{-1} and with R_1=1 (i.e. K_1=K_1') both at baseline and at follow-up. For comparison, BP_{ND}+1 obtained with RPM2 and reference Logan are indicated at 90 min p.i. Note that RPM2 and reference Logan results for all simulated K_1 values are plotted at 90 min p.i. The x-axis represents the mid-time of a 10-min period for calculating SUVr measures.

Both SUVr measures overestimated RPM2 values with 9 to 14%. Carson et al [13] using [^{18}F]cyclofoxy, showed that tissue ratios like SUVr can overestimate specific binding substantially due to its sensitivity to differences in clearance rate. In addition, it was shown that this bias was different for high and low binding areas. Using [^{11}C]PIB, Lopresti et al. [18] were the first to describe that $SUVr_{40\text{-}60}$ and $SUVr_{40\text{-}90}$ showed a large positive bias compared with quantitative methods, but that the percentage bias was fairly similar between low and high binding areas. Overestimation of SUVr compared with quantitative methods has also been observed using the novel amyloid tracers [^{18}F]flutemetamol [23] and [^{18}F]florbetapir [24]. Reference Logan estimates were about 6% lower than RPM2 estimates, likely due to sensitivity of reference Logan graphical analysis to statistical noise [25]. In the present study, there was a difference of 17-19% between SUVr and reference Logan values. In a recent study in MCI patients [26], SUVr values were up to 31% higher than reference Logan DVR. These discrepancies between methods have important implications for determination of quantitative thresholds for "PIB-positivity", as these thresholds depend critically on the analytical method used to analyze the data.

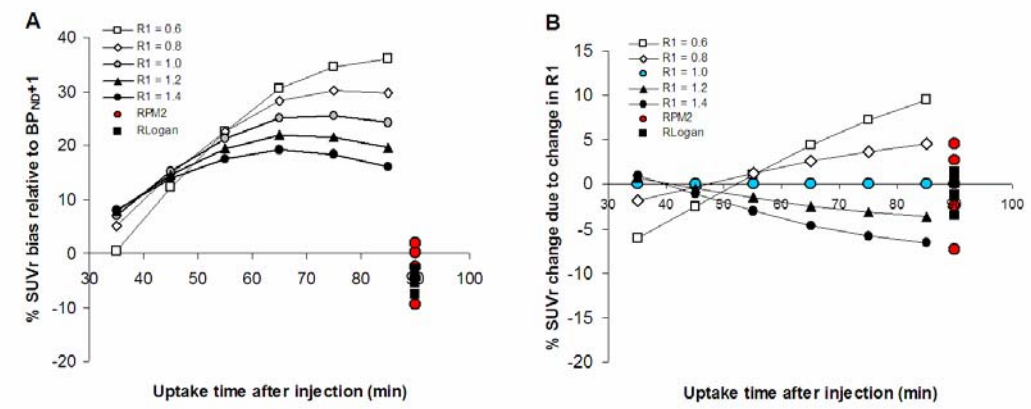

Figure 5: Regional flow (i.e. K_1 in the simulations) variation effects (R1). (A) % bias in SUVr compared to true (simulated) DVR=BPnd+1 as function of uptake time. For comparison results obtained using RPM2 and reference Logan are indicated at 90 min p.i. (B) % change in SUVr as function of regional flow variation indicating artificial variation in SUVr as a result of variations in R1. For comparison results obtained using RPM2 and reference Logan are indicated at 90 min p.i. Small biases are now also observed for RPM2 and reference Logan, but with a smaller range than those seen with SUVR. Note that RPM2 and reference Logan results for all simulated R_1 values are plotted at 90 min p.i.

Both SUVr measures showed larger variability than RPM2 values, especially at follow-up. This can be explained by two processes. First, at later time points the SUVr becomes constant over time. Yet, SUVr will overestimate the true DVR as the tissue curves follow the clearance of plasma input curves. In other words, there is no true equilibrium between plasma concentration and tissue concentration (because the concentration in plasma is lower than in tissue, there will be a net transport of tracer from tissue to plasma). The violation of equilibrium between reference and target regions will be different due to differences in specific binding between these regions and subjects. Because of these differences in non-equilibrium between subjects there will more variability of SUVr between subjects. By performing dynamic scans and kinetic analysis, the change and variability of the input function (that affects both reference and target region) is taken into account and, consequently, BP_{ND} estimated with RPM2 can be expected to be more reproducible. A second reason may be the variations in flow. In order to see to what degree the various parametric methods (SUVr, reference Logan and RPM2) are affected by flow, we performed several simulations. In general, the simulation data are in good agreement with the clinical findings. Firstly, SUVr generally overestimated simulated BP_{ND}+1 (=DVR) values, while RPM2 and reference Logan based values showed minimal bias. Secondly, these simulations showed that both global and regional (i.e.

heterogeneous) K_1 changes over time could result in artificial changes in SUVr over time, a phenomenon that was less prominent for RPM2 or reference Logan. Yet, some small biases and dependence on changes in K_1 were also observed for RPM2 and reference Logan. This can be explained by the contribution of signal from the blood volume fraction. Blood volume fractions were included in the simulations to generate realistic time activity curves, but are, by definition, not taken into account by both RPM2 and reference Logan. Finally, results obtained using SUVr strongly depended on the specific uptake interval, with slightly less bias and flow dependence for earlier time intervals. This is consistent with clinical data where $SUVr_{40\text{-}60}$ seemed to show less variability over time than $SUVr_{60\text{-}90}$. It is already known that, in AD patients, flow changes over time occur due to disease progression [22] and, consequently, it may be expected that this will result in more variability in SUVr over time. Changes in R_1 seen in AD patients indicate that these flow changes are indeed present. Therefore, it is highly likely that changes in SUVr observed in the present series of AD patients do not reflect changes in specific [^{11}C]PIB binding, but rather are due to changes in perfusion during the course of the disease. Apart from heterogeneous flow changes (reflected by changes in R1). Also relatively large global flow changes are likely to occur both in healthy subjects and patients. A recent study of Bremmer et al. [27] showed that day-to-day variations in global cerebral blood flow were about 30% under normal conditions. As shown by the simulations, these global flow variations could add to the clinically observed variability in SUVr. Similar effects of flow on SUVr values may be expected when employing radiotracers other than [^{11}C]PIB. The flow dependence is caused by the lack of equilibrium of tracer distributions between blood and tissue and the tissue compartments. Therefore this occurs for any tracer, although the degree of this effect differs between tracers depending on their kinetic behaviour. As such, these findings imply that any study (but particularly when using [^{11}C]PIB or tracers with similar kinetic behaviour) where variations in blood flow can be expected should not be analysed using SUVr. Consequently, for accurate quantification of longitudinal amyloid imaging studies, dynamic scanning protocols and fully quantitative data analysis methods are essential. This is especially true for longitudinal studies with disease modifying agents aiming to lower amyloid load in the brain. Studies that use suboptimal methods such as SUVr carry the inherent risk that ineffective drugs are not identified appropriately or, more importantly, that potential effective drugs are dismissed, especially when effect sizes are small.

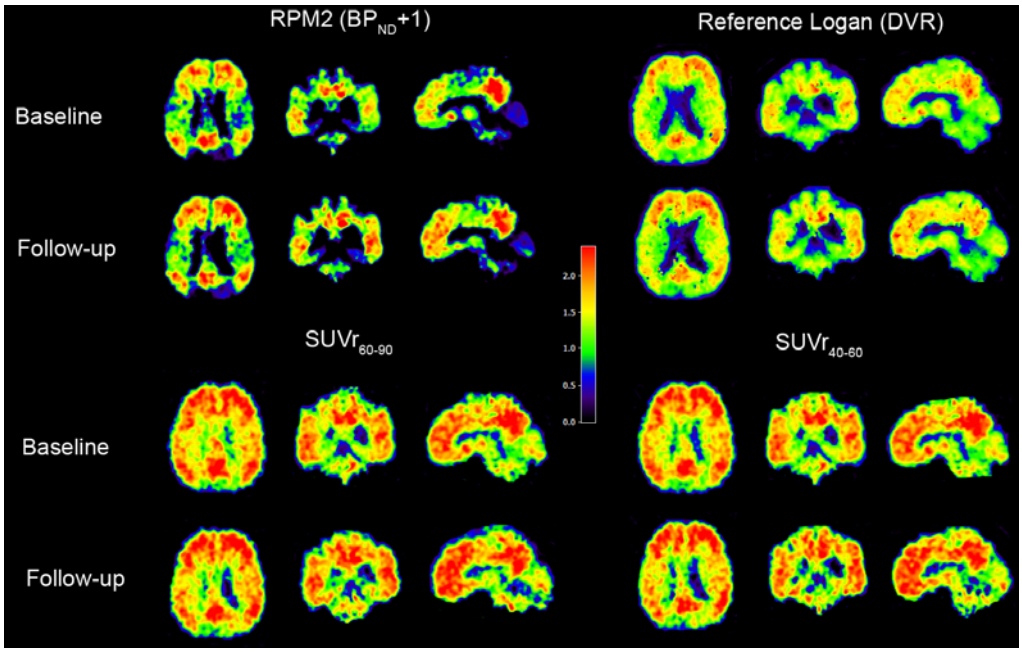

Figure 2: Parametric images of an AD patient with 27 months of follow-up, showing increased RPM2 BP_{ND}(+1) (4%), Reference Logan DVR (2%) and $SUVr_{40-60}$ (2%), whereas $SUVr_{60-90}$ decreased with 10%. R1 was 2% lower at follow-up.

Recently, effects of bapineuzumab on fibrillar amyloid load in AD patients, as measured using [^{11}C]PIB and PET, were reported [28]. This study found a significant reduction in mean [^{11}C]PIB uptake across six targeted regions of interest in patients in the bapineuzumab group compared with those in the placebo group. This is a landmark study, as it was the first to show a central effect of a therapeutic approach, aimed at lowering cerebral amyloid load in patients with AD. For the analysis of [^{11}C]PIB PET scans $SUVr_{60-90}$ was used. Results of the present study, however, indicate that $SUVr_{60-90}$ is susceptible to flow changes, which may be different in bapineuzumab and placebo groups. As such, it is impossible to differentiate between decreases in amyloid load due to the treatment or to flow artefacts. This is important as potentially, with more stringent methodology, the ineffectiveness of bapineuzumab in the treatment of AD could have been identified earlier, saving costly phase II and even phase III trials.

One could argue that repeated 90 minutes dynamic scans cause a selection bias, as only relatively few patients can undergo such a demanding procedure. This may indeed be true for patients with moderate to severe AD. It is, however, most likely that amyloid lowering

drugs are most effective in the very early stages of the disease. This justifies inclusion of patients with mild AD or, preferably, prodromal AD or individuals with autosomal dominant AD in a preclinical stage. Dynamic scanning protocols and fully quantitative data analysis methods are necessary in these patients, as a solid baseline measurement to monitor their disease course and treatment response is needed since these patients will progress to advances stages with associated blood flow changes. These subjects are perfectly capable of undergoing dynamic scans when carefully prepared and monitored during scanning.

In case of longitudinal [^{11}C]PIB studies, a steady state approach could be an alternative for dynamic scanning [29]. Steady state levels of [^{11}C]PIB can be achieved using a bolus with continuous infusion protocol, which can be performed outside the PET camera. When a reliable steady state has been achieved, usually a short scanning period is sufficient. This method would combine advantages of a good quantitative measure that is independent of (relative) flow changes with short scan duration. However, this still needs to be tested and validated for [^{11}C]PIB.

In conclusion, SUVr should not be used for longitudinal [^{11}C]PIB studies, especially when only small changes in specific binding can be expected.

REFERENCES

1. Braak H., Braak E. Neuropathological stageing of Alzheimer-related changes. *Acta Neuropathology*. 1991;82:239-259.
2. Klunk WE, Engler H, Nordberg A et al. Imaging brain amyloid in Alzheimer's disease with Pittsburgh Compound-B. *Ann Neurol*. 2004;55(3):306-319.
3. Tolboom N, Yaqub M, van der Flier WM et al. Detection of Alzheimer pathology in vivo using both 11C-PIB and 18F-FDDNP PET. *J Nucl Med*. 2009;50(2):191-197.
4. Engler H, Forsberg A, Almkvist O et al. Two-year follow-up of amyloid deposition in patients with Alzheimer's disease. *Brain*. 2006;129(Pt 11):2856-2866.
5. Ossenkoppele R, Tolboom N, Foster-Dingley JC et al. Longitudinal imaging of Alzheimer pathology using [11C]PIB, [18F]FDDNP and [18F]FDG PET. *Eur J Nucl Med Mol Imaging*. 2012;39(6):990-1000.
6. Scheinin NM, Aalto S, Koikkalainen J et al. Follow-up of [11C]PIB uptake and brain volume in patients with Alzheimer disease and controls. *Neurology*. 2009;73(15):1186-1192.
7. Jack CR, Jr., Lowe VJ, Weigand SD et al. Serial PIB and MRI in normal, mild cognitive impairment and Alzheimer's disease: implications for sequence of pathological events in Alzheimer's disease. *Brain*. 2009;132(Pt 5):1355-1365.
8. Rinne JO, Brooks DJ, Rossor MN et al. 11C-PIB PET assessment of change in fibrillar amyloid-beta load in patients with Alzheimer's disease treated with bapineuzumab: a phase 2, double-blind, placebo-controlled, ascending-dose study. *Lancet Neurol*. 2010;9(4):363-372.
9. Villain N, Chetelat G, Grassiot B et al. Regional dynamics of amyloid-beta deposition in healthy elderly, mild cognitive impairment and Alzheimer's disease: a voxelwise PIB-PET longitudinal study. *Brain*. 2012;135(Pt 7):2126-2139.
10. Lammertsma AA, Hume SP. Simplified reference tissue model for PET receptor studies. *NeuroImage*. 1996;4(3 Pt 1):153-158.
11. Yaqub M, Tolboom N, Boellaard R et al. Simplified parametric methods for [11C]PIB studies. *NeuroImage*. 2008;42(1):76-86.
12. Logan J, Fowler JS, Volkow ND, Wang GJ, Ding YS, Alexoff DL. Distribution volume ratios without blood sampling from graphical analysis of PET data. *J Cereb Blood Flow Metab*. 1996;16(5):834-840.
13. Carson RE, Channing MA, Blasberg RG et al. Comparison of bolus and infusion methods for receptor quantitation: application to [18F]cyclofoxy and positron emission tomography. *J Cereb Blood Flow Metab*. 1993;13(1):24-42.
14. Brix G, Zaers J, Adam LE et al. Performance Evaluation of a Whole-Body PET Scanner Using the NEMA Protocol. *J Nucl Med*. 1997;38(10):1614-1623.
15. Svarer C, Madsen K, Hasselbalch SG et al. MR-based automatic delineation of volumes of interest in human brain PET images using probability maps. *NeuroImage*. 2005;24(4):969-979.
16. Gunn RN, Lammertsma AA, Hume SP, Cunningham VJ. Parametric Imaging of Ligand-Receptor Binding in PET Using a Simplified Reference Region Model. *NeuroImage*. 1997;6(4):279-2787.
17. Wu Y, Carson R. Noise reduction in the simplified reference tissue model for neuroreceptor functional imaging. *J Cereb Blood Flow Metab*. 2002;22(12):1440-1452.
18. Lopresti BJ, Klunk WE, Mathis CA et al. Simplified quantification of Pittsburgh Compound B amyloid imaging PET studies: a comparative analysis. *J Nucl Med*. 2005;46(12):1959-1972.
19. Yamaguchi H, Hirai S, Morimatsu M, Shoji M, Nakazato Y. Diffuse type of senile plaques in the cerebellum of Alzheimer-type dementia demonstrated by beta protein immunostain. *Acta Neuropathology*. 1989;77:314-319.
20. Lammertsma AA, Hume SP. Simplified Reference Tissue Model for PET Receptor Studies. *NeuroImage*. 1996;4(3):153-158.
21. Tolboom N, Yaqub M, Boellaard R et al. Test-retest variability of quantitative [11C]PIB studies in Alzheimer's disease. *Eur J Nucl Med Mol Imaging*. 2009;36(10):1629-1638.
22. Yaqub M, Boellaard R, Kropholler MA, Lammertsma AA. Optimization algorithms and weighting factors for analysis of dynamic PET studies. *Phys Med Biol*. 2006;51(17):4217-4232.

23. Nelissen N, Van LK, Thurfjell L et al. Phase 1 study of the Pittsburgh compound B derivative 18F-flutemetamol in healthy volunteers and patients with probable Alzheimer disease. *J Nucl Med*. 2009;50(8):1251-1259.
24. Wong DF, Rosenberg PB, Zhou Y et al. In vivo imaging of amyloid deposition in Alzheimer disease using the radioligand 18F-AV-45 (florbetapir [corrected] F 18). *J Nucl Med*. 2010;51(6):913-920.
25. Slifstein M, Laruelle M. Effects of statistical noise on graphic analysis of PET neuroreceptor studies. *J Nucl Med*. 2000;41(12):2083-2088.
26. Zhou Y, Sojkova J, Resnick SM, et al. Relative equilibrium plot improves graphical analysis and allows bias correction of standardized uptake value ratio in quantitative 11C-PIB PET studies. *J Nucl Med*. 2012;53(4):622-628.
27. Bremmer JP, van Berckel BN, Persoon S et al. Day-to-day test-retest variability of CBF, CMRO2, and OEF measurements using dynamic 15O PET studies. *Mol Imaging Biol*. 2011;13(4):759-768.
28. Rinne JO, Brooks DJ, Rossor MN et al. 11C-PIB PET assessment of change in fibrillar amyloid-beta load in patients with Alzheimer's disease treated with bapineuzumab: a phase 2, double-blind, placebo-controlled, ascending-dose study. *Lancet Neurol*. 2010;9(4):363-372.
29. Koeppe RA, Frey KA. Equilibrium analysis of [C-11]PIB studies. *NeuroImage*. 2008;41:T30.

Chapter 2.2

Longitudinal Imaging of Alzheimer Pathology using [^{11}C]PIB, [^{18}F]FDDNP and [^{18}F]FDG PET

European Journal of Nuclear Medicine and Molecular Imaging 2012 39(6):990-1000

Rik Ossenkoppele, Nelleke Tolboom, Jessica C. Foster-Dingley, Sofie F. Adriaanse, Ronald Boellaard, Maqsood Yaqub, Albert D. Windhorst, Frederik Barkhof, Adriaan A. Lammertsma, Philip Scheltens, Wiesje M. van der Flier & Bart N.M. van Berckel.

ABSTRACT

Introduction

[^{11}C]PIB and [^{18}F]FDDNP are PET tracers for *in vivo* detection of the neuropathology underlying Alzheimer's disease (AD). [^{18}F]FDG is a glucose analogue and its uptake reflects metabolic activity. The purpose of this study was to examine longitudinal changes in these tracers in AD and mild cognitive impairment (MCI) patients and in healthy controls.

Methods

Longitudinal, paired, dynamic [^{11}C]PIB and [^{18}F]FDDNP (90 minutes each) and static [^{18}F]FDG (15 minutes) PET scans were obtained in 11 controls, 12 MCI patients and 8 AD patients. Mean interval between baseline and follow-up was 2.5 years (range, 2.0-4.0 years). Parametric [^{11}C]PIB and [^{18}F]FDDNP images of binding potential (BP_{ND}) and [^{18}F]FDG standardized uptake value ratio (SUVr) images were generated.

Results

A significant increase in global cortical [^{11}C]PIB BP_{ND} was found in the MCI group, but no changes were observed in AD patients and controls. Subsequent regional analysis revealed that this increase in [^{11}C]PIB BP_{ND} in MCI patients was most prominent in the lateral temporal lobe ($p<0.05$). For [^{18}F]FDDNP, no changes in global BP_{ND} were found. [^{18}F]FDG uptake was reduced at follow-up in the AD group only, especially in frontal, parietal and lateral temporal lobes (all $p<0.01$). Changes in global [^{11}C]PIB binding ($\rho=-0.42$, $p<0.05$) and posterior cingulate [^{18}F]FDG uptake ($\rho=0.54$, $p<0.01$) correlated with changes in MMSE over time across groups, whilst [^{18}F]FDDNP ($\rho=-0.18$, $p=0.35$) did not.

Conclusion

[^{11}C]PIB and [^{18}F]FDG track molecular changes in different stages of AD: we showed increased amyloid load in MCI patients and progressive metabolic impairment in AD patients. [^{18}F]FDDNP seems to be less useful for examining disease progression.

INTRODUCTION

Alzheimer's disease (AD) is a progressive neurodegenerative disorder characterized by decline in cognitive functions, progressive impairment of activities of daily living and neuropsychiatric symptoms. The neuropathological characteristics underlying AD are senile plaques consisting of amyloid-β (Aβ) and neurofibrillary tangles consisting of hyperphosphorylated tau, possibly leading to loss of synaptic density and network connections and ultimately generalized cortical atrophy [1,2]. To date, several PET tracers are available to assess molecular aspects of this neuropathological process *in vivo*. ^{18}F-2-fluoro-2-deoxy-D-glucose ([^{18}F]FDG) is a glucose analogue and, as such, its uptake is strongly associated with neuronal function. [^{18}F]FDG is a well validated and widely used PET tracer with a sensitivity of 94% and a specificity of 73% for diagnosing AD [3]. More recently, [^{11}C]PIB (Pittsburgh Compound-B) [4] and [^{18}F]FDDNP (2-(1-{6-[(2-[^{18}F]fluoroethyl)(methyl)amino]-2-naphthyl}ethylidene)malononitrile) [5] have been developed for *in vivo* imaging of the neuropathology underlying AD.

[^{11}C]PIB has high diagnostic accuracy for the detection of AD [4,6] and can easily be used for visual assessment [7;8]. Furthermore, high [^{11}C]PIB binding is a strong predictor for progression of mild cognitive impairment (MCI) to AD [9-12]. Longitudinal imaging studies in AD, however, showed inconsistent results with no [13-15] or only modest [11,16,17] changes in [^{11}C]PIB binding over time in AD. [^{18}F]FDDNP also discriminates between AD and healthy controls on a group level [5,6,18], but in AD patients it has a 9-fold lower specific binding signal than [^{11}C]PIB [6]. The unique feature of [^{18}F]FDDNP, however, is its affinity to bind to both amyloid plaques and neurofibrillary tangles *in vitro* [19]. This is important, as tangle load, rather than amyloid burden, is strongly related to both cognitive performance and disease progression. In the only published longitudinal study with [^{18}F]FDDNP to date, cognitive decline was associated with increased [^{18}F]FDDNP binding over time [5]. As such, [^{18}F]FDDNP might be a suitable, or even better, PET tracer for monitoring the time course of the disease.

The purpose of this longitudinal study was to examine global and regional changes in specific [^{11}C]PIB and [^{18}F]FDDNP binding and [^{18}F]FDG uptake over time in the same set of patients with AD and MCI, and in healthy controls.

METHODS

Subjects

At baseline, 15 subjects for each diagnostic group were included [6]. In the AD group, six patients were not capable of undergoing follow-up PET scans due to disease progression, whilst one patient experienced a severe stroke. Three MCI patients refused to participate in this follow-up study due to lack of motivation. Of the MCI patients that dropped out, one progressed to AD and the others remained cognitively stable. Two healthy controls developed diseases other than dementia, one subject could not participate because of family affairs and one control was lost to follow-up. Consequently, 8 AD patients, 12 MCI patients and 11 healthy controls were included in this longitudinal study.

All subjects received a standard dementia screening at baseline that included medical history, physical and neurological examinations, screening laboratory tests, brain MRI and extensive neuropsychological testing [6]. Clinical diagnosis was established by consensus in a multidisciplinary team, without awareness of the PET results. After 2-3 years, a renewed clinical consensus diagnosis was established using repeated brain MRI, neuropsychological testing and clinical data.

All AD patients met criteria proposed by the National Institute of Neurological and Communicative disorders and Stroke and the Alzheimer's Disease and Related Disorders Association (NINCDS-ADRDA) for probable AD [20]. At follow-up, six out of eight AD patients were taking acetylcholinesterase inhibitors and one AD patient used a selective serotonin reuptake inhibitor. MCI patients of the amnestic subtype met Petersen criteria based on subjective and objective cognitive impairment, in the absence of dementia or significant functional loss [21]. At follow-up, one MCI patient used an acetylcholinesterase inhibitor and another a benzodiazepine. Controls were recruited through advertisements in newspapers and underwent the same diagnostic procedures. None of the controls used psychotropic medication on both occasions or developed cognitive complaints.

Exclusion criteria were a history of major psychiatric or neurological (other than AD) illness and the use of non-steroidal anti-inflammatory drugs, as the latter have been reported to compete with [^{18}F]FDDNP for binding to Aβ fibrils *in vitro* and to Aβ plaques *ex vivo* [19]. Additional exclusion criteria for controls were subjective memory complaints

or clinically relevant abnormalities on MRI. Patients with severe vascular events during the follow-up period, such as stroke or haemorrhage, were also excluded. Written informed consent was obtained from all subjects after a complete written and verbal description of the study. The study protocol was approved by the Medical Ethics Review Committee of the VU University Medical Center.

PET

[^{11}C]PIB and [^{18}F]FDDNP PET scans were performed on the same day, except for five subjects at baseline (1 AD; 3 MCI; 1 HC) and seven subjects at follow-up (3 AD; 3 MCI; 1 HC), all due to radiosynthesis failure. PET scans were obtained on an ECAT EXACT HR+ scanner (Siemens/CTI, Knoxville, TN, USA) equipped with a neuroinsert to reduce the contribution of scattered photons. This scanner enables the acquisition of 63 transaxial planes over a 15.5 cm axial field of view, thus allowing the whole brain to be imaged in one bed position. The properties of this scanner have been reported elsewhere [22]. All subjects received a venous cannula for tracer injection. First, a 10 minute transmission scan was obtained in 2-dimensional acquisition mode using three retractable rotating line sources. This scan was used to correct the subsequent emission scan for photon attenuation. Next, a dynamic emission scan in 3-dimensional acquisition mode was started simultaneously with the intravenous injection of 351 ± 82 MBq (at baseline) and 377 ± 91 MBq (at follow-up) [^{11}C]PIB, using an infusion pump (Med-Rad, Beek, The Netherlands) at a rate of 0.8mL s^{-1}, followed by a flush of 42 mL of saline at 2.0 mL s^{-1}. [^{11}C]PIB was synthesized according to a modified procedure of Wilson et al.[23], resulting in a specific activity of 41 ± 22 GBq μmol^{-1} (at baseline) and 88 ± 40 GBq μmol^{-1} (at follow-up). The [^{11}C]PIB scan consisted of 23 frames increasing progressively in duration (1x15, 3x5, 3x10, 2x30, 3x60, 2x150, 2x300, 7x600 s) for a total scan duration of 90 minutes. Finally, after a resting period of at least an hour to allow for decay of ^{11}C, exactly the same procedure was repeated but now using an injection of [^{18}F]FDDNP [24] (177 ± 14 MBq at baseline and 189 ± 15 MBq at follow-up), with a specific activity of 86 ± 51 GBq μmol^{-1} (at baseline) and 70 ± 43 GBq μmol^{-1} (at follow-up). Patient motion was restricted by a head holder and regularly checked during scanning using laser beams.

[^{18}F]FDG PET scans were obtained for all subjects within an average interval of one month to the [^{11}C]PIB and [^{18}F]FDDNP scans. [^{18}F]FDG was injected after subjects rested for 10

minutes with the eyes closed and ears unplugged in a dimly lit room with minimal background noise. An intravenous bolus injection (150±17 MBq at baseline and 186±7 MBq at follow-up) of FDG was injected. Thirty-five minutes after injection, a 10 minute transmission scan followed by a 15 minute emission scan (3 x 5 minute frames) was performed.

MRI

All subjects underwent repeated structural MRI using a 1.5T Sonata scanner (Siemens, Erlingen, Germany). The scan protocol included a coronal T1-weighted 3-dimensional magnetization-prepared-acquisition gradient echo (MPRAGE) (slice thickness 1.5 mm; 160 slices; matrix size 256 x 256; voxel size 1 x 1 x 1.5 mm; echo time 3.97 ms; repetition time 2,700 ms; inversion time 950 ms; flip angle 8°), which was used for co-registration, segmentation and region-of-interest (ROI) definition.

Image and Data Analysis

All PET sinograms were corrected for dead time, tissue attenuation using the transmission scan, decay, scatter, and randoms. Next, data were reconstructed using a standard filtered back projection algorithm and a Hanning filter with a cut-off at 0.5 times the Nyquist frequency. A zoom factor of 2 and a matrix size of 256 x 256 x 63 were used, resulting in voxel size of 1.2 x 1.2 x 2.4 mm and spatial resolution of approximately 7 mm full width at half-maximum at the centre of the field of view.

MR images were aligned to corresponding PET images using a mutual-information algorithm. Data were further analyzed using PVE-lab, a software program that uses a probability map based on 35 delineated ROI that have been validated previously [25]. ROI were projected onto [^{11}C]PIB and [^{18}F]FDDNP parametric non-displaceable binding potential (BP_{ND}) images. These parametric images were generated using a 2-step basis-function implementation of the simplified reference tissue model (RPM2) [26], to the full dynamic 90 minute PET data. RPM2, a fully quantitative method for assessing the data, was identified as the parametric model of choice [26-28]. BP_{ND} is a quantitative measure of specific binding and reflects the concentration of specifically bound tracer relative to that of free plus non-specifically bound tracer in tissue under equilibrium. For [^{18}F]FDG, standardized uptake value ratio (SUVr) images (45-60 minutes post injection) were

generated. Cerebellar grey matter was chosen as reference tissue for this triplet of PET tracers because of its (histopathological) lack of Congo red and thioflavin-S-positive plaques, and its insensitivity to metabolic changes during disease progression [29].

For regional analysis, BP_{ND} ([^{11}C]PIB and [^{18}F]FDDNP) and SUVr ([^{18}F]FDG) of frontal (volume weighted average of orbital frontal, medial inferior frontal, and superior frontal), parietal, and lateral temporal (volume weighted average of superior temporal and medial inferior temporal) cortices and medial temporal lobe (MTL: volume weighted average of enthorinal cortex and hippocampus) and posterior cingulate were calculated. In addition, two global cortical ROI were defined. First, for direct comparison between [^{11}C]PIB and [^{18}F]FDDNP, a global cortical BP_{ND} based on the volume-weighted average of frontal, parietal and lateral temporal cortices, MTL, and posterior cingulate was computed. Secondly, another global cortical BP_{ND} excluding the MTL was calculated as this brain region shows substantially less amyloid deposition compared to the other ROI [4;6]. Finally, [^{11}C]PIB scans were classified into either positive or negative, based on visual inspection of parametric BP_{ND} images by a trained nuclear medicine physician (BvB).

Statistics

Group differences in subject characteristics were assessed using one-way ANOVA with post hoc LSD tests. Longitudinal changes in global cortical BP_{ND} and SUVr were assessed using ANOVA for repeated measures with diagnosis as between subjects factor, time as within subjects factor and global cortical BP_{ND} and SUVr as variables. Next, groups were stratified according to baseline global [^{11}C]PIB BP_{ND} (<0.1, 0.1-0.75, and >0.75) and paired samples t-tests were performed between baseline and follow-up global measures of [^{11}C]PIB, [^{18}F]FDDNP and [^{18}F]FDG. Subsequently, regional changes over time were investigated using paired samples t-tests in each group separately. Spearman correlation analysis was used to assess the relationships between changes in global cortical BP_{ND} and SUVr and changes in MMSE scores over time and the relationships between changes in global cortical [^{11}C]PIB BP_{ND} and [^{18}F]FDDNP BP_{ND} and posterior cingulate [^{18}F]FDG SUVr. Level of significance was set at $p<0.05$, except for the interaction terms in ANOVA for repeated measures where $p<0.10$ was considered significant.

RESULTS

Subjects

The three diagnostic groups did not differ with respect to age, gender, education or mean interval between baseline and follow-up (Table 1).

Table 1. Characteristics according to diagnostic group

Variable	Diagnostic group			
	Controls (n=11)	MCI (n=12)	AD (n=8)	P Value
Age at baseline, year	66±7	67±7	62±6	0.23
Sex % m (m/f)	73(8/3)	75(9/3)	87(7/1)	0.60
APOE ε4 (0/1/2)	9/2/0	4/5/3	2/4/2	<0.05
Education*	6(2-7)	6(3-7)	6(4-7)	0.58
Mean interval, years	2.5±0.3	2.5±0.5	2.7±0.6	0.49
MMSE, baseline	29±1	27±3	25±2	<0.0001[a]
MMSE, follow-up	29±1	25±1**	22±5**	<0.0001[b]
RAVLT, baseline				
Immediate recall	37±10	29±5	27±5	<0.05[c]
Delayed recall	7±2	3±3	2±2	<0.05[c]
Recognition	29±5	27±2	24±3	<0.05[d]
RAVLT, follow-up				
Immediate recall	39±13	29±10	20±4	<0.05[c]
Delayed recall	8±4	3±4	1±1	<0.05[c]
Recognition	28±4	26±3	22±5	<0.05[d]

* Education using Verhage's classification [41] on a 1-7 scale, indicated as median (range) ** Decline on MMSE during follow-up, p<0.05

[a]Post-hoc LSD tests: AD<MCI, p<0.05; AD<Controls, p<0.0001; MCI<Controls, p<0.05; [b]Post-hoc LSD tests: AD<MCI, p<0.05; AD<Controls, p<0.0001; MCI<Controls, p<0.01; [c] Post-hoc LSD tests: AD<HC, p<0.05, MCI<HC, p<0.05;

[d] Post-hoc LSD tests: AD<MCI, p<0.05, AD<HC, p<0.05

MMSE scores decreased over time in MCI and AD patients ($p<0.05$) and remained stable in controls. During the follow-up period, four MCI patients progressed to AD and one converted to frontotemporal lobar degeneration. Furthermore, two MCI patients demonstrated clear cognitive improvement and were no longer classified as MCI at follow-up. The other five MCI patients remained cognitively stable.

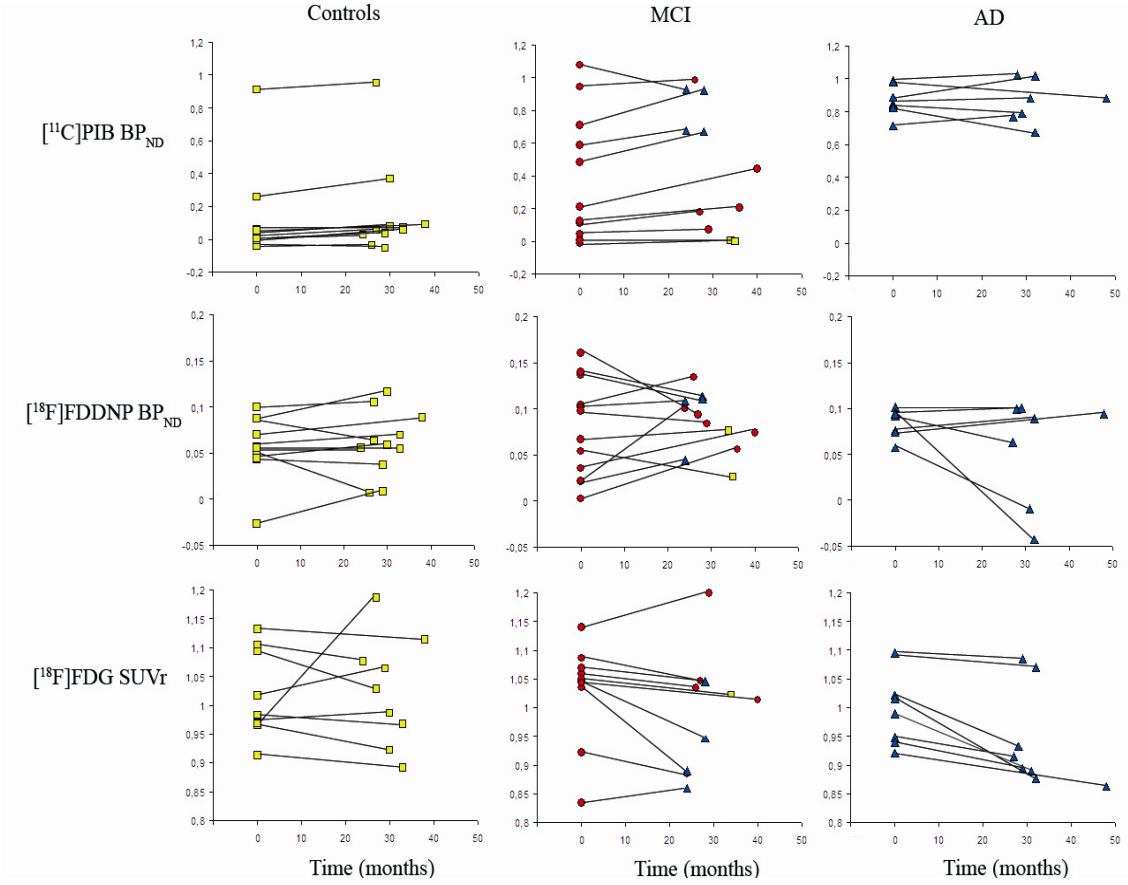

Figure 1. Overview of global cortical [^{11}C]PIB BP_{ND} (upper row), [^{18}F]FDDNP BP_{ND} (middle row) and [^{18}F]FDG SUVr (lower row) in the same healthy controls (left panel, yellow squares), MCI patients (middle panel, red circles) and AD patients (right panel, blue triangles). In the MCI group, several diagnoses changed during the follow-up period. The X-axis represents the follow-up period in months. Baseline and follow-up measurements are connected for each individual subject. ANOVA for repeated measures revealed increased [^{11}C]PIB binding in the MCI group and decreased [^{18}F]FDG uptake in the AD group over time. No longitudinal change in [^{18}F]FDDNP binding was found.

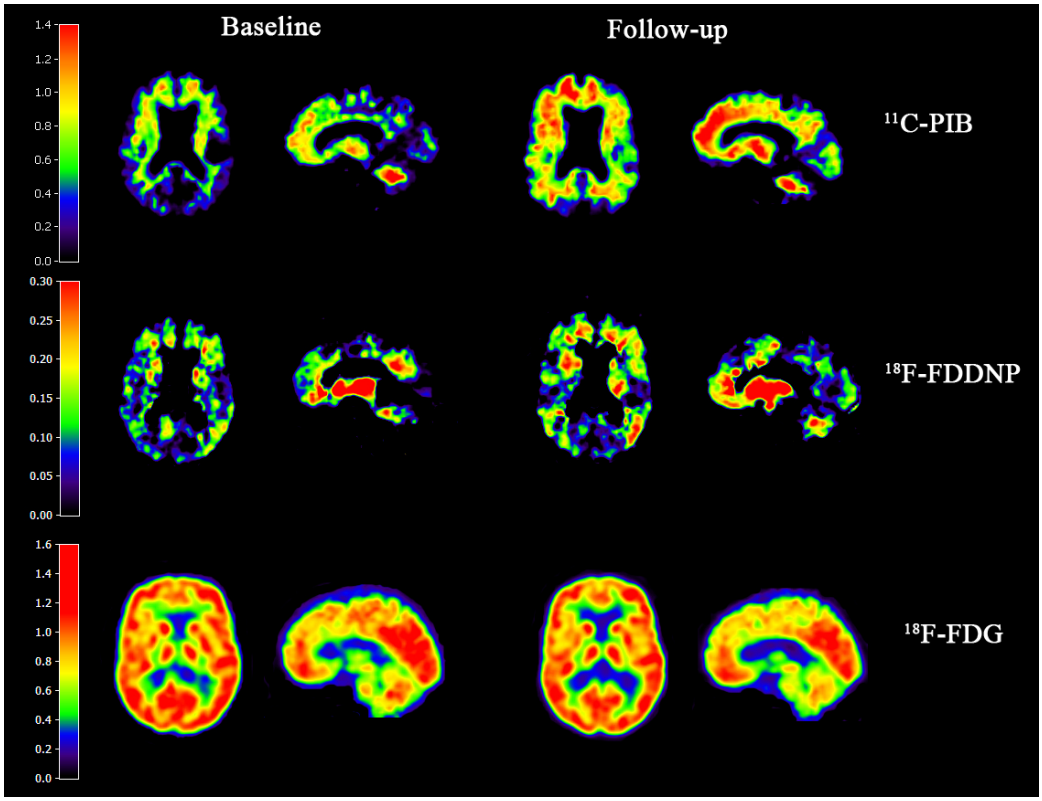

Figure 2. Baseline and follow-up parametric [^{11}C]PIB BP_{ND} (upper row) and [^{18}F]FDDNP BP_{ND} (middle row) and [^{18}F]FDG SUVr (lower row) images of a patient with mild cognitive impairment, who did not convert to AD during the follow-up period. The [^{11}C]PIB PET scans show a clear shift from predominantly non-specific binding in subcortical structures at baseline towards generalized cortical binding at follow-up. The latter pattern typically is observed in patients with Alzheimer's disease. In addition, the [^{18}F]FDDNP scans of this patient display increased cortical binding over time. The [^{18}F]FDG scans show minor longitudinal changes but both baseline and follow-up scans are within the normal range. Longer follow-up is needed to determine whether the increased amyloid burden eventually will lead to progression to AD.

[^{11}C]PIB

At baseline, global cortical BP_{ND} for [^{11}C]PIB was 0.87±0.10 in patients with AD, 0.39±0.39 in MCI patients and 0.12±0.27 in controls. At follow-up, global cortical BP_{ND} was 0.86±0.13 in AD patients, 0.46±0.39 in MCI patients and 0.15±0.29 in controls. Figure 1 (upper row) shows the individual changes over time for each individual subject in the three groups. Four out of five PIB-positive amnestic MCI patients progressed to AD during the follow-up period. The two MCI subjects with lowest BP_{ND} at baseline showed clear cognitive improvement and were no longer classified as MCI patients at follow-up. Furthermore, one PIB-negative MCI patient converted to frontotemporal lobe degeneration, the other

PIB-negative MCI patients remained cognitively stable. ANOVA for repeated measures showed a main effect for diagnosis ($p<0.05$) but no significant main effect for time ($p=0.08$). There was no significant interaction between time and diagnosis for global cortical BP_{ND} including MTL ($p=0.11$). There was an interaction, however, between time and diagnosis for global cortical BP_{ND} without MTL ($p<0.10$), which was attributable to an increase of [^{11}C]PIB binding over time in the MCI group. (Figure 1). Subsequent regional analysis using paired samples t-tests in diagnostic groups revealed a significant increase of [^{11}C]PIB binding in the lateral temporal lobe in the MCI group ($p<0.05$, Table 2). [^{11}C]PIB binding in MTL of the AD group decreased over time ($p<0.05$).

Table 2. Regional [^{11}C]PIB BP_{ND} over time by diagnostic group

[^{11}C]PIB	**Controls**		**MCI**		**AD**	
Region	Baseline	Follow-up	Baseline	Follow-up	Baseline	Follow-up
Frontal	0.13±0.33	0.15±0.34	0.43±0.44	0.50±0.43	0.93±0.09	0.94±0.14
Parietal	0.12±0.27	0.15±0.28	0.39±0.42	0.47±0.39	0.95±0.20	0.93±0.19
PC	0.12±0.21	0.14±0.23	0.41±0.43	0.44±0.40	0.88±0.18	0.82±0.21
MTL	0.06±0.08	0.09±0.09	0.09±0.07	0.08±0.07	0.18±0.04	0.12±0.06[b]
Temporal	0.12±0.24	0.14±0.26	0.38±0.36	0.46±0.39[a]	0.81±0.10	0.79±0.12

Regional changes within groups were assessed using paired samples t-tests.

MCI, Mild cognitive impairment; AD, Alzheimer's disease; PC, posterior cingulate; MTL, Medial temporal lobe

[a] Increased [^{11}C]PIB binding over time at a $p<0.05$ level

[b] Decreased [^{11}C]PIB binding over time at a $p<0.05$ level

Correlation analysis using Spearman's ρ revealed a negative correlation between increase in global cortical [^{11}C]PIB binding and decline in MMSE scores across groups ($\rho=-0.42$, $p<0.05$, Figure 3A). There was a modest, albeit non-significant, correlation between changes in global [^{11}C]PIB and [^{18}F]FDDNP BP_{ND} across groups ($\rho=0.33$, $p=0.08$). Changes in global [^{11}C]PIB BP_{ND}, however, did not correlate with change in global [^{18}F]FDG SUVr ($\rho=0.02$, $p=0.94$). Paired samples t-tests showed that subjects with low amyloid burden at baseline ([^{11}C]PIB BP_{ND} <0.1) showed no significant changes in [^{11}C]PIB binding ($p=0.09$), [^{18}F]FDDNP binding ($p=0.72$) and [^{18}F]FDG uptake ($p=0.99$) over time (Table 3). Subjects

with baseline [^{11}C]PIB BP_{ND} between 0.1 and 0.75 showed increased [^{11}C]PIB binding ($p<0.01$) and decreased [^{18}F]FDG uptake ($p<0.05$) during the follow-up period, whilst [^{18}F]FDDNP binding did not change ($p=0.95$). Subjects with high amyloid burden at baseline ([^{11}C]PIB BP_{ND} >0.75) showed a marked decrease in [^{18}F]FDG uptake ($p<0.01$) over time, whereas [^{11}C]PIB binding ($p=0.63$) and [^{18}F]FDDNP binding ($p=0.71$) remained stable.

Table 3. Longitudinal changes in global [^{11}C]PIB binding, [^{18}F]FDDNP binding and [^{18}F]FDG uptake in relation to baseline global [^{11}C]PIB BP_{ND}

	Baseline [^{11}C]PIB BP_{ND}		
	<0.1 (n=12)	0.1-0.75 (n=9)	>0.75 (n=9)
Δ [^{11}C]PIB BP_{ND}	0.01±.0.03	0.13±0.07[b]	-0.02±0.11
Δ [^{18}F]FDDNP BP_{ND}	0.00±0.08	-0.00±0.04	-0.01±0.06
Δ [^{18}F]FDG SUVr	0.00±0.08	-0.03±0.03[a]	-0.08±0.07[b]

BP_{ND}, non-displaceable binding potential; SUVr, standardized uptake value ratio

Differences between groups were assessed using paired samples t-tests:

[a] $p<0.05$, [b] $p<0.01$

[^{18}F]FDDNP

At baseline, global cortical BP_{ND} for [^{18}F]FDDNP was 0.08±0.02 in AD patients, 0.08±0.05 in MCI patients and 0.06±0.04 in controls. At follow-up, global cortical BP_{ND} was 0.06±0.06 in patients with AD, 0.09±0.03 for MCI patients and 0.06±0.04 in controls. Figure 1 (middle row) shows individual changes over time for the three groups. The majority of AD patients and two of the four MCI converters showed a non-significant decrease of [^{18}F]FDDNP binding over time. ANOVA for repeated measures showed no main effect of diagnosis ($p=0.28$) or time ($p=0.45$), nor was there an interaction between diagnosis and time ($p=0.16$). These results did not change when the MTL was left out of the global ROI. Subsequent regional analysis within groups showed an increase of specific [^{18}F]FDDNP binding in parietal lobe ($p<0.05$) and a decrease in MTL ($p<0.05$) of healthy controls. All other brain areas in the diagnostic groups remained unchanged (Table 4). There was no correlation between changes in global [^{18}F]FDDNP binding and MMSE scores over time

(ρ=-0.18, p=0.35, Figure 3B). Change in global [^{18}F]FDDNP BP_{ND} did not correlate with change in global [^{18}F]FDG SUVr (ρ=0.14, p=0.51).

Table 4. Regional [^{18}F]FDDNP BP_{ND} over time by diagnostic group

[^{18}F]FDDNP	**Controls**		**MCI**		**AD**	
Region	Baseline	Follow-up	Baseline	Follow-up	Baseline	Follow-up
Frontal	0.05±0.04	0.06±0.05	0.08±0.06	0.08±0.04	0.08±0.02	0.06±0.07
Parietal	0.02±0.05	0.05±0.04[a]	0.04±0.04	0.05±0.02	0.04±0.02	0.02±0.06
PC	0.06±0.03	0.03±0.04	0.06±0.07	0.06±0.04	0.08±0.05	0.04±0.07
MTL	0.12±0.04	0.11±0.03[b]	0.12±0.05	0.13±0.04	0.15±0.05	0.10±0.03
Temporal	0.08±0.03	0.07±0.04	0.09±0.06	0.11±0.04	0.10±0.02	0.07±0.06

Regional changes within groups were assessed using paired samples t-tests.

[a] Increased [^{18}F]FDDNP binding and [b] decreased [^{18}F]FDDNP binding: p<0.05.

[^{18}F]FDG

Global cortical SUVr for [^{18}F]FDG at baseline was 1.00±0.07 in AD patients, 1.03±0.09 in MCI patients and 1.02±0.08 in controls. At follow-up, global cortical SUVr was 0.93±0.07 in AD, 1.00±0.10 in MCI and 1.03±0.09 in controls. Figure 1 (lower row) shows individual changes over time for all subjects in the three diagnostic groups. Progressive decrease in [^{18}F]FDG uptake was observed in all AD patients and in three of four MCI converters. ANOVA for repeated measures showed no main effect of diagnosis (p=0.30), but there was a main effect of time (p<0.05). Furthermore, there was an interaction between time and diagnosis (p<0.05). The observed decrease in [^{18}F]FDG uptake over time was largely attributable to patients with AD (Figure 1). Subsequent regional analysis in the AD group showed decreased glucose metabolism in frontal (p<0.01), parietal (p<0.01) and lateral temporal lobes (p<0.01) over time, but not in posterior cingulate (p=0.09) and MTL (p=0.42). No regional changes over time were observed in controls or MCI patients (Table 5). Changes in posterior cingulate gyrus [^{18}F]FDG uptake was correlated with decline in MMSE scores across groups (ρ=0.54, p<0.01, Figure 3C).

Table 5. Regional [18F]FDG SUVr over time by diagnostic group

[18F]FDG	Controls		MCI		AD	
Region	Baseline	Follow-up	Baseline	Follow-up	Baseline	Follow-up
Frontal	1.07±0.09	1.08±0.12	1.05±0.22	1.05±0.10	1.10±0.07	1.03±0.07[a]
Parietal	1.07±0.08	1.10±0.10	1.10±0.06	1.06±0.19	0.95±0.14	0.86±0.17[a]
PC	1.09±0.09	1.11±0.11	1.10±0.07	1.10±0.11	0.98±0.17	0.91±0.19
MTL	0.75±0.03	0.74±0.04	0.79±0.20	0.73±0.08	0.75±0.05	0.73±0.10
Temporal	1.00±0.07	1.00±0.09	1.04±0.09	0.97±0.10	0.97±0.07	0.88±0.09[a]

Regional changes within groups were assessed using paired samples t-tests.

[a] Decreased [18F]FDG uptake over time at a $p<0.01$ level

DISCUSSION

In this study temporal changes in specific [11C]PIB and [18F]FDDNP binding and in [18F]FDG uptake were investigated using repeat scans in the same set of AD, MCI and control subjects. We found an increase of [11C]PIB in the MCI group which was most prominent in the lateral temporal lobe. No changes in the AD group and the controls were observed. [18F]FDDNP binding did not change over time in any of the groups. [18F]FDG uptake decreased over time in the AD group only, particularly in frontal, parietal and lateral temporal cortices. Changes in global [11C]PIB binding and [18F]FDG uptake in the posterior cingulate correlated with changes in MMSE scores over time across diagnostic groups, whilst changes in [18F]FDDNP did not.

Recently, Jack et al. [30] proposed a biomarker model based on the assumption that the formation of senile plaques reaches a relative plateau by the time clinical symptoms emerge. The present data, however, show increased [11C]PIB binding over time in the vast majority of both MCI converters and non-converters. This finding is in agreement with three recent papers that also identified longitudinal changes of amyloid load in MCI patients using [11C]PIB [11,12,16].The dynamic change in [11C]PIB binding over time during the MCI stage is exemplified by a cognitively stable MCI patient, who made a transition from a negative to a positive PIB scan during the follow-up period (Figure 2). This particular finding is not consistent with the aforementioned neuropathological

pathway in AD, and suggests that other pathological processes than fibrillary Aβ in this patient may drive cognitive complaints at the time of initial MCI diagnosis. Four out of five PIB-positive MCI patients progressed to AD during the follow-up period, whilst this did not happen to any of the PIB-negative MCI patients. Interestingly, the two MCI subjects with the lowest [^{11}C]PIB binding at baseline showed clear cognitive improvement and were no longer classified as MCI patients at follow-up. These findings together with previous reports [9-12] show that [^{11}C]PIB-positive scans strongly predict progression to AD in MCI patients and underscore the high negative predictive value of [^{11}C]PIB for AD.

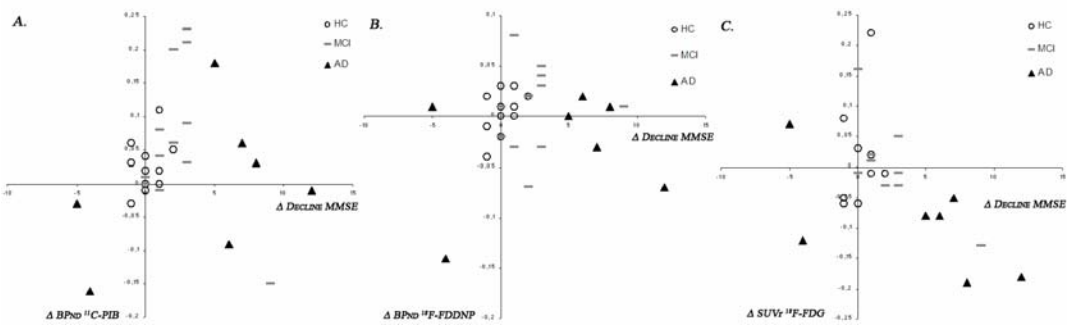

Figure 3. Correlation analysis (Spearman's ρ) was used to assess the relationships between changes in global cortical BP_{ND} and posterior cingulate SUVr and decline in MMSE scores over time. Across diagnostic groups, there were moderate correlations between [^{11}C]PIB BP_{ND} (ρ=-0.42, $p<0.05$) and [^{18}F]FDG SUVr (ρ=0.54, $p<0.01$) with MMSE. No significant correlation was found for [^{18}F]FDDNP BP_{ND} with MMSE (ρ=-0.18, p=0.35). AD patients are represented with filled triangles, MCI patients with circles and controls with squares.

Despite progression of disease, as indicated by a decline in MMSE, [^{11}C]PIB BP_{ND} in AD patients was stable over time. This finding is in agreement with the amyloid-cascade-hypothesis [31] which states that accumulation of Aβ during early stages of the disease precedes a cascade of neuropathological events that eventually leads to AD. In later stages of the disease, the equilibrium between amyloid deposition and resolution is restored, leading to stable amyloid levels. The observed amyloid plateau in the present AD patients is consistent with data from post-mortem studies [32] and transgenic mouse models [33], as well as CSF studies [34]. Furthermore, these results are in accordance with some [13-15] but not all [11,16,17] previous longitudinal studies using [^{11}C]PIB in AD.

In a previous study [7], it was shown that the diagnostic accuracy of [^{18}F]FDDNP for detection of AD is lower than that of [^{11}C]PIB. Both tracers bind to fibrillar aggregates of senile plaques, although [^{3}H]FDDNP has a 10-fold lower affinity than [^{3}H]PIB *in vitro* (8.5±1.3 nM versus 85.0±2.0 nM) [35]. This is reflected in a lower signal-to-noise ratio *in vivo* with a 9-fold lower BP_{ND} (0.09±0.02 versus 0.85±0.10) in AD patients [6]. It should be noted, however, that uptake of [^{18}F]FDDNP *in vitro*, results from binding to both amyloid plaques and neurofibrillary tangles [19]. Furthermore, [^{18}F]FDDNP BP_{ND} showed strong correlations with tau levels in cerebrospinal fluid [36] and performance on episodic memory tasks [37]. It was therefore hypothesized that [^{18}F]FDDNP might be an eligible PET tracer for monitoring the time course of the disease. This hypothesis could not be confirmed as no longitudinal changes in [^{18}F]FDDNP binding and no relationship between disease progression and increase of global [^{18}F]FDDNP BP_{ND} were observed. We were thus unable to replicate the only longitudinal study on [^{18}F]FDDNP published to date in which cognitive decline was associated with increased [^{18}F]FDDNP binding over time [5]. This can possibly be explained by several methodological considerations such as differences in subject selection and the use of different kinetic models for the analysis of PET data. More importantly, however, in the aforementioned study repeat [^{18}F]FDDNP PET scans were only performed in a subset (nine controls and three MCI subjects) of the baseline participants (83 subjects in total). In contrast, in the present study repeat measurements were performed not only in controls and MCI patients, but also in AD patients. This larger study population allowed for a statistical analysis of the longitudinal data, rather than only exploring a subset of the study sample.

However, all of the above does not explain why no increase in [^{18}F]FDDNP binding over time was found in both AD patients and MCI converters, as it is known that tangle pathology is closely related to disease progression. Therefore, the stable [^{18}F]FDDNP levels over time may be modified by reduced availability of binding sites due to brain atrophy, in particular because [^{18}F]FDDNP binding is highest in MTL. Another consideration is that the component of [^{18}F]FDDNP that binds to neurofibrillary tangles may not be as substantial [35] as initially suggested [19]. The low BP_{ND} of [^{18}F]FDDNP further complicates its interpretation and applicability.

Progressive decrease of glucose metabolism throughout the neocortex was observed in the AD group only. The utility of [^{18}F]FDG PET to monitor disease progression has been described consistently in previous studies [14,38]. The absence of a correlation between temporal changes in global [^{18}F]FDG SUVr and [^{11}C]PIB BP_{ND} across groups, together with interaction effects in different diagnostic groups indicate that both tracers track molecular changes in different stages of AD. In early stages of the disease, accumulation of Aβ is an ongoing event while no or only minor metabolic changes occur. As the clinical course of AD progresses, the amyloid curve flattens and evident generalized glucose hypometabolism arise. This notion is supported by a previous study showing that metabolic impairment follows anatomical patterns of amyloid deposition with a temporal delay [39]. For diagnostic purposes, [^{18}F]FDG and [^{11}C]PIB PET provide complementary information and can be used in combination for early and accurate detection of AD. The time course of AD should preferably be monitored by [^{18}F]FDG.

One of the strengths of the present study is its unique study design that allows direct comparison of repeat [^{11}C]PIB, [^{18}F]FDDNP and [^{18}F]FDG PET scans in the same set of patients with AD and MCI and in controls. For both [^{11}C]PIB and [^{18}F]FDDNP optimal quantitative parametric methods were used. RPM2 provides an estimation of specific binding that is independent of potential blood flow changes, which can occur during disease progression. In contrast, semi-quantitative methods such as SUVr are more sensitive to alterations in blood flow and/or tracer delivery. On the other hand, RPM2 requires a dynamic PET scan of 90 minutes, which may have led to diminished participation in the AD group. This could have introduced some selection bias, since patients with major disease progression were not able to participate in the follow-up condition. This, in turn, is reflected by the relatively small decline in MMSE scores (Table 1) in AD patients. Furthermore, sample sizes of the diagnostic groups were relatively small, thereby diminishing the statistical power. Another possible limitation of this study is that subjects were relatively young, and the time course of the disease may differ between younger and older AD patients [40]. Finally, use of acetylcholinesterase inhibitors by several AD patients may have affected the semi-quantitative assessment of [^{18}F]FDG uptake.

Conclusions

Increased cortical [^{11}C]PIB binding was seen in MCI patients and decreased [^{18}F]FDG uptake in AD patients. Based on the limited series of patients in the present study, [^{18}F]FDDNP seems to be of less value for monitoring disease progression.

REFERENCES

1. Cummings JL. Alzheimer's Disease. *N Engl J Med* 2004;351:56-67.
2. Stam CJ, de Haan W, Daffertshofer A et al. Graph theoretical analysis of magnetoencephalographic functional connectivity in Alzheimer's disease. *Brain* 2009;132:213-224.
3. Silverman DHS, Small GW, Chang CY et al. Positron Emission Tomography in Evaluation of Dementia. *JAMA* 2001;286:2120-2127.
4. Klunk WE, Engler H, Nordberg A et al. Imaging Brain Amyloid in Alzheimer's Disease with Pittsburgh Compound-B. *Ann Neurol* 2004;55:306-319.
5. Small GW, Kepe V, Ercoli LM et al. PET of Brain Amyloid and Tau in Mild Cognitive Impairment. *N Engl J Med* 2006;355:2652-2663.
6. Tolboom N, Yaqub M, van der Flier WM et al. Detection of Alzheimer Pathology In Vivo Using Both 11C-PIB and 18F-FDDNP PET. *J Nucl Med* 2009;50:191-197.
7. Tolboom N, Flier WM, Boverhoff J et al. Molecular imaging in the diagnosis of Alzheimer's disease: visual interpretation of [11C]PIB and [18F]FDDNP PET images. *J Neurol Neurosurg Psychiatry* 2010;81:882-884.
8. Ng S, Villemagne VL, Berlangieri S et al. Visual Assessment Versus Quantitative Assessment of 11C-PIB PET and 18F-FDG PET for Detection of Alzheimer's Disease. *J Nucl Med* 2007;48:547-552.
9. Forsberg A, Engler H, Almkvist O et al. PET imaging of amyloid deposition in patients with mild cognitive impairment. *Neurobiol Aging* 2008;29:1456-1465.
10. Okello A, Koivunen J, Edison P et al. Conversion of amyloid positive and negative MCI to AD over 3 years: An 11C-PIB PET study. *Neurology* 2009;73:754-760.
11. Villemagne VL, Pike K, Chetelat G et al. Longitudinal assessment of Aß and cognition in aging and Alzheimer disease. *Ann Neurol* 2011;69:181-192.
12. Koivunen J, Scheinin M, Virta JR et al. Amyloid PET imaging in patients with mild cognitive impairment: a 2-year follow-up study. *Neurology* 2011;76:1085-1090.
13. Engler H, Forsberg A, Almkvist O et al. Two-year follow-up of amyloid deposition in patients with Alzheimer's disease. *Brain* 2006;129:2856-2866.
14. Kadir A, Almkvist O, Forsberg A et al. Dynamic changes in PET amyloid and FDG imaging at different stages of Alzheimer's disease. *Neurobiology of Aging* 2012;33:198.e1-14.
15. Scheinin NM, Aalto S, Koikkalainen J et al. Follow-up of [11C]PIB uptake and brain volume in patients with Alzheimer disease and controls. *Neurology* 2009;73:1186-1192.
16. Jack CR, Jr., Lowe VJ, Weigand SD et al. Serial PIB and MRI in normal, mild cognitive impairment and Alzheimer's disease: implications for sequence of pathological events in Alzheimer's disease. *Brain* 2009;132:1355-1365.
17. Rinne JO, Brooks DJ, Rossor MN et al. 11C-PIB PET assessment of change in fibrillar amyloid-[beta] load in patients with Alzheimer's disease treated with bapineuzumab: a phase 2, double-blind, placebo-controlled, ascending-dose study. *Lancet Neurol* 2010;9:363-372.
18. Shin J, Lee SY, Kim SH et al. Multitracer PET imaging of amyloid plaques and neurofibrillary tangles in Alzheimer's disease. *NeuroImage* 2008;43:236-244.
19. Agdeppa ED, Kepe V, Liu J et al. Binding Characteristics of Radiofluorinated 6-Dialkylamino-2-Naphthylethylidene Derivatives as Positron Emission Tomography Imaging Probes for beta -Amyloid Plaques in Alzheimer's Disease. *J Neurosci* 2001;21:189RC.
20. McKhann G, Drachman D, Folstein M et al. Clinical diagnosis of Alzheimer's disease: report of the NINCDS-ADRDA Work Group under the auspices of Department of Health and Human Services Task Force on Alzheimer's disease. *Neurology* 1984;34:939-944.
21. Petersen RC, Smith GE, Waring SC et al. Mild Cognitive Impairment: Clinical Characterization and Outcome. *Arch Neurol* 1999;56:303-308.
22. Brix G, Zaers J, Adam LE et al. Performance Evaluation of a Whole-Body PET Scanner Using the NEMA Protocol. *J Nucl Med* 1997;38:1614-1623.
23. Wilson A.A., Garcia A, Chestaskova A et al. A rapid one-step radiosynthesis of the beta-amyloid imaging radiotracer N-methyl-[C-11]2-('4-methylaminophenyl)-6-hydroxybenzothiazole ([C-11]-6-OH-BTA-1). *Journal of labelled compounds and radiopharmaceuticals* 2004;47:679-682.

24. Klok RP, Klein PJ, van Berckel BNM et al. Synthesis of 2-(1,1-dicyanopropen-2-yl)-6-(2-[18F]-fluoroethyl)-methylamino-naphthalene ([18F]FDDNP). *Appl Radiat Isot* 2008;66:203-207.
25. Svarer C, Madsen K, Hasselbalch SG et al. MR-based automatic delineation of volumes of interest in human brain PET images using probability maps. *NeuroImage* 2005;24:969-979.
26. Wu Y, Carson R. Noise reduction in the simplified reference tissue model for neuroreceptor functional imaging. *J Cereb Blood Flow Metab* 2002;22:1440-1452.
27. Yaqub M, Tolboom N, Boellaard R et al. Simplified parametric methods for [11C]PIB studies. *NeuroImage* 2008;42:76-86.
28. Yaqub M, Tolboom N, van Berckel BNM et al.Simplified parametric methods for [18F]FDDNP studies. *NeuroImage* 2010;49:433-441.
29. Yamaguchi H, Hirai S, Morimatsu M et al. Diffuse type of senile plaques in the cerebellum of Alzheimer-type dementia demonstrated by beta protein immunostain. *Acta Neuropath* 1989;77:314-319.
30. Jack Jr CR, Knopman DS, Jagust WJ et al. Hypothetical model of dynamic biomarkers of the Alzheimer's pathological cascade. *Lancet Neurol* 2010;9:119-128.
31. Hardy JA, Selkoe DJ. The amyloid hypothesis of Alzheimer's disease: progress and problems on the road to therapeutics. *Science* 2002;197:353-356.
32. Hyman, Marzloff K, Arriagada PV. The lack of accumulation of senile plaques or amyloid burden in Alzheimer's disease suggests a dynamic balance between amyloid deposition and resolution. *J Neuropathol Exp Neurol* 1993;52:594-600.
33. Christie RH, Bacskai BJ, Zipfel WR et al. Growth Arrest of Individual Senile Plaques in a Model of Alzheimer's Disease Observed by In Vivo Multiphoton Microscopy. *J Neurosci* 2001;21:858-864.
34. Bouwman FH, van der Flier WM, Schoonenboom NSM et al. Longitudinal changes of CSF biomarkers in memory clinic patients. *Neurology* 2007;69:1006-10 11.
35. Thompson PW, Ye L, Morgenstern JL et al. Interaction of the Amyloid Imaging Tracer FDDNP with Hallmark Alzheimer's Disease Pathologies. *J Neurochemy* 2009;109:623-630.
36. Tolboom N, van der Flier WM, Yaqub M et al. Relationship of Cerebrospinal Fluid Markers to 11C-PIB and 18F-FDDNP Binding. *J Nucl Med* 2009;50:1464-1470.
37. Tolboom N, Flier WM, Yaqub M et al. Differential association of [11C]PIB and [18F]FDDNP binding with cognitive impairment. *Neurology* 2009;73:2079-2085.
38. Alexander GE, Chen K, Pietrini P et al. Longitudinal PET Evaluation of Cerebral Metabolic Decline in Dementia: A Potential Outcome Measure in Alzheimer's Disease Treatment Studies. *Am J Psychiatry* 2002;159:738-745.
39. Forster S, Grimmer T., Miederer I et al. Regional expansion of hypometabolism in Alzheimer's disease follows amyloid deposition with temporal delay. *Biol Psychiatry* 2012;71:792-797.
40. van der Vlies AE, Koedam ELGE, Pijnenburg YAL et al. Most rapid cognitive decline in APOE E4 negative Alzheimer's disease with early onset. *Psychol Med* 2009;39:1907-11.
41. Verhage F. Intelligentie en leeftijd: onderzoek bij Nederlanders van twaalf tot zevenenzeventig jaar [Intelligence and age: study with Dutch people aged 12 to 77]. In: Van Gorcum, ed. Assen: 1964.

Chapter 3

Molecular imaging in cognitively normal elderly

Is Verbal Episodic Memory in Elderly with Amyloid Deposits Preserved Through Altered Neuronal Function?

Cerebral Cortex (in press)

Rik Ossenkoppele, Cindee Madison, Hwamee Oh, Miranka Wirth,
Bart N.M. van Berckel, William J. Jagust

ABSTRACT

A potential mechanism that enables intellectual preservation in cognitively normal elderly that harbor beta-amyloid (Aβ) pathology is heightened cerebral glucose metabolism. To investigate cross-sectional inter-relationships between Aβ, glucose metabolism and cognition, 81 subjects (mean age: 75±7) underwent [^{11}C]Pittsburg Compound-B and [^{18}F]fluorodeoxyglucose positron emission tomography scans and neuropsychological testing. They were divided into low-Aβ (n=53), intermediate-Aβ (n=13) and high-Aβ (n=15) groups as defined by their global cortical [^{11}C]PIB retention. Glucose metabolism was assessed using a MetaROI mask that covers metabolically critical regions in Alzheimer's disease (AD) (i.e. posterior cingulate and bilateral angular and inferior temporal gyri). Previously validated factor scores for verbal and visual episodic memory, semantic memory, working memory and executive functioning were used to evaluate cognitive performance Greater Aβ deposition in the precuneus was associated with higher metabolic activity (at trend level) and lower visual episodic memory scores. Glucose metabolism did not correlate with cognition across all subjects. However, heightened metabolic activity was associated with better verbal episodic memory performance in subjects with elevated amyloid levels. This preliminary study suggests that neural compensation, as a manifestation of brain reserve, enables elderly supposedly on the path to AD, at least temporarily, to preserve cognitive function.

INTRODUCTION

Deposition of amyloid-beta (Aβ) is a neuropathological hallmark of Alzheimer's disease (AD), but significant plaque burden is frequently present in cognitively normal elderly at autopsy as well [1-3]. *In vivo* positron emission tomography (PET) studies employing [^{11}C]Pittsburgh compound-B (PIB, [4]) confirmed that approximately 30% of persons over 70 years display cerebral amyloidosis [5-7]. According to new research criteria, these individuals are in a preclinical stage of AD [8]. In a recently proposed biomarker model [9], it was hypothesized that Aβ deposition precedes tau mediated neuronal dysfunction, brain atrophy and cognitive deterioration that eventually lead to the onset of dementia. The estimated time between initial Aβ accumulation and manifestation of symptoms is 15 years [10,11]. Following this model, it may be expected that some individuals with high Aβ burden already show subtle signs of neurodegeneration. Indeed, morphological reductions in AD specific regions were observed in elderly with amyloid deposits on structural magnetic resonance imaging (MRI) [12-16]. Functional MRI studies, paradoxically, demonstrated increased brain activation in aging [17-20] and genetic risk populations [21,22] that potentially capture the earliest stage of AD development. Similarly in patients with mild cognitive impairment, increased cerebral glucose metabolism as measured using [^{18}F]fluorodeoxyglucose (FDG) PET was associated with greater Aβ load [23]. Heightened synaptic activity could be a manifestation of cognitive brain reserve that reflects a compensatory response to counteract neurotoxic effects of Aβ. Increased neuronal activity may enable the brain to suppress pathological insult and maintain normal cognitive function for a longer period. In keeping with this idea, the cross-sectional effect of Aβ on cognition, if any, is small. Some studies showed a negative correlation between the presence of amyloid and cognitive performance in cognitively normal elderly [24-26], whereas others could not replicate this [27,10]. There is more robust evidence for long-term effects of amyloid pathology as individuals with elevated Aβ are at higher risk for cognitive decline over time [28-30,6].

[^{18}F]FDG PET is an eligible marker of resting state synaptic activity and is capable of capturing up- and down-regulation of brain function [31-32]. Neuronal activity as measured with [^{18}F]FDG PET may provide more insight in the complex relationship between Aβ deposition and cognitive performance. The objectives of this cross-sectional

study were to investigate the relationships between 1) Aβ load and glucose metabolism, 2) Aβ load and cognition, 3) glucose metabolism and cognition and 4) glucose metabolism and cognition as a function of amyloid-status in a group of cognitively normal elderly.

MATERIALS AND METHODS

Subjects

Eighty-one cognitively normal elderly subjects with available [^{11}C]PIB and [^{18}F]FDG PET data were included in the present study. All volunteers were recruited through the Berkeley Aging Cohort study (BACs); a community-dwelling cohort that is a convenience sample of healthy individuals who are older than 60 years and reside in the San Francisco Bay Area of California. BACs participants were recruited through advertisements in senior centers and in local newspapers. Inclusion criteria were independent daily living, absence of any neurological or psychiatric condition that potentially affects brain structure and function, absent cognitive complaints, normal performance on cognitive tests (maximally 1.5 SD's below age-, years of education-, and sex- adjusted means), no use of psychoactive drugs and absence of sensory impairment that might interfere with cognitive testing. Subjects completed genotyping for apolipoprotein E (APOE) ε4 carrier status. The local ethics committee approved the study and subjects gave written informed consent.

Neuropsychological testing

Seventy-four subjects underwent an extensive neuropsychological test battery, thus cognitive data was missing for seven subjects. Previously, a principal component analysis was conducted on 189 cognitively normal elderly (mean age: 73±7; 63 males; mean MMSE: 29±1) and 108 young adults (mean age: 25±4; 62 males; mean MMSE: 29±1) in order to obtain concise and reliable cognitive component scores [33]. This revealed five major cognitive components: 1) verbal episodic memory (Free recall trials 1-5, Short-delay free recall, Short-delay cued recall, Long-delay free recall and Long-delay cued recall of the California Verbal Learning Test) [34], 2) visual episodic memory (Immediate recall, Delayed recall, Retention and Recognition from the Visual Reproduction Test in the Wechsler Memory Scale) [35], 3) semantic memory (Category fluency "vegetables" and "animals") [36], 4) working memory (Digit span forward and backward) [35] and 5) executive functioning ("Trail B minus A" score from Trail Making Test[37], Symbol Digit

Modalities Test [38] and Stroop Test [39]. Factor loadings for individual neuropsychological tests were used to calculate factor scores for participants in this study on these cognitive component scales. Factor score=0 represents the mean of the derivation sample, with a standard deviation of 1. Negative component scores indicate worse cognitive performance and positive values mean better test scores compared to the derivation sample.

Imaging data acquisition

[^{11}C]PIB PET

All PET scans were performed at Lawrence Berkeley National Laboratory (LBNL) using a Siemens ECAT EXACT HR scanner (Siemens, Inc., Iselin, NJ, USA) in 3-dimensional acquisition mode. The dynamic [^{11}C]PIB scans consisted of 34 frames increasing progressively in duration (4x15, 8x30, 9x60, 2x180, 8x300 and 3x600 seconds) for a total scanning time of 90 minutes. More details on the [^{11}C]PIB-PET imaging data acquisition and data analysis can be found in a previously published study [15].

[^{18}F]FDG PET

[^{18}F]FDG PET imaging was performed approximately two hours after [^{11}C]PIB injection. Following an injection of 6-10 mCi of the tracer, 6x5 min frames of emission data were collected starting 30 min post-injection. All PET data were reconstructed using an ordered subset expectation maximization algorithm with weighted attenuation. Images were smoothed with a 4x4x4 mm Gaussian kernel with scatter correction.

Structural MRI

High-resolution structural MRI scans were performed at LBNL on a 1.5 T Magnetom Avanto system (Siemens, Inc.) with a 12-channel head coil run in triple mode. Three T1-weighted magnetization-prepared rapid gradient echo (MPRAGE) scans were collected axially for each subject (repetition time: 2110 msec; echo time: 3.58 ms; flip angle: 15°; field-of-view: 256x256 mm; matrix size: 256x256; slices: 160; voxel size: 1x1x1 mm^3). Reference regions and regions-of-interest (ROI) for [^{11}C]PIB and [^{18}F]FDG were generated using the FreeSurfer Version 4.4 software package (surfer.nmr.mgh.harvard.edu). In addition, total cortical gray matter volumes were obtained using the automated segmentation of the Freesurfer software (Version 5.1) and entered as covariate to correct

for potential confounding by brain atrophy in models including both [^{11}C]PIB and [^{18}F]FDG.

Imaging data analysis

[^{11}C]PIB

PIB-PET data analysis methods are described elsewhere [15]. In summary, all PET images were preprocessed using Statistical Parametric Mapping 8 (SPM8; www.fil.ion.ucl.ac.uk/spm). Frames 6-34 collected over 90 minutes were realigned to the middle frame (17th frame) and co-registered to the subject's structural MRI image. Global index (encompassing frontal, temporal, parietal and anterior and posterior cingulate cortices) and precuneus distribution volume ratio's (DVR) of [^{11}C]PIB were calculated using Logan graphical analysis with cerebellar gray matter as reference region [40,41]. In a previous study, elderly BACs subjects were contrasted against 11 young control subjects (25±3 years) and classified as low-PIB (index DVR: <1.08), intermediate-PIB (1.08-1.16) or high-PIB (>1.16) [42]. We adopted this classification in the present study. In previous reports we have characterized intermediate- and high-PIB subjects as PIB-positive (PIB+) [42,33].

[^{18}F]FDG-PET

The six [^{18}F]FDG PET frames were aligned to the first frame and averaged. Then, each [^{18}F]FDG frame was realigned to the resultant mean image. The native space realigned images were summed to create one [^{18}F]FDG image that was then intensity normalized to the pons, as pontine glucose metabolism is known to be preserved in AD patients [43].

In the present study, [^{18}F]FDG data was analyzed using the MetaROI approach [44]. This method comprises five ROIs (posterior cingulate cortex (PCC), bilateral angular gyri and bilateral inferior temporal gyri) that were most strongly associated with metabolic and cognitive decline indicative of AD dementia in a literature review of published reports. To generate [^{18}F]FDG SUVr within the MetaROI, at first, structural MRI scans were co-registered to corresponding [^{18}F]FDG scans in native space. Subsequently, all co-registered MRI scans were registered to MNI space to generate a study specific template using the DARTEL tool in SPM8. Next, [^{18}F]FDG scans were warped to MNI space using the flowfields obtained with the transformation of the MRI scans. Finally, a MetaROI mask was

applied to extract mean [^{18}F]FDG uptake values for the composite ROI and the individual regions comprising this ROI.

Statistics

Differences between groups for baseline characteristics were assessed using ANOVA and X^2 tests, where appropriate. We adjusted the analyses for age, education and APOE genotype given their effects on [^{11}C]PIB retention, [^{18}F]FDG uptake and cognitive scores in the present study (see Table 2) and in previous studies. Pearson correlations were used to assess assocations between age, education, APOE genotype, precuneus [^{11}C]PIB, composite [^{18}F]FDG MetaROI and cognitive factor scores. Linear regression analyses, adjusted for age, education and APOE, were used to test the relationships between precuneus [^{11}C]PIB retention (as a continuous variable) and composite and regional [^{18}F]FDG MetaROI uptake. In an additional model we adjusted for partial volume effects by entering cortical gray matter volumes as covariate. We also performed a voxelwise analysis in SPM8 using a MetaROI [^{18}F]FDG mask to define the search region as dependent variable, precuneus [^{11}C]PIB as regressor and age, education, APOE and cortical gray matter volume as nuisance variables. This analysis was performed in MNI space (see subsection "[^{18}F]FDG-PET" for transformation), and results were displayed at $p<0.05$ (2-tailed, uncorrected) with a cluster size of 10 voxels. Next, linear regression analyses were performed to assess the relationships between precuneus [^{11}C]PIB/[^{18}F]FDG MetaROI and the cognitive factor scores. In the first model we entered no covariates while in the second model we adjusted for age, education and APOE. Finally, interactions between [^{11}C]PIB status (low, intermediate or high) and composite [^{18}F]FDG MetaROI on the cognitive factor scores were assessed using multivariate ANCOVA with adjustment for age, education and APOE status. Post-hoc linear regression analyses were used to further explore these relationships within [^{11}C]PIB groups.

RESULTS

Subjects

Demographics, cognitive scores, index [^{11}C]PIB and composite [^{18}F]FDG are presented in Table 1. 53 subjects were completely amyloid negative while the balance had evidence of Aβ deposition ranging from mild to extensive. There were no group differences in terms of

age, gender, level of education, APOE genotype, MMSE, any of the cognitive factor scores or composite [^{18}F]FDG MetaROI. By design, the high-PIB group showed increased global [^{11}C]PIB retention compared to both intermediate-PIB and low-PIB groups ($p<0.001$), and intermediate-PIB subjects had higher index compared to the low-PIB group ($p<0.01$).

Table 1. Demographics, cognition, [^{11}C]PIB index and composite [^{18}F]FDG

	All *(n=81)*	Low-PIB *(n=53)*	Intermediate-PIB *(n=13)*	High-PIB *(n=15)*
Age	75.0±6.6	74.8±6.2	72.4±6.9	78.1±7.0
Gender (male/female)	29/52	19/34	5/8	5/10
Education	17.0±1.8	17.2±1.8	16.9±1.6	16.5±1.8
APOE ε4 carriers (%)	27	21	25	47
MMSE	29.0±1.2	29.1±1.2	29.5±0.7	28.5±1.2
Verbal episodic memory	-0.04±1.04	-0.05±1.1	-0.21±0.85	0.10±1.07
Visual episodic memory	-0.15±0.89	-0.05±0.89	0.04±0.93	-0.61±0.73
Working memory	-0.04±1.05	-0.08±1.08	0.17±1.20	-0.10±0.83
Semantic memory	0.03±1.18	-0.10±1.09	0.41±1.52	0.15±1.15
Executive functions	-0.28±1.03	-0.27±1.00	-0.36±0.54	-0.26±1.42
[^{11}C]PIB index	1.11±0.18	1.02±0.04	1.11±0.02*	1.43±0.18**
Composite [^{18}F]FDG MetaROI	1.65±0.18	1.65±0.18	1.61±0.17	1.67±0.18

Data are presented as mean ± standard deviation unless indicated otherwise.

* Intermediate-PIB > low-PIB: $p<0.01$;

** High-PIB > low and intermediate-PIB: $p<0.001$

Across groups, Pearson correlations revealed significant associations between age and precuneus [^{11}C]PIB ($r=0.23$), age and composite [^{18}F]FDG MetaROI ($r=-0.25$), education and executive functions ($r=0.25$), APOE genotype and precuneus [^{11}C]PIB ($r=0.28$), precuneus [^{11}C]PIB and visual episodic memory ($r=-0.30$), executive functions and semantic memory ($r=-0.29$, all $p<0.05$) and between age and visual episodic memory ($r=-0.39$, $p<0.01$). No other significant correlations were found (Table 2).

Correlations between Precuneus PIB and FDG MetaROI

Linear regression analysis with adjustment for age, education and APOE showed an association at trend level between precuneus [^{11}C]PIB retention and composite [^{18}F]FDG MetaROI (standardized β: 0.21, p=0.10, Figure 1A). Additional adjustment for partial volume effects using cortical gray matter volumes revealed an even stronger association (standardized β: 0.33, p<0.05). Precuneus [^{11}C]PIB retention was significantly correlated with PCC (standardized β: 0.36, p<0.05) and right angular (standardized β: 0.28, p<0.05) [^{18}F]FDG uptake, which was confirmed in a voxelwise analysis in SPM8 within MetaROIs (Figure 1B). Precuneus [^{11}C]PIB retention did not correlate significantly with left angular gyrus (standardized β: 0.16, p=0.25) and left (standardized β: 0.19, p=0.15) and right (standardized β: 0.17, p=0.18) inferior temporal gyri uptake.

Precuneus PIB and Cognitive Factor Scores

Linear regression analysis showed a negative association between precuneus [^{11}C]PIB retention and performance on visual episodic memory tasks across groups (standardized β: -0.30, p<0.05, Figure 2A). This result was no longer significant after adjustment for age, education and APOE (standardized β: -0.19, p=0.12). Post-hoc analysis revealed a borderline significant correlation between precuneus [^{11}C]PIB and visual episodic memory factor scores in the high-PIB group (adjusted: standardized β: -0.55, p=0.08; unadjusted: standardized β: -0.64, p<0.05), whereas this association was absent in intermediate-PIB (standardized β: -0.17, p=0.69) and low-PIB (standardized β: 0.12, p= 0.43) groups. Across and within groups, there were no associations between precuneus [^{11}C]PIB retention and verbal episodic memory, working memory, semantic memory and executive functions (all p>0.05).

MetaROI FDG and Cognitive Factor Scores

Linear regression analyses, irrespective of whether or not adjusted for age, education and APOE, showed no association between the composite and regional [^{18}F]FDG MetaROI and any of the cognitive factor scores across groups (all p>0.05).

Table 2. Correlations between age, education, APOE genotype, [^{11}C]PIB, [^{18}F]FDG and cognition

	Age	Education	APOE	[^{11}C]PIB	[^{18}F]FDG	Verbal EM	Visual EM	WM	SM	EXE
Age	X									
Education	-0.05	X								
APOE ε4 status	-0.03	0.17	X							
Precuneus [^{11}C]PIB	0.23*	-0.18	0.28*	X						
Composite [^{18}F]FDG MetaROI	-0.25*	0.10	0.02	0.11	X					
Verbal episodic memory	-0.15	-0.03	0.01	0.10	0.12	X				
Visual episodic memory	-0.39**	0.01	-0.10	-0.30*	0.03	-0.18	X			
Working memory	0.15	0.02	0.03	-0.07	0.10	-0.15	-0.13	x		
Semantic memory	-0.15	0.09	0.10	0.01	0.13	0.05	0	-0.03	X	
Executive functions	-0.07	0.25*	0.13	0.04	0.01	0.12	-0.19	-0.16	-0.29*	X

Associations between age, education, APOE genotype, [^{11}C]PIB, [^{18}F]FDG and cognition were assessed using Pearson correlations.

** $p<0.01$; * $p<0.05$

Relationships between FDG and cognition according to PIB status

Multivariate ANOVA with adjustment for age, education and APOE status showed a significant interaction between [^{11}C]PIB status (low, intermediate or high) and composite [^{18}F]FDG MetaROI on verbal episodic memory ($p<0.05$), but not on other cognitive factor scores (all $p>0.05$). Post-hoc linear regression analyses with adjustment for age, education and APOE, revealed strong associations between the composite ROI (standardized β: 0.68, $p<0.01$, Figure 2B) and left (standardized β: 0.80, $p<0.01$, Figure 2C) and right (standardized β: 0.68, $p=0.01$, Figure 2D) angular gyrus [^{18}F]FDG uptake and verbal episodic memory in subjects with intermediate [^{11}C]PIB retention. Moderate, albeit non-significant, correlations with verbal episodic memory were found in the left (standardized β: 0.52, $p=0.11$) and right (standardized β: 0.59, $p=0.17$) inferior temporal gyri and in the PCC (standardized β: 0.28, $p=0.38$) of intermediate-PIB subjects (Table 3). In the high-PIB group, there was an association between left inferior medial temporal [^{18}F]FDG uptake and verbal episodic memory (standardized β: 0.57, $p<0.05$). No other significant correlations were found in any of the groups between composite or regional [^{18}F]FDG uptake and cognitive factor scores (see Supplementary material).

Table 3. Relationships between [^{18}F]FDG and verbal EM according to PIB-status

	Low-PIB	Intermediate-PIB	High-PIB
Verbal episodic memory versus:			
Composite [^{18}F]FDG MetaROI	-0.14	0.68**	0.33
Right angular gyrus	-0.10	0.80**	0.31
Left angular gyrus	-0.10	0.68*	0.44
PCC	-0.16	0.28	-0.10
Right inferior temporal gyrus	-0.11	0.59	0.57*
Left inferior temporal gyrus	-0.01	0.52	0.36

Estimates are presented as standardized β-values, to allow comparison of effect sizes. All analyses were adjusted for age, education and APOE genotype.

** $p<0.01$; * $p<0.05$

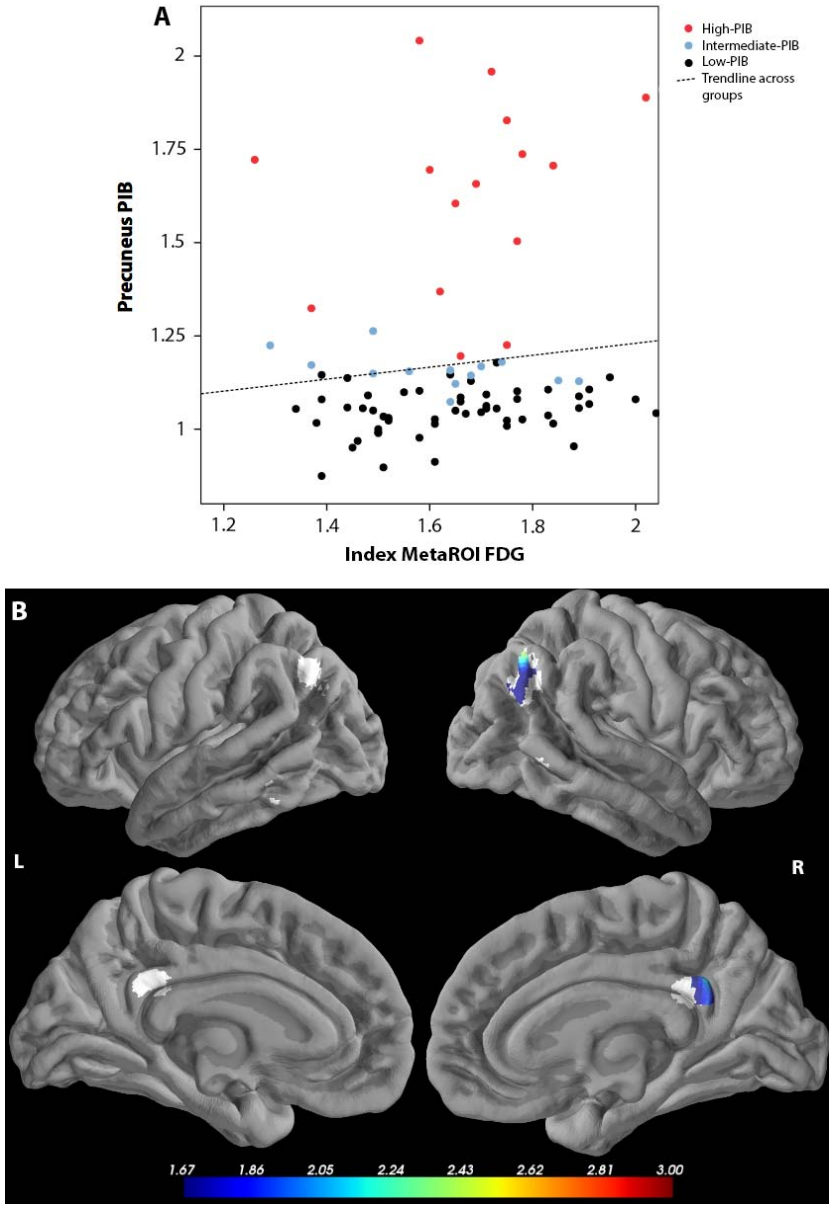

Figure 1. Linear regression analyses, with adjustment for age, education and APOE, showed an association at trend level between precuneus [^{11}C]PIB DVR and composite [^{18}F]FDG MetaROI **(A)** (standardized β: -0.21, p=0.10). Additionally, we performed a voxelwise regression analysis within MetaROI regions (in white), thresholded at an uncorrected p<0.05 (k > 10 voxels) **(B)**. Colormaps represent mean T-values. Effects in the right angular gyrus and posterior cingulate mainly drive the relationship between precuneus [^{11}C]PIB and composite [^{18}F]FDG MetaROI.

DISCUSSION

In the present study, cognitively normal subjects underwent [^{11}C]PIB and [^{18}F]FDG PET and extensive neuropsychological testing, allowing exploration of the inter-relationships between amyloid burden, glucose metabolism and cognition. We found that greater Aβ pathology was associated with heightened metabolic activity in AD specific regions (at trend level) and worse performance on visual episodic memory tasks. Across all subjects, cerebral glucose metabolism was not associated with cognitive performance. In individuals with intermediate or high amyloid burden, however, metabolic activity in several AD specific regions was positively correlated to verbal episodic memory scores. This potential mechanism of cognitive brain reserve may reflect neural compensation that suppresses neurotoxic effects of Aβ pathology. These findings suggest that asymptomatic elderly with cerebral amyloidosis are, at least temporarily, able to preserve cognitive function through increased brain activity.

Aβ burden and glucose metabolism

In the present study we used highly sensitive PET measures to detect biological processes related to AD. [^{11}C]PIB retention was used to quantify fibrillary amyloid plaque deposition in the precuneus, one of the regions earliest affected in AD [42]. In addition, we used a meta-analysis based approach (MetaROI) for [^{18}F]FDG to measure cerebral glucose metabolism in AD specific regions [44]. The association between heightened metabolic activity and increased amyloid deposition is consistent with other functional imaging studies showing elevated brain activation in aging, mild cognitive impairment and genetic risk populations [17-23]. There are at least two mechanisms that may account for this phenomenon. The first is that the brain starts to recruit neuronal resources more intensively as a response to neurotoxicity of Aβ. This neural compensation may be an appearance of cognitive brain reserve, a concept that is often used to explain why some individuals can tolerate substantial pathological burden longer before showing cognitive loss, whereas others have less resilient brain capacity and decline earlier [45].

A second interpretation of our data is that increased neural activity leads to Aβ accumulation in the brain [46]. Animal studies have shown that a state of wakefulness and long-term unilateral vibrissal stimulation in transgenic mice enhance Aβ release and the formation and growth of amyloid plaques [47,48]. In addition, Aβ plaques preferentially accumulate in metabolically highly active regions found in multimodal association cortices and the default mode network in the human brain [49]. The link between increased neural activity and amyloid pathology could not be attributed separately to low-, intermediate- or high-PIB groups. In a previous study [50], amyloid-positive cognitively normal elderly had minor metabolic reductions compared to their amyloid-negative counterparts. Discrepancies with the present study may be explained by the fact that we used [^{11}C]PIB as a continuous variable and that both studies selected different target regions to assess glucose metabolism. In addition, we included only subjects with cerebral amyloidosis who had glucose metabolism (and cognitive function) in the normal range. Potentially, the relationships between Aβ deposition and metabolic activity change along the spectrum of preclinical AD.

Aβ burden and cognition

Primarily driven by subjects with high [^{11}C]PIB retention, greater precuneus Aβ burden was associated with worse visual episodic memory performance. This result was no longer significant after adjustment for age, education and APOE genotype and there were no associations with other cognitive functions, including verbal episodic memory performance. It could be speculated that the discrepancy between modalities is a consequence of a higher degree of complexity of our episodic memory task or, alternatively, it may be harder to process visual information rather than verbal stimuli. This would be consistent with a recent study [55] showing that highly demanding cognitive tasks increase the sensitivity to detect subtle Aβ related impairment. Previous reports on the effect of amyloid burden on cognition have been equivocal; some have shown significantly lower memory scores in subjects with Aβ [24-26] whereas others did not [27,10]. Assuming that Aβ deposition eventually leads to clinical symptoms, mediating factors are needed to explain the weak cross-sectional association between amyloid

plaques and cognition. These mediators could boost the effects of Aβ pathology (e.g. neuroinflammation, tau pathology or vascular damage) [51] or, conversely, suppress them by means of cognitive brain reserve factors.

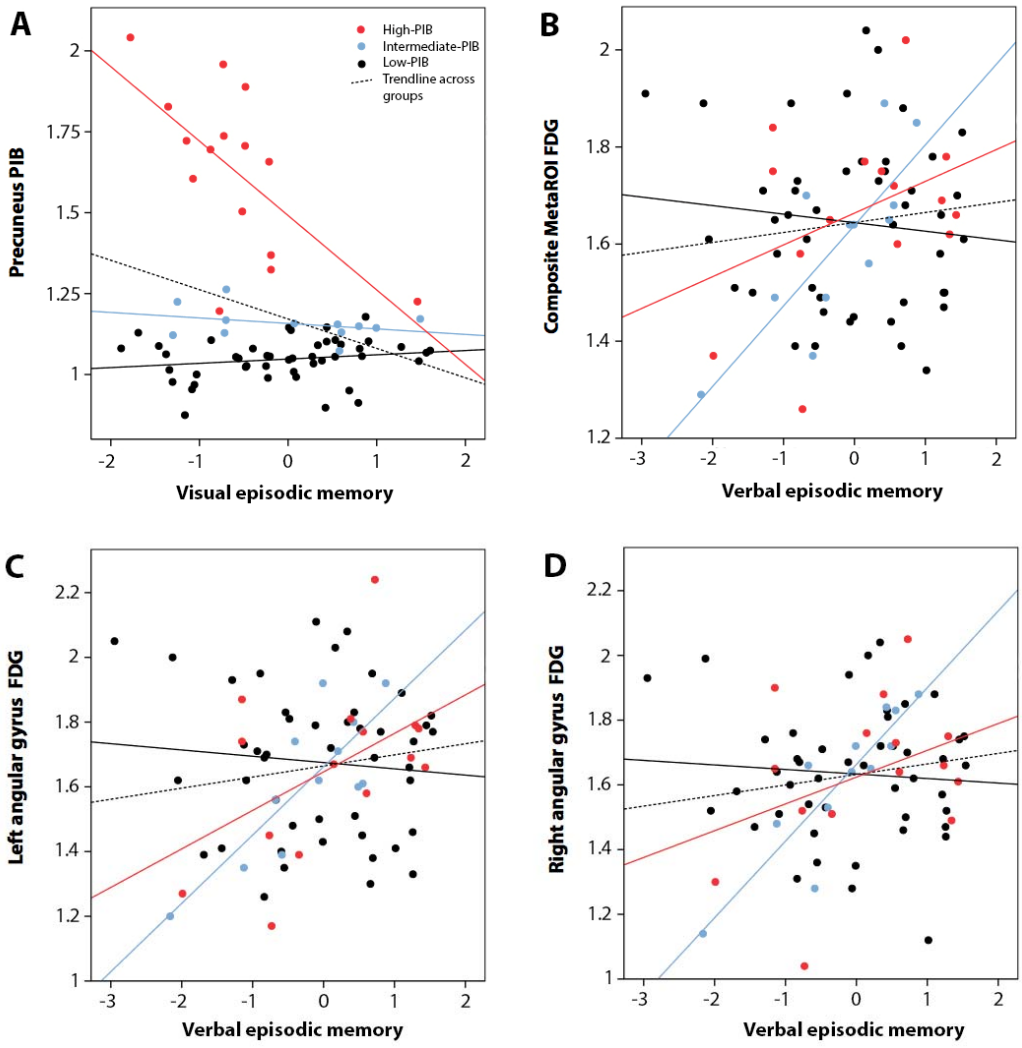

Figure 2. Linear regression analysis showed an association between increased [^{11}C]PIB retention in the precuneus and lower visual episodic memory factor scores **(A)** (standardized β: -0.30, p<0.05). Across groups, there was no effect of [^{18}F]FDG on cognition. In subjects with intermediate-PIB levels, verbal episodic memory performance was positively associated with **(B)** composite (standardized β: 0.68, p<0.01), **(C)** left (standardized β: 0.80, p<0.01) and **(D)** right (standardized β: 0.68, p=0.01) angular gyri [^{18}F]FDG SUVr.

Glucose metabolism and cognition

Across all subjects, metabolic activity was not associated with cognitive factor scores. The majority (53 of 81 subjects) of subjects in the present study showed no *in vivo* evidence of cerebral amyloidosis. These subjects with low [^{11}C]PIB retention, however, displayed comparable basal cerebral glucose metabolism as subjects with intermediate and high levels of Aβ (Figure 1A) and there was a wide dynamic range. Relatively low metabolic activity in these subjects is most likely independent of AD pathology and could be due to developmental factors or life-long experiences. Stronger correlates with cognition may be expected in prodromal AD or AD dementia patients who have crossed the threshold for abnormal [^{18}F]FDG uptake and display clinical symptoms (Chetelat et al. 2003; Ossenkoppele et al. 2012; Landau et al. 2012).

Glucose metabolism and cognition as a function of Aβ

Looking specifically at subjects harboring Aβ pathology in the brain, there was a positive correlation between metabolic activity and verbal episodic memory scores. This was most prominent in the intermediate-PIB group that comprised individuals with [^{11}C]PIB retention 2-4 standard deviations above the mean distribution volume ratio of young healthy controls. In a previous study it was shown that this elevation of [^{11}C]PIB occurred in a pathologically confirmed AD like pattern and is therefore of likely biological relevance [42]. In this group, composite (weighted average of the five MetaROIs) and bilateral angular gyri [^{18}F]FDG uptake related strongly to one of the earliest cognitive functions affected in AD, namely verbal episodic memory [52]. In other words, among elderly supposedly on the path to AD, those who display heightened cerebral glucose metabolism have better preserved cognitive function than those with lower metabolic activity. It is unclear if increased neuronal activity is an adaptive response of the brain to the presence of Aβ pathology or that individuals just start out differently and show distinct cognitive trajectories when Aβ comes into play.

In high-PIB subjects, [^{18}F]FDG uptake in the left inferior temporal lobe correlated with verbal episodic memory performance. In addition, moderate correlations were

appreciated for the metabolic composite, bilateral angular gyri and right inferior temporal cortex, but due to small sample size the statistical threshold was not reached. The pattern of better cognitive performance in individuals with higher metabolic activity was thus similar to that seen in the intermediate-PIB group, only to a smaller extent. Longitudinal imaging studies have shown amyloid plaque growth in normal elderly, particularly in those that already have substantial Aβ load [53,54,6]. Individuals with strongly elevated [^{11}C]PIB retention are potentially more advanced in the amyloid cascade model and thus closer towards entering the clinical stage of AD [9]. This could imply that neural compensation is temporarily beneficial but long-term exposure of Aβ will eventually tip over glucose metabolism and subsequent cognitive performance. This model fits well with previous studies that report only a modest effect of Aβ on cross-sectional cognitive performance [10, 24-27], whereas subjects harboring Aβ are consistently more prone to longitudinal cognitive deterioration [6, 28-30]. An alternative explanation is that these are "survivors" and are protected against cognitive deterioration not only via neuronal mechanisms but also by interactions of currently unknown genetic and environmental factors.

Limitations

The main limitation of the present study is the relatively small sample size of the intermediate- (n=13) and high-PIB (n=15) groups. The results, however, seem not to be driven by outliers and effects are often appreciated in multiple brain regions, indicating a certain robustness of the findings. Also, the cross-sectional design of this study does only allow speculation that individuals with Aβ pathology who are no longer capable of compensation through neural circuits are the most likely to decline cognitively. Longitudinal studies that include more subjects could help to test this hypothesis. Finally, the present study was not designed to assess the impact of cognitive reserve variables on preservation of cognitive function by means of increased metabolic function.

Conclusions

We found relationships between presence of Aβ pathology and higher metabolic activity (at trend level) and lower visual episodic memory scores. Glucose metabolism did not correlate with cognition across all subjects, but heightened metabolic activity was associated with better verbal episodic memory performance in subjects with moderately elevated amyloid levels. This preliminary study indicates that neural compensation, as a manifestation of cognitive brain reserve, is a mechanism of action that enables elderly with amyloid deposits to preserve cognitive function.

REFERENCES

1. Price JL, Morris JC. Tangles and plaques in nondemented aging and "preclinical" Alzheimer's disease. Ann Neurol 1999; 45: 358-68.
2. Wolf D, Gearing M, Snowdon D, et al. Progression of regional neuropathology in Alzheimer disease and normal elderly: findings from the Nun study. Alz Dis Assoc Disord 1999; 13: 226-31.
3. Bennett DA, Schneider JA, Arvanitakis Z, et al. Neuropathology of older persons without cognitive impairment from two community-based studies. Neurology 2006; 66: 1837-44.
4. Klunk WE, Engler H, Nordberg A, et al. Imaging brain amyloid in Alzheimer's disease with Pittsburgh Compound-B. Ann Neurol 2004; 55: 306-19.
5. Morris, JC, Roe, CM, Xiong, C, et al. APOE predicts amyloid-beta but not tau Alzheimer pathology in cognitively normal aging. Ann Neurol 2010; 67: 122-31.
6. Villemagne VL, Pike KE, Chételat G, et al. Longitudinal assessment of Aβ and cognition in aging and Alzheimer disease. Ann Neurol 2011; 69: 181-92.
7. Jack CR, Knopman DS, Weigand SD, et al. An operational approach to National Institute on Aging-Alzheimer's Association criteria for preclinical AD. Ann Neurol 2012; 71: 765-75.
8. Sperling RA, Aisen PS, Beckett LA, et al. Toward defining the preclinical stages of Alzheimer's disease: recommendations from the National Institute on Aging-Alzheimer's Association workgroups on diagnostic guidelines for Alzheimer's disease. Alzheimers Dement 2011; 7: 280-92.
9. Jack CR, Knopman DS, Jagust WJ, et al. Hypothetical model of dynamic biomarkers of the Alzheimer's pathological cascade. Lancet Neurol 2010; 9: 119-28.
10. Rowe CC, Ellis KA, Rimajova M, et al. Amyloid imaging results from the Australian Imaging, Biomarkers and Lifestyle (AIBL) study of aging. Neurobiol Aging 2010; 31: 1275-83.
11. Bateman RJ, Xiong C, Benzinger TL, et al. Clinical and Biomarker Changes in Dominantly Inherited Alzheimer's Disease. N Engl J Med. 2012; [Epub ahead of print].
12. Dickerson BC, Bakkour A, Salat DH, et al. The cortical signature of Alzheimer's disease: regionally specific cortical thinning relates to symptom severity in very mild to mild AD dementia and is detectable in asymptomatic amyloid-positive individuals. Cerebral cortex 2009; 19: 497-510.
13. Mormino EC, Kluth JT, Madison CM, et al. Episodic memory loss is related to hippocampal-mediated beta-amyloid deposition in elderly subjects. Brain 2009; 132: 1310-23.
14. Chételat G, Villemagne VL, Bourgeat P, Pike et al. Relationship between atrophy and beta-amyloid deposition in Alzheimer disease. Ann Neurol 2010; 67: 317-24.
15. Oh H, Mormino EC, Madison C, et al. β-Amyloid affects frontal and posterior brain networks in normal aging. NeuroImage 2011; 54: 1887-95.
16. Becker JA, Hedden T, Carmasin J, et al. Amyloid-β associated cortical thinning in clinically normal elderly. Ann Neurol 2011; 69: 1032-42.
17. Cabeza R, Anderson ND, Locantore JK, et al. Aging gracefully: compensatory brain activity in high-performing older adults. NeuroImage 2002; 17: 1394-402.
18. Rosen AC, Prull MW, O'Hara R, et al. Variable effects of aging on frontal lobe contributions to memory. Neuroreport 2002; 13: 2425-8.
19. Park DC, Reuter-Lorenz P. The adaptive brain: aging and neurocognitive scaffolding. Annu Rev Psychol 2009; 60: 173-96.
20. Mormino EC, Brandel MG, Madison CM, et al. Aβ Deposition in Aging Is Associated with Increases in Brain Activation during Successful Memory Encoding. Cerebral cortex 2012a; 22: 1813-23.
21. Bookheimer SY, Strojwas MH, Cohen MS, et al. Patterns of brain activation in people at risk for Alzheimer's disease. New Engl J Med 2000; 343: 450-6.

22. Filippini N, MacIntosh BJ, Hough MG, et al. Distinct patterns of brain activity in young carriers of the APOE-epsilon4 allele. Proc Natl Acad Sci USA 2009; 106: 7209-14.
23. Cohen AD, Price JC, Weissfeld LAet al. Basal cerebral metabolism may modulate the cognitive effects of Abeta in MCI: an example of brain reserve. J Neurosci 2009; 29: 14770-8.
24. Pike KE, Savage G, Villemagne VL, et al. Beta-amyloid imaging and memory in non-demented individuals: evidence for preclinical Alzheimer's disease Brain 2007; 130: 2837-44.
25. Rentz DM, Locascio JJ, Becker JA, et al. Cognition, reserve, and amyloid deposition in normal aging. Ann Neurol 2010; 67: 353-64.
26. Rodrigue KM, Kennedy KM, Devous MD, et al. β-Amyloid burden in healthy aging: regional distribution and cognitive consequences, Neurology 2012; 78: 387-95.
27. Aizenstein HJ, Nebes RD, Saxton JA, et al. Frequent amyloid deposition without significant cognitive impairment among the elderly. Arch Neurol 2008; 65: 1509-17.
28. Morris JC, Roe CM, Grant EA, et al. Pittsburgh compound B imaging and prediction of progression from cognitive normality to symptomatic AD. Arch Neurol 2009; 66: 1469-75.
29. Storandt M, Mintun MA, Head D, et al. Cognitive decline and brain volume loss as signatures of cerebral amyloid-beta deposition identified with Pittburgh compound B: cognitive decline associated with Abeta deposition. Arch Neurol 2009; 66: 1476-81.
30. Resnick SM, Sojkova J, Zhou Y, et al. Longitudinal cognitive decline is associated with fibrillar amyloid-beta measured by [11C]PIB. Neurology 2010; 74: 807-15.
31. Attwell D, Laughlin SB. An energy budget for signaling in the grey matter of the brain. J Cereb Blood Flow Metab 2001; 21: 1133-45.
32. Rocher AB, Chapon F, Blaizot X, et al. Resting-state brain glucose utilization as measured by PET is directly related to regional synaptophysin levels: a study in baboons. NeuroImage 2003; 20: 1894-8.
33. Oh H, Madison C, Haight TJ, et al. Effects of age and β-amyloid on cognitive changes in normal elderly people, Neurobiology of aging 2012; [Epub ahead of print].
34. Delis D, Kramer J, Kaplan E, et al. California Verbal Learning Test. Psychological Coorporation 2000; San Antonio.
35. Wechsler D. Wechsler Adult Intelligence Scale-III (WAIS-III) manual. The Psychological Coorporation 1997; New York.
36. Benton A, Hamsher K, Sivan A. Multilingual Aphasia Examination. AJA Associates 1983; Iowa City.
37. Reitan R. Validity of the Trail Making Test as an indicator of organic brain damage. Percept Mot Skills 1958; 8: 271-6.
38. Smith A. Symbol Digit Modalities Test. Western Psychological Services 1982; Los Angeles.
39. Golden C. Stroop Color and Word Test: A Manual for Clinical and Experimental Uses. Stoelting 1978; Chicago.
40. Logan J, Fowler JS, Volkow ND, et al. Distribution volume ratios without blood sampling from graphical analysis of PET data. J Cereb Blood Flow Metab 1996; 16: 834-40.
41. Price JC, Klunk WE, Lopresti BJ, et al. Kinetic modeling of amyloid binding in humans using PET imaging and Pittsburgh Compound-B. J Cereb Blood Flow Metab 2005; 25: 1528-47.
42. Mormino. EC, Brandel MG, Madison CM, et al. Not quite PIB-positive, not quite PIB-negative: slight PIB elevations in elderly normal control subjects are biologically relevant. NeuroImage 2012b; 59: 1152-60.
43. Minoshima S, Frey KA, Foster NL, et al. Preserved pontine glucose metabolism in Alzheimer disease: a reference region for functional brain image (PET) analysis. J Comp Assist Tomogr 1995; 19: 541-7.

44. Landau SM, Harvey D, Madison CM, et al. Associations between cognitive, functional, and FDG-PET measures of decline in AD and MCI. Neurobiol Aging 2011; 32: 1207-18.
45. Stern Y. Cognitive reserve and Alzheimer disease. Alz Dis Assoc Disord 2006; 20: 112-7.
46. Jagust WJ, Mormino EC. Lifespan brain activity, β-amyloid, and Alzheimer's disease. Trends Cog Sci 2011; 15: 520-6.
47. Kang JE, Lim MM, Bateman RJ, et al. Amyloid-beta dynamics are regulated by orexin and the sleep-wake cycle. Science 2009; 326: 1005-7.
48. Bero AW, Yan P, Roh JH, et al. Neuronal activity regulates the regional vulnerability to amyloid-β deposition. Nat Neurosci 2011; 14:750-6.
49. Buckner RL, Snyder AZ, Shannon BJ, et al. Molecular, structural, and functional characterization of Alzheimer's disease: evidence for a relationship between default activity, amyloid, and memory. J Neurosci 2005; 25: 7709-17.
50. Drzezga A, Becker JA, Van Dijk KR, et al. Neuronal dysfunction and disconnection of cortical hubs in non-demented subjects with elevated amyloid burden. Brain 2011; 134: 1635-46.
51. Desikan RS, McEvoy LK, Thompson WK, et al. Amyloid-β associated clinical decline occurs only in the presence of elevated P-tau. Arch Neurol 2012; 69: 709-13.
52. Salmon D. Disorders of memory in Alzheimer's disease. Handbook of neuropsychology vol. 2: Memory and its disorders 2000; Elsevier Amsterdam: 155-95.
53. Sojkova J, Zhou Y, An Y, et al. Longitudinal patterns of β-amyloid deposition in nondemented older adults. Arch Neurol 2011; 68: 644-9.
54. Vlassenko AG, Mintun MA, Xiong C, et al. Amyloid-beta plaque growth in cognitively normal adults: longitudinal [11C]Pittsburgh compound B data. Ann Neurol 2011; 70: 857-61.
55. Rentz DM, Amariglio RE, Becker JA, et al. Face-name associative memory performance is related to amyloid burden in normal elderly. Neuropsychologia 2011; 49: 2776-83.

Chapter 4

Molecular imaging in AD: mechanisms of clinical heterogeneity

Chapter 4.1

Amyloid Burden and Metabolic Function in Early Onset Alzheimer's Disease: Parietal Lobe Involvement

Brain 2012 135(Pt 7):2115-2125

Rik Ossenkoppele, Marissa D. Zwan, Nelleke Tolboom, Danielle M.E. van Assema, Sofie F. Adriaanse, Reina W. Kloet, Ronald Boellaard, Albert D. Windhorst, Frederik Barkhof, Adriaan A. Lammertsma, Philip Scheltens, Wiesje M. van der Flier & Bart N.M. van Berckel.

ABSTRACT:

Alzheimer's disease with early onset often presents with a distinct cognitive profile, potentially reflecting a different distribution of underlying neuropathology. The purpose of this study was to examine the relationships between age and both *in vivo* fibrillary amyloid deposition and glucose metabolism in patients with Alzheimer's disease. Dynamic [^{11}C]Pittsburgh compound-B (90 minutes) and static [^{18}F]fluorodeoxyglucose (15 minutes) scans were obtained in 100 patients with Alzheimer's disease and 20 healthy controls. Parametric non-displaceable binding potential images of [^{11}C]Pittsburgh compound-B and standardized uptake value ratio images of [^{18}F]fluorodeoxyglucose were generated using cerebellar grey matter as reference tissue. Nine [^{11}C]Pittsburgh compound-B negative patients were excluded. The remaining patients were categorized into younger (n=45, age: 56±4) and older (n=46, age: 69±5) groups, based on the median age (62) at time-of-diagnosis. Younger patients showed more severe impairment on visuo-spatial function, attention and executive function composite scores ($p<0.05$), while we found a trend towards poorer memory performance for older patients ($p=0.11$). Differences between groups were assessed using a general linear model with repeated measures (gender adjusted) with age as between subjects factor, region (frontal, temporal, parietal and occipital and posterior cingulate cortices) as within subjects factor and [^{11}C]Pittsburgh compound-B binding/[^{18}F]fluorodeoxyglucose uptake as dependent variables. There was no main effect of age for [^{11}C]Pittsburgh compound-B or [^{18}F]fluorodeoxyglucose, suggesting that overall, the extent of amyloid deposition or glucose hypometabolism did not differ between groups. Regional distributions of [^{11}C]Pittsburgh compound-B binding and [^{18}F]fluorodeoxyglucose uptake (both p for interaction <0.05) differed between groups, however, largely due to increased [^{11}C]Pittsburgh compound-B binding and decreased [^{18}F]fluorodeoxyglucose uptake in the parietal cortex of younger patients (both $p<0.05$). Linear regression analyses showed negative associations between visuo-spatial functioning and parietal [^{11}C]Pittsburgh compound-B binding for younger patients (standardized β: -0.37) and between visuo-spatial functioning and occipital binding for older patients (standardized β: -0.39). For [^{18}F]fluorodeoxyglucose, associations were found between parietal uptake with

visuo-spatial (standardized β: 0.55), attention (standardized β: 0.39) and executive functioning (standardized β: 0.37) in younger patients, and between posterior cingulate uptake and memory in older patients (standardized β: 0.41, all $p<0.05$). These *in vivo* findings suggest that clinical differences between younger and older Alzheimer's disease patients are not restricted to topographical differentiation in downstream processes, but may originate from distinctive distributions of early upstream events. As such, increased amyloid burden, together with metabolic dysfunction, in the parietal lobe of younger Alzheimer's disease patients may contribute to the distinct cognitive profile in these patients.

INTRODUCTION

Alzheimer's disease is the most common form of dementia and its prevalence increases progressively with age [1,2]. The first symptom in late-onset Alzheimer's disease is usually episodic memory dysfunction, followed by deficits in other cognitive domains as the disease progresses. In Alzheimer's disease with early onset, however, a more heterogeneous cognitive presentation has been described. In about 30% of these patients, focal cortical symptoms such as aphasia, apraxia and agnosia, precede memory disturbances [3-5].

The disparity between early-onset and late-onset Alzheimer's disease potentially reflects differences in distribution of underlying neuropathology. Post-mortem studies have described higher burdens of amyloid plaques and neurofibrillary tangles in early-onset Alzheimer's disease patients [6-10]. Major disadvantages of post-mortem studies, however, are that usually only a few slices of a small number of brain areas are examined, and that in general they are performed years after disease onset. Furthermore, the increased pathological burden in early-onset Alzheimer's disease may be explained by a more advanced stage of the disease at time of death as older Alzheimer's disease patients more frequently die due to other age related conditions. This may introduce a systematic bias in post-mortem studies [8,11].

Brain amyloid plaque load can be quantified *in vivo* using positron emission tomography (PET) and carbon-11-labelled Pittsburgh compound-B ([^{11}C]PIB) [12]. In the first study comparing [^{11}C]PIB retention in early-onset and late-onset Alzheimer's disease, these earlier pathological observations could not be replicated in the living human brain as no global and regional differences in amyloid burden were found [13]. In line with this finding, amyloid-beta 1-42 and hyperphosphorylated tau levels in cerebrospinal fluid (CSF) did not differ according to age-at-onset [14].

The absence of conclusive evidence for an effect of age on deposition of amyloid plaques is remarkable given the distinct phenotype often observed in early-onset

Alzheimer's disease patients. Differences in downstream processes according to age-at-onset, however, have been reported more consistently. Early-onset Alzheimer's disease patients show more severe cortical atrophy, cerebral hypoperfusion, and glucose hypometabolism and more profound abnormalities on electroencephalography than their late-onset counterparts [13,15-22]. Furthermore, in early onset Alzheimer's disease, the posterior parts of the brain are affected most prominently, whilst in late-onset Alzheimer's disease this is the case for medial temporal regions [13,15,18,23].

The purpose of the present study was to examine the extent and distribution of specific [^{11}C]PIB binding and [^{18}F]fluorodeoxyglucose (FDG) uptake in order to test the hypothesis that early-onset Alzheimer's disease is associated with more posterior-oriented amyloid load and glucose hypometabolism as compared with late-onset Alzheimer's disease.

METHODS

Subjects

100 Alzheimer's disease patients and 20 healthy controls were included. Patients with Alzheimer's disease were categorized into younger and older groups, based on median age (62 years) at time of diagnosis. All subjects received a standard dementia screening that included medical history, informant-based history, physical and neurological examinations, screening laboratory tests, brain magnetic resonance imaging (MRI) and neuropsychological testing [24]. Clinical diagnosis was established by consensus in a multidisciplinary team, without awareness of the PET results. All Alzheimer's disease patients met criteria proposed by the National Institute on Aging and the Alzheimer's Association (NIA-AA) workgroup for probable Alzheimer's disease with at least intermediate likelihood due to abnormal [^{11}C]PIB PET [25]. Controls were recruited through advertisements in newspapers and underwent the same diagnostic procedures.

Exclusion criteria were a history of major psychiatric or neurological (other than Alzheimer's disease) illness, drug and/or alcohol abuse, major vascular events such as stroke or haemorrhage, and known genetic mutations (presenilin-1, presenilin-2, and amyloid-β precursor protein). Furthermore, [^{11}C]PIB negative Alzheimer's disease patients were excluded. Parametric images of [^{11}C]PIB were assessed visually and scored binary (e.g. positive or negative) by an experienced nuclear medicine physician (BvB). [^{11}C]PIB scans were interpreted conservatively and were only considered positive if there was binding in more than one brain region (e.g. frontal, parietal, temporal, occipital) to such an extent that differentiation between grey and white matter was either blurred or absent, indicating substantial cortical uptake. Consequently, 9 patients were excluded, leaving 45 younger and 46 older Alzheimer's disease patients for analysis. Additional exclusion criteria for controls were subjective memory complaints or clinically relevant abnormalities on MRI. Written informed consent was obtained from all subjects after a complete written and verbal description of the study. The study was approved by the Medical Ethics Review Committee of the VU University Medical Center.

Cognition

In 43 younger and 44 older Alzheimer's disease patients, cognitive functioning was assessed using a neuropsychological test battery covering five major cognitive domains: memory (immediate recall, recognition and delayed recall of a Dutch version of the Rey Auditory Verbal Learning Test and the Visual Association Test (VAT)), visuo-spatial functioning (number location, dot counting and fragmented letters derived from the Visual Object Space and Perception (VOSP) battery, and the Rey Complex Figure copy test), executive functions (Digit Span backwards, Trail Making Test (TMT) part B and Stroop Color-Word card subtask), attention (TMT part A, Stroop test Word and Color subtasks, and digit span forward), and language (VAT picture naming and category fluency (animals: 1 minute) [26-33]. For each cognitive task, raw test scores were converted to z-scores. Next, composite z-scores were calculated for each cognitive domain by averaging z-scores for all cognitive tasks within a cognitive domain. Composite z-scores were calculated when at least one neuropsychological task was available in each cognitive domain

(n=43 younger, n=44 older Alzheimer's disease patients). Z-transformation was performed within the Alzheimer's disease group without taking into account a normative group. Z=0 therefore reflects the average test performance of our Alzheimer's disease patients in a given domain. Level of education was rated according to Verhage [34].

PET

PET scans were obtained on an ECAT EXACT HR+ scanner (Siemens/CTI, Knoxville, TN, USA) equipped with a neuroinsert to reduce the contribution of scattered photons. This scanner enables the acquisition of 63 transaxial planes over a 15.5 cm axial field of view, thus allowing the whole brain to be imaged in one bed position. The properties of this scanner have been reported elsewhere [35]. All subjects received a venous cannula for tracer injection. First, a 10 minute transmission scan was obtained in 2-dimensional acquisition mode using three retractable rotating line sources in order to correct the subsequent emission scan for photon attenuation. Next, a dynamic emission scan in 3-dimensional acquisition mode was started simultaneously with the intravenous injection of 365±32 MBq [^{11}C]PIB in younger and 382±44 [^{11}C]PIB in older Alzheimer's disease patients (p=0.67), using an infusion pump (Med-Rad; Beek, the Netherlands) at a rate of 0.8mL/s, followed by a flush of 42 mL of saline at 2.0 mL/s. [^{11}C]PIB was synthesized according to a modified procedure [36], with a specific activity of 91±37 GBq/μmol in younger and 104±57 GBq/μmol in older patients (p=0.37). The [^{11}C]PIB scan consisted of 23 frames increasing progressively in duration (1 x 15, 3 x 5, 3 x 10, 2 x 30, 3 x 60, 2 x 150, 2 x 300, 7 x 600s) for a total scan duration of 90 minutes. After an interval of at least two hours to allow for decay of [^{11}C]PIB, an intravenous bolus injection of approximately 185 MBq of [^{18}F]FDG was injected. All subjects rested for 15 minutes before injection and thirty-five minutes after injection with the eyes closed and ears unplugged in a dimly lit room with minimal background noise. Next, patients underwent a 10 minute transmission scan followed by a 15 minute emission scan (3 x 5 minute frames). Patient motion was restricted by a head holder and regularly checked during the PET scans using laser beams. Due to tracer synthesis failure, 15 patients did not undergo [^{11}C]PIB and [^{18}F]FDG PET scans on the same day but with

an interval of at most 4 weeks. [^{11}C]PIB and [^{18}F]FDG PET scans were performed 4±3 months after the clinical diagnosis was made.

MRI

All subjects underwent structural MRI using a 1.5T Sonata (Siemens, Erlangen, Germany) scanner (16 younger and 12 older Alzheimer's disease patients and all controls) or a 3T Signa HDxt (General Electric, Milwaukee, USA) scanner (29 younger and 34 older Alzheimer's disease patients). The scan protocol included a coronal T1-weighted 3-dimensional magnetization-prepared-acquisition gradient echo (MPRAGE) (1.5T scanner: slice thickness 1.5 mm, 160 slices, matrix size 256 x 256, voxel size 1 x 1 x 1.5 mm, echo time 3.97 ms, repetition time 2,700 ms, flip angle, 8°; 3T scanner: slice thickness 1 mm, 180 slices, matrix size 256 x 256, voxel size 1 x 1 x 1.5 mm, echo time 3 ms, repetition time 708 ms, flip angle 12°). The MRI scan was used for co-registration, segmentation and region-of-interest (ROI) definition. Furthermore, medial temporal lobe atrophy (MTA) and white matter hyperintensities were assessed visually using standardized rating scales [23,37].

Image and Data Analysis

All PET sinograms were corrected for dead time, tissue attenuation using the transmission scan, decay, scatter, and randoms and were reconstructed using a standard filtered back projection algorithm and a Hanning filter with a cut-off at 0.5 times the Nyquist frequency. A zoom factor of 2 and a matrix size of 256 x 256 x 63 were used, resulting in voxel size of 1.2 x 1.2 x 2.4 mm and spatial resolution of approximately 7-mm full width at half-maximum at the center of the field of view.

MR images were aligned to corresponding PET images using a mutual-information algorithm. Data were further analyzed using PVE-lab, a software program that uses a probability map based on 35 delineated ROIs that have been validated previously [38]. ROIs were projected onto [^{11}C]PIB parametric non-displaceable binding potential (BP_{ND}) images. These images were generated by applying a 2-step basis-function implementation of the simplified reference tissue model (RPM2) [39], to the full dynamic 90 minute PET data. RPM2, a fully quantitative method for

assessing the data, was identified as the parametric model of choice [40]. The outcome measure BP_{ND} is a quantitative measure of specific binding. It reflects the concentration of specifically bound tracer relative to the concentration of free and non-specifically bound tracer in tissue under equilibrium. For [^{18}F]FDG, parametric images of standardized uptake value ratio (SUVr) were extracted from the interval between 45 and 60 minutes after injection. Cerebellar gray matter was chosen as reference tissue for both PET tracers because of its (histopathological) lack of Congo red and thioflavin-S-positive plaques [41], and its relative insensitivity to metabolic changes during disease progression [42].

For regional analysis, BP_{ND} ([^{11}C]PIB) and SUVr ([^{18}F]FDG) of frontal (volume weighted average of orbital frontal, medial inferior frontal, and superior frontal), parietal (including the precuneus), occipital and temporal (volume weighted average of superior temporal and medial inferior temporal) cortices and posterior cingulate were calculated. In addition, global cortical BP_{ND} and SUVr were calculated, based on the aforementioned regions.

APOE

APOE genotyping was performed after DNA isolation from 10 ml ethylenediaminetetraacetic acid (EDTA) blood, using the LightCycler APOE mutation detection method (Roche Diagnostics GmbH, Mannheim, Germany).

Statistics

Differences between groups for baseline characteristics were assessed using ANOVA, Kruskal Wallis tests and χ^2 tests, where appropriate. ANOVAs, adjusted for gender and education in model 1, and additionally adjusted for MMSE and APOE in model 2, were used to compare cognitive test performance between Alzheimer's disease groups only, and to compare global [^{11}C]PIB BP_{ND} and [^{18}F]FDG SUVr between patients and controls. Regional differences in [^{11}C]PIB BP_{ND} and [^{18}F]FDG SUVr between younger and older Alzheimer's disease patients were assessed using a general linear model (GLM) with repeated measures (model 1: adjusted for gender, model 2: additionally adjusted for education, MMSE, and APOE) entering

age (dichotomous) as between subjects factor, region (frontal, temporal, parietal and occipital and posterior cingulate cortices) as within subjects factor and regional BP_{ND}/SUVr as dependent variables. The analyses were repeated entering age-at-diagnosis as continuous variable. ANOVAs (model 1: adjusted for gender, model 2: additionally adjusted for education, MMSE, and APOE) were used to further assess differences between younger and older Alzheimer's disease patients in regional BP_{ND}/SUVr. Linear regression analyses were used to assess the spatial relationships between [^{11}C]PIB and [^{18}F]FDG, and to assess the relationships between regional BP_{ND}/SUVr and composite cognitive domain scores for younger and older Alzheimer's disease patients separately. Statistical significance was set at $p<0.05$.

RESULTS

Subject characteristics

Characteristics according to diagnostic group are presented in Table 1. At time of diagnosis, the younger Alzheimer's disease patients were on average 56±4 (median: 56, range: 40-62) and the older Alzheimer's disease patients 69±5 (median: 67, range: 62-78) years. Younger and older patients did not differ in gender, level of education, disease duration or MMSE scores. Alzheimer's disease patients had a slightly lower level of education than controls ($p<0.05$).

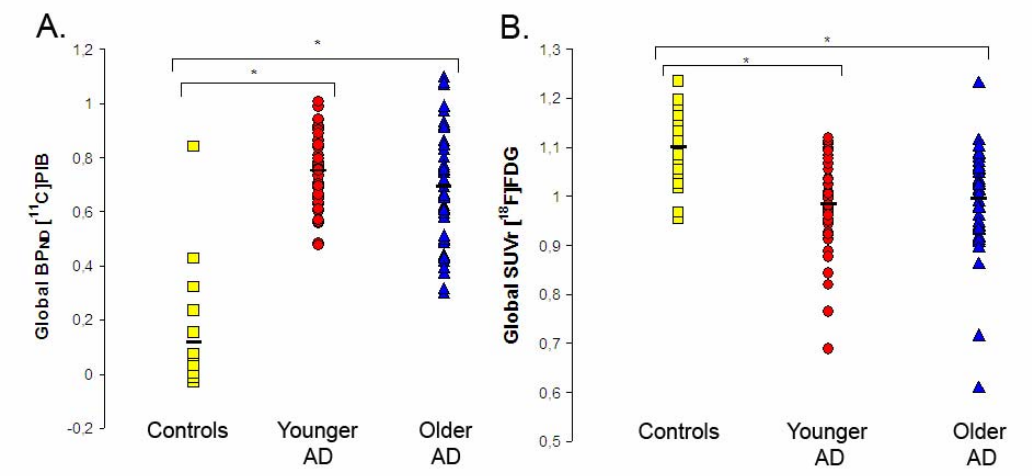

Figure 1. Global (A) [^{11}C]PIB BP_{ND} and (B) [^{18}F]FDG SUVr in controls and in younger and older Alzheimer's disease patients. Horizontal lines between symbols represent mean values. * post hoc Bonferonni tests: $p<0.001$).

Adjusted for gender and education, younger patients showed more severe impairment on visuo-spatial function, executive function and attention composite scores than older patients ($p<0.05$, Table 2). In contrast, there was a trend towards worse memory performance for the older Alzheimer's disease group compared with younger patients ($p=0.11$). No differences in language skills were observed ($p=0.51$). After additional adjustment for MMSE and APOE, the difference in memory performance between groups became significant ($p<0.05$).

Global [^{11}C]PIB BP BP_{ND} and [^{18}F]FDG SUVr

Adjusted for gender, global cortical [^{11}C]PIB BP_{ND} did not differ between younger (0.75±0.13) and older Alzheimer's disease (0.69±0.21, $p=0.29$), both being higher than that of controls (0.12±0.21, both $p<0.001$, Figure 1A). Global cortical [^{18}F]FDG uptake was essentially the same in younger (0.98±0.09) and older (0.99±0.10) Alzheimer's disease patients ($p=0.30$), which was lower than that in controls (1.10±0.07, both $p<0.001$, Figure 1B). Additional adjustment for education, MMSE, and APOE did not change the results essentially.

Table 1. Subject characteristics according to diagnostic group

	Younger AD (n=45)	**Older AD (n=46)**	**Controls (n=20)**
Age at diagnosis	56±4[a]	69±5	67±7
Disease duration	3±2	3±2	n/a
Gender (m,f)	29,16	26,20	14,6
Education	5(3-7)[b]	5(3-7)[b]	6(2-7)
MMSE	23±5[b]	24±3[b]	29±1
% APOE ε4 carrier	67	80	18
MTA score	0.9±0.8	1.3±1.0[#]	n/a
Fazekas score	0.8±0.6	0.9±0.6	n/a

Data are presented as mean ± standard deviation unless indicated otherwise.
[a] Younger Alzheimer's disease < older Alzheimer's disease and controls: $p<0.05$
[b] Younger and older Alzheimer's disease < controls: $p<0.05$
[#] Older Alzheimer's disease > Younger Alzheimer's disease: $p=0.06$

Table 2. Composite cognitive scores according to age

	Younger Alzheimer's disease	Older Alzheimer's disease
Memory	0.10±0.13	-0.19±0.13+
Visuo-spatial functions	-0.46±0.19*	0.19±0.11
Executive functions	-0.30±0.15*	0.16±0.11
Language	-0.10±0.18	-0.09±0.14
Attention	-0.27±0.14*	0.20±0.08

Data are presented as Mean±SE. Composite scores were calculated by averaging z-scores for all tests within a cognitive domain. Neuropsychological data were available for 43 younger and 44 older Alzheimer's disease patients.
* $p<0.05$
+ $p=0.11$ after adjustment for gender and education, $p<0.05$ after additional adjustment for MMSE and APOE

Regional [^{11}C]PIB BP_{ND} and [^{18}F]FDG SUVr

GLM with repeated measures (adjusted for gender) was used to assess the regional distributions of [^{11}C]PIB and [^{18}F]FDG in relation to age in Alzheimer's disease patients only. For [^{11}C]PIB BP_{ND}, the main effect for age, treated as dichotomous variable, was not significant ($p=0.22$), but there was a main effect for region ($p<0.001$). Moreover, there was an interaction between age and region ($p<0.01$), which could be attributed to increased [^{11}C]PIB binding in the parietal cortex of younger Alzheimer's disease patients (Figure 2A). Additional adjustment for education, MMSE, and APOE did not change the results (p for interaction <0.05). Results were comparable when the analysis was repeated using age as continuous variable (interaction between age and region $p<0.01$). ANOVAs with adjustment for gender, education, MMSE and APOE, showed higher parietal [^{11}C]PIB BP_{ND} in younger patients compared with older patients ($p<0.05$). There were no significant differences between groups in other regions.

For [^{18}F]FDG, the main effect for age was not significant ($p=0.37$), but there was a main effect for region ($p<0.001$). Furthermore, there was an interaction between age and region ($p<0.05$), mainly driven by reduced parietal [^{18}F]FDG uptake in

younger Alzheimer's disease patients (Figure 2B). The interaction between age and region lost significance after additional adjustment for education, MMSE, and APOE (p for interaction 0.15). When the analysis was repeated using age as continuous variable results did not change essentially. ANOVAs, adjusted for gender, revealed lower [^{18}F]FDG SUVr in the parietal cortex of younger patients compared with older patients ($p<0.05$). This finding was no longer significant after additional adjustment for education, MMSE, and APOE. There were no significant differences between groups in other regions. Linear regression analyses (adjusted for gender, education, MMSE, and APOE) for the whole group and for younger and older Alzheimer's disease patients separately showed no correlation between [^{11}C]PIB BP_{ND} and [^{18}F]FDG SUVr in any of the cortical ROIs.

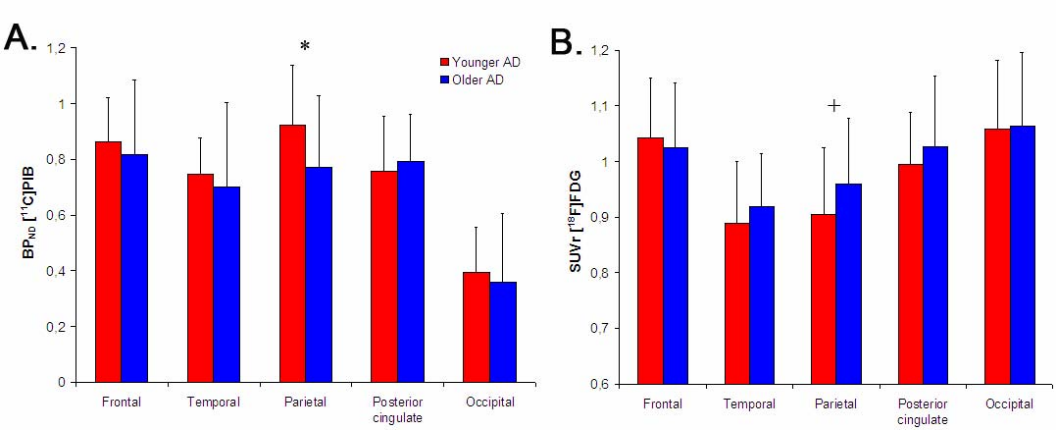

Figure 2. Regional (A) [^{11}C]PIB BP_{ND} and (B) [^{18}F]FDG SUVr in younger and older Alzheimer's disease patients. Differences between groups were assessed using a general linear model with repeated measures, adjusted for gender, education, MMSE, and APOE. For both tracers there were interactions between age and region ([^{11}C]PIB: $p<0.01$, [^{18}F]FDG: $p<0.05$). ANOVAs for individual regions showed that this was largely attributable to increased [^{11}C]PIB binding (* $p<0.05$) and decreased [^{18}F]FDG uptake (+ $p<0.05$ after adjustment for gender, $p>0.05$ after additional adjustment for education, MMSE, and APOE) in the parietal lobe of younger Alzheimer's disease patients.

Cognition and regional [^{11}C]PIB BP_{ND} and [^{18}F]FDG SUVr

Linear regression analyses with adjustment for gender and education showed a negative association between visuo-spatial functioning composite scores and parietal [^{11}C]PIB BP_{ND} for young Alzheimer's disease patients ($p<0.05$) (Table 3, Figure 3A), and between visuo-spatial functioning composite scores and occipital

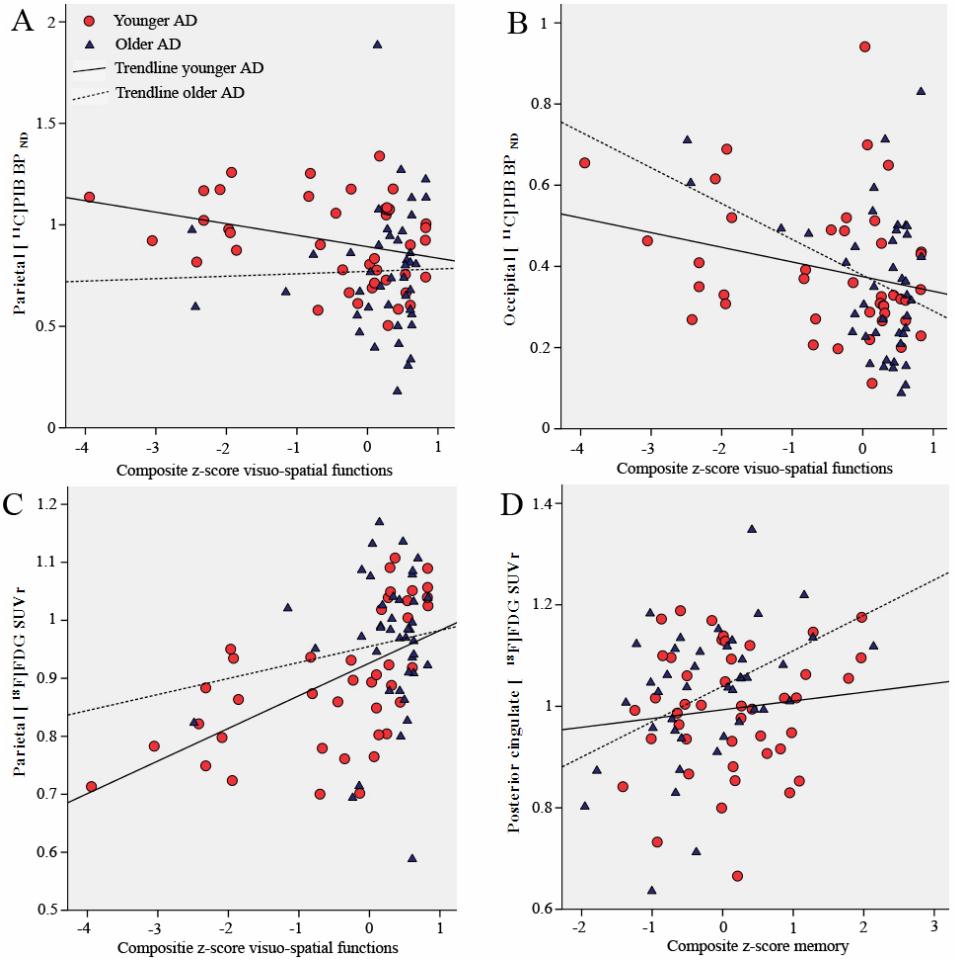

Figure 3. Linear regression analyses showed correlations between parietal amyloid deposition (A) and glucose metabolism (C) with visuo-spatial function composite scores in younger Alzheimer's disease patients (standardized β [^{11}C]PIB: -0.37; [^{18}F]FDG: 0.55, both $p<0.05$). In older Alzheimer's disease patients, there was a relationship between occipital [^{11}C]PIB binding and visuo-spatial functioning (B) (standardized β: -0.39, $p<0.05$). Furthermore, metabolic activity in the posterior cingulate was correlated with memory performance in older Alzheimer's disease patients (D) (standardized β: 0.41, $p<0.05$).

[^{11}C]PIB BP_{ND} for older Alzheimer's disease patients ($p<0.05$) (Figure 3B). For [^{18}F]FDG, linear regression showed associations between parietal SUVr with visuo-spatial (Figure 3C), attention, and executive functioning composite scores in younger Alzheimer's disease patients (all $p<0.05$) (Table 4). In older Alzheimer's disease patients, increased posterior cingulate SUVr was associated with worse memory (Figure 3D) and language performance ($p<0.05$). After additional adjustment for MMSE and APOE only the correlation between posterior cingulate SUVr and language lost significance. There were no other associations between regional [^{11}C]PIB BP_{ND}/[^{18}F]FDG SUVr and composite cognitive domain scores.

DISCUSSION

The main findings of the present study are an increased amyloid burden and modestly increased metabolic dysfunction in the parietal cortex of younger Alzheimer's disease patients. Parietal amyloid load was related to visuo-spatial functioning in younger patients, whilst metabolic impairment in the parietal cortex of these patients was related to visuo-spatial skills, executive functions, and attention. In older patients, memory performance was associated with metabolic activity in the posterior cingulate. This suggests that clinical differences between younger and older Alzheimer's disease patients are related not only to topographical differentiation in downstream processes, but may originate from distinctive distributions of early upstream events.

The spatial relationship between amyloid deposition and its downstream effects in sporadic Alzheimer's disease is not completely understood. Several studies have shown anatomical overlap between amyloid deposition and glucose metabolism in parieto-temporal, posterior cingulate and precuneus regions, indicating metabolic vulnerability in amyloid plaque enriched brain regions [43,44]. In contrast, amyloid deposition in the frontal cortex often coincides with relatively spared metabolism and, vice versa, low levels of fibrillary amyloid plaques in medial temporal regions are often accompanied by severe neurodegeneration. Previously, it has been found that early-onset Alzheimer's disease patients show differently distributed glucose

Table 3. Associations of regional [^{11}C]PIB binding with cognition in younger and older Alzheimer's disease patients

[^{11}C]PIB binding		Frontal		Temporal		Parietal		Post. cingulate		Occipital	
Cognitive domain	**Model**	**younger**	**older**	**younger**	**older**	**younger**	**older**	**younger**	**older**	**younger**	**older**
Memory	**1**	-0.17	0.2	-0.17	-0.03	-0.04	-0.02	-0.29	-0.04	-0.08	0.02
	2	-0.24	0.16	-0.16	0	-0.08	0.07	-0.30	0	-0.13	-0.09
Visuo-spatial	**1**	-0.08	-0.02	-0.19	-0.04	-0.30*	0.04	0.03	-0.06	-0.25	-0.39*
	2	-0.16	0.04	-0.26	0.11	-0.37*	0.13	-0.03	0	-0.18	-0.39*
Executive functions	**1**	0.10	0.07	0.14	0.07	-0.05	-0.03	0.07	0.07	-0.09	-0.14
	2	0.02	0.04	0	0.12	0.03	0	0.06	0.09	-0.09	-0.18
Language	**1**	0.02	0.07	0.08	0.09	-0.07	0.03	-0.01	0.09	0.11	-0.07
	2	-0.04	0.04	-0.03	0.09	-0.13	0.04	-0.07	0.16	0.15	-0.08
Attention	**1**	0.07	-0.07	0.08	-0.03	-0.04	-0.04	0.06	0.05	-0.07	-0.15
	2	-0.05	0.06	-0.03	0.21	-0.15	0.08	0.07	0.07	0.08	0.05

Associations between regional [^{11}C]PIB binding with composite scores of five major cognitive domains were assessed using linear regression analyses. Estimates are presented as standardized β values, to allow for comparison of effect sizes. Model 1: gender and education as covariates. Model 2: gender, education, MMSE, and APOE as covariates.
* $p<0.05$ for both model 1 and model 2

Table 4. Associations of regional [18F]FDG uptake with cognition in younger and older Alzheimer's disease patients

[18F]FDG uptake		Frontal		Temporal		Parietal		Post. cingulate		Occipital	
Cognitive domain	**Model**	**younger**	**older**	**younger**	**older**	**younger**	**older**	**younger**	**older**	**younger**	**older**
Memory	**1**	0.02	0.11	0.10	0.18	-0.07	0.02	0.03	0.42*	-0.15	-0.11
	2	0	0.20	0	0.12	-0.16	0.09	0.02	0.41*	-0.17	0.01
Visuo-spatial	**1**	-0.16	0	0.13	0.15	0.56*	0.20	0.11	0.22	0.18	0.09
	2	-0.19	0.02	0	0.13	0.55*	0.22	0.10	0.21	0.13	0.15
Executive functions	**1**	0.06	-0.15	0.26	0.03	0.56*	0.09	0.02	-0.10	0.05	-0.01
	2	0.01	-0.18	0	-0.01	0.37*	0.09	0.19	-0.14	0.02	0.01
Language	**1**	0.13	0	0.25	0.22	0.02	0.19	0.01	0.31*	-0.04	0.10
	2	0.11	0.02	0.11	0.18	-0.13	0.19	-0.01	0.29	-0.07	0.15
Attention	**1**	-0.09	-0.12	0.19	0	0.52*	-0.17	-0.01	-0.23	0.09	-0.28
	2	-0.13	-0.09	-0.02	-0.04	0.39*	-0.15	0.08	-0.24	0.06	-0.23

Associations between regional [18F]FDG uptake with composite scores of five major cognitive domains were assessed using linear regression analyses. Estimates are presented as standardized β values, to allow for comparison of effect sizes. Model 1: gender and education as covariates. Model 2: gender, education, MMSE, and APOE as covariates.
* $p<0.05$ for both model 1 and model

hypometabolism in the absence of a regionally specific pattern of amyloid deposition [13]. This raised the question whether other pathological processes such as neurofibrillary tangle formation or neuroinflammation may account for this region-specific metabolic impairment. Based on the present study, however, it may be worthwhile to reconsider the possibility of an amyloidogenic predisposition for metabolic vulnerability, especially in the parietal cortex as this brain structure was most severely affected by both amyloid deposition and glucose hypometabolism in younger Alzheimer's disease patients. These findings are in line with current theories on the pathogenesis of Alzheimer's disease proposing that amyloid-beta initiates a cascade of neuropathological events that eventually lead to neuronal damage and cell death [45]. As such, disproportionate parietal amyloid-beta accumulation may precede parietal metabolic brain dysfunction in early-onset Alzheimer's disease patients.

The finding of a different amyloid distribution in younger Alzheimer's disease patients is in contrast with two previous studies. In a recent study, increased global [^{11}C]PIB retention without specific differences in distribution was shown in early-onset Alzheimer's disease [46]. Observed effects in that study, however, were mainly due to inclusion of a number of PIB-negative patients in the late-onset Alzheimer's disease group in the absence of PIB-negative early-onset Alzheimer's disease patients. In contrast, we included only PIB-positive patients, thereby minimising the possibility of misdiagnosis. In the first [^{11}C]PIB study comparing early-onset with late-onset Alzheimer's disease, however, no global or topographical differences in amyloid burden were reported [13]. Discrepancies with the present study may be due to differences in group characterization, sample sizes, or the use of different methods for analysing the [^{11}C]PIB PET data. Furthermore, Rabinovici et al. used an age cut-off of 65 years at time of disease onset to categorize early-onset and late-onset Alzheimer's disease patients. Patients in the present study were relatively young, leading to an age cut-off of 62 years at time of diagnosis. This may suggest that the present findings may be driven by Alzheimer's disease patients with very early onset. Potentially, the marked

increased parietal [^{11}C]PIB binding is most prominent in very young patients, whilst [^{18}F]FDG uptake differs most between early-onset and late-onset Alzheimer's disease patients. This would fit a recently proposed hypothetical biomarker model [47] and possibly explains discrepant findings between this and a previous study [13]. Adding an even older Alzheimer's disease group in a future study would be of major interest. An alternative explanation for the increased parietal [^{11}C]PIB binding in younger Alzheimer's disease patients could be their clinical presentation. In the present study, younger and older patients had comparable MMSE scores, disease duration, level of education and APOE genotype. Yet, younger patients performed relatively worse on non-memory tasks, whilst older patients exhibited most severe impairment on memory tasks. These different phenotypes may be an ultimate expression of topographical differences as younger Alzheimer's disease patients showed an increased parietal amyloid burden. This notion was further supported by the association we found between parietal [^{11}C]PIB binding and visuo-spatial functioning in young Alzheimer's disease patients. Distinct distributions of amyloid load, however, were not found in patients with focal variants of Alzheimer's disease such as posterior cortical atrophy [48,49] (PCA, characterized by impairment in vision and visuospatial skills) or logopenic aphasia [50,51] (characterized by word finding problems, anomia and difficulty in sentence repetition), when compared with patients with typical Alzheimer's disease. Despite similar distributions of [^{11}C]PIB retention in PCA, these patients did show reduced [^{18}F]FDG uptake in occipito-temporal regions [49], suggesting that not amyloid plaque deposition but metabolic impairment drives the clinical presentation. Sample sizes in these studies were small, however, and further investigation is needed to unravel the pathways that eventually lead to distinct phenotypes of Alzheimer's disease.

The origin of an apparent parietal predilection for both amyloid deposits and glucose hypometabolism in early-onset Alzheimer's disease remains unknown. Early and subtle changes in brain network activity may play a role in this intriguing phenomenon. The parietal lobe is an important component of the default mode network (DMN) which consists of a set of interconnected brain regions that

typically activate during task-free imaging [52]. Basal neural network activity is highest in DMN structures that are also vulnerable for amyloid deposition such as frontal cortex, posterior cingulate and parietal cortex. It has been hypothesized that amyloid plaques preferentially develop in brain areas susceptible to very early network changes [53,54]. Due to unknown, possibly genetic or environmental factors, changes in DMN integrity may be most pronounced in the parietal cortex in early-onset Alzheimer's disease patients, thereby anticipating parietal amyloid-beta accumulation and progressive metabolic impairment. Another possibility is that early-onset and late-onset Alzheimer's disease patients exhibit disruptions in different brain networks. Late-onset Alzheimer's disease patients may predominantly show DMN, thus hippocampal-cortical memory system, disruptions, whilst early-onset Alzheimer's disease patients may more often exhibit reduced connectivity in the dorsal attention network [55] or in the frontoparietal control system [56]. Whether indeed age-of-onset is related to specific changes in functional connectivity in Alzheimer's disease patients remains to be investigated.

In early-onset Alzheimer's disease, patients often present with cognitive deficits linked to parietal cortex such as acalculia, spatial disorientation and apraxia [3-5]. Younger Alzheimer's disease patients in this study had most severe impairment in visuo-spatial skills, executive functions and attention, in addition to an increased amyloid burden and modestly decreased glucose metabolism in the parietal lobe. We also showed a direct association between amyloid deposition in the parietal cortex and visuo-spatial functioning, and between parietal glucose metabolism and visuo-spatial abilities, executive functions, and attention in these patients. These relationships were independent of gender, education, MMSE scores and APOE genotype. Data of the present study fit a hypothetical model in which disproportionate accumulation of amyloid-beta precedes disproportional neuronal dysfunction in the parietal cortex of younger Alzheimer's disease patients, in turn leading to decline in cognitive functions that are typically associated with parietal brain structures. Older Alzheimer's disease patients showed a trend towards worse memory performance compared with younger patients. Memory performance was related strongly to reduced metabolic activity in the posterior cingulate, a critical

brain region in sporadic Alzheimer's disease. Furthermore, there was an association between amyloid deposition in the occipital cortex and visuo-spatial functioning. This effect is strongly driven by two patients with high [^{11}C]PIB binding and low visuo-spatial composite scores (Figure 3B). One of these older patients was diagnosed with PCA, illustrating that an atypical presentation is not restricted to early-onset Alzheimer's disease. Furthermore, our data suggest that dysfunction of the brain (i.e. reduced glucose metabolism) is more closely related to cognitive dysfunction in younger than in older Alzheimer's disease patients. It may be hypothesized that cognitive deficits in younger patients are a direct effect of Alzheimer's disease pathology or its downstream effects, whilst in older patients other aging related factors confound this relation.

Despite previously reported differences in extent and pattern of brain atrophy between early-onset and late-onset Alzheimer's disease [15,16], PET data were not corrected for partial volume effects. Many uncertainties affect both accuracy and precision of (MR based) partial volume correction methods, such as coregistration and segmentation errors [57]. To date, there is no consensus on the best method for [^{11}C]PIB and [^{18}F]FDG data. It is possible that application of partial volume correction would have resulted in even higher [^{11}C]PIB binding values in the parietal cortex of younger Alzheimer's disease patients. For [^{18}F]FDG, however, lack of partial volume correction may have led to underestimation and could, therefore, have affected observed differences between younger and older Alzheimer's disease patients. This is not necessarily the case as partial volume correction did not make any difference in a previous study [13]. Another limitation of the present study is that Alzheimer's disease patients in the older group were relatively young (69 years on average at time of diagnosis). Amongst the strengths of this study is the large sample of patients with a clinical diagnosis of Alzheimer's disease and *in vivo* evidence of amyloidosis. Furthermore, younger and older Alzheimer's disease patients were comparable in terms of gender, disease duration, education and disease severity, yet showed a clearly distinct cognitive profile, thereby providing sharp contrast between Alzheimer's disease phenotypes according to age. Finally,

an optimal quantitative parametric method (RPM2) was used for analysing [^{11}C]PIB data.

The present study provides *in vivo* evidence for a different topography of amyloid deposition and glucose hypometabolism in younger Alzheimer's disease patients compared to older patients. Increased amyloid burden, together with metabolic dysfunction, in the parietal cortex of younger Alzheimer's disease patients may explain the distinct cognitive profile in these patients. This study adds to the understanding of heterogeneity in terms of age-at-onset and clinical presentation and shows for the first time a more direct relationship between amyloid deposition and clinical signs.

REFERENCES

1. Fratiglioni L, Launer L, Andersen K et al. Incidence of dementia and major subtypes in Europe: A collaborative study of population-based cohorts. Neurologic diseases in the elderly research group. *Neurology* 2000;54:S10-S15.
2. Cummings J. Alzheimer's Disease. *N Engl J Med* 2004;351:56-67.
3. Koedam E, Lauffer V, van der Vlies A et al. Early- versus late-onset Alzheimer's disease: more than age alone. *J Alzheimers Disease* 2010;19:1401-1408.
4. Koss E, Edland S, Fillenbaum G, et al. Clinical and neuropsychological differences between patients with earlier and later onset of Alzheimer's disease: A CERAD analysis, part XII. *Neurology* 1996;46:136-141.
5. Stopford CL, Snowden JS, Thompson JC et al. Variability in cognitive presentation of Alzheimer's disease. *Cortex* 2008;44:185-195.
6. Mann DM, Yates PO, Marcyniuk B. Alzheimer's presenile dementia, senile dementia of Alzheimer type and Down's syndrome in middle age form an age related continuum of pathological changes. *Neuropathol Appl Neurobiol* 1984;10:185-207.
7. Hansen LA, DeTeresa R, Davies P et al. Neocortical morphometry, lesion counts, and choline acetyltransferase levels in the age spectrum of Alzheimer's disease. *Neurology* 1988;38:48-54.
8. Berg L, McKeel DW, Miller JP et al. Clinicopathologic Studies in Cognitively Healthy Aging and Alzheimer Disease: Relation of Histologic Markers to Dementia Severity, Age, Sex, and Apolipoprotein E Genotype. *Arch Neurol* 1998;55:326-335.
9. Bigio EH, Hynan LS, Sontag E et al. Synapse loss is greater in presenile than senile onset Alzheimer disease: implications for the cognitive reserve hypothesis. *Neuropathol Appl Neurobiol* 2002;28:218-227.
10. Marshall GA, Fairbanks LA, Tekin S et al. Early-onset Alzheimer's disease is associated with greater pathological burden. J *Geriatr Psychiatry Neurol* 2007;20:29-33.
11. Ho GJ, Hansen LA, Alford MF et al. Age at onset is associated with disease severity in Lewy body variant and Alzheimer's disease. *Neuroreport* 2002;13:1825-1828.
12. Klunk WE, Engler H, Nordberg A et al. Imaging Brain Amyloid in Alzheimer's Disease with Pittsburgh Compound-B. *Ann Neurol* 2004;55:306-319.
13. Rabinovici GD, Furst AJ, Alkalay A et al. Increased metabolic vulnerability in early-onset Alzheimer's disease is not related to amyloid burden. *Brain* 2010;133:512-528.
14. Bouwman FH, Schoonenboom NSM, Verwey NA et al. CSF biomarker levels in early and late onset Alzheimer's disease. *Neurobiol Aging* 2009;30:1895-1901.
15. Frisoni GB, Pievani M, Testa C et al. The topography of grey matter involvement in early and late onset Alzheimer's disease. *Brain* 2007;130:720-730.
16. Karas G, Scheltens P, Rombouts S et al. Precuneus atrophy in early-onset Alzheimer's disease: a morphometric structural MRI study. *Neuroradiol* 2007;49:967-976.
17. Jagust WJ, Reed BR, Seab JP et al. Alzheimer's disease: Age at onset and single-photon emission computed tomographic patterns of regional cerebral blood flow. *Arch Neurol* 1990;47:628-633.
18. Kemp PM, Holmes C, Hoffman SM et al. Alzheimer's disease: differences in technetium-99m HMPAO SPECT scan findings between aerly onset and late onset dementia. *J Neurol Neurosurg Psychiatry* 2003;74:715-719.
19. Yasuno F, Imamura T, Hirono et al. Age at onset and regional cerebral glucose metabolism in Alzheimer´s disease. *Dement Geriatr Cogn Dis* 1998;9:63-67.
20. Sakamoto S, Ishii K, Sasaki M et al. Differences in cerebral metabolic impairment between early and late onset types of Alzheimer's disease. *J Neurol Sci* 2002;200:27-32.
21. Kim EJ, Cho SS, Jeong Y et al. Glucose metabolism in early onset versus late onset Alzheimer's disease: an SPM analysis of 120 patients. *Brain* 2005;128:1790-1801.

22. de Waal H, Stam CJ, Blankenstein MA et al. EEG abnormalities in early and late onset Alzheimer's disease: understanding heterogeneity. *J Neurol Neurosurg Psychiatry* 2011;82:67-71.
23. Scheltens P, Leys D, Barkhof F et al. Atrophy of medial temporal lobes on MRI in "probable" Alzheimer's disease and normal ageing: diagnostic value and neuropsychological correlates. *J Neurol Neurosurg Psychiatry* 1992;55:967-72.
24. Tolboom N, Yaqub M, van der Flier WM et al. Detection of Alzheimer Pathology In Vivo Using Both 11C-PIB and 18F-FDDNP PET. *J Nucl Med* 2009; 50: 191-197.
25. McKhann G, Knopman D, Chertkow H et al. The diagnosis of dementia due to Alzheimer's disease: Recommendations from the National Institute on Aging-Alzheimer's Association workgroups on diagnostic guidelines for Alzheimer's disease. *Alzheimers Dement* 2011;7:263-269.
26. Saan RJ, Deelman BG. De 15-Woorden test A en B (Een voorlopige handleiding, in Dutch). 1986.
27. Lindeboom J, Schmand B, Tulner L, Walstra G, Jonker C. Visual association test to detect early dementia of the Alzheimer type. *J Neurol Neurosurg Psychiatry* 2002;73:126-33.
28. Warrington EK, James M. The visual object and space perception battery. Bury St. Edmunds UK: Thames Valley test company. 1991.
29. Osterrieth PA. Le test de copie dúne figure complexe: contribution a l'etude de l'aperception et de la memoire. *Archives de Psychologie* 1944;30:205-353.
30. Lindeboom J, Matto D. [Digit series and Knox cubes as concentration tests for elderly subjects]. *Tijdschr Geront Geriatr* 1994;25:63-68.
31. Reitan RM. Validity of the Trail Making Test as an indicator of organic brain damage. *Percept Mot skills* 1958;8:271-276.
32. Stroop JR. Studies of interference in serial verbal reactions. *J Exp Psychol* 1935;18:643-662.
33. Luteijn F, van der Ploeg. GIT. Groninger Intelligentie Test (in Dutch). Lisse: Swets & Zeitlinger; 1982.
34. Verhage F. Intelligentie en leeftijd: onderzoek bij Nederlanders van twaalf tot zevenenzeventig jaar [Intelligence and age: study with Dutch people aged 12 to 77]. In: Van Gorcum, editor. Assen: 1964.
35. Brix G, Zaers J, Adam LE et al. Performance Evaluation of a Whole-Body PET Scanner Using the NEMA Protocol. *J Nucl Med* 1997;38:1614-23.
36. Wilson AA, Garcia A, Chestaskova A et al. A rapid one-step radiosynthesis of the beta-amyloid imaging radiotracer N-methyl-[C-11]2-('4-methylaminophenyl)-6-hydroxybenzothiazole ([C-11]-6-OH-BTA-1). *J Labelled Comp Radiopharm* 2004;47:679-82.
37. Fazekas F, Chawluk JB, Alavi A, Hurtig HI, Zimmerman RA. MR signal abnormalities at 1.5 T in Alzheimer's disease and normal aging. *AJR* 1987;149:351-356.
38. Svarer C, Madsen K, Hasselbalch SG et al. MR-based automatic delineation of volumes of interest in human brain PET images using probability maps. *NeuroImage* 2005;24:969-979.
39. Wu Y, Carson R. Noise reduction in the simplified reference tissue model for neuroreceptor functional imaging. *J Cereb Blood Flow Metab* 2002;22:1440-1452.
40. Yaqub M, Tolboom N, Boellaard R et al. Simplified parametric methods for [11C]PIB studies. *NeuroImage* 2008;42:76-86.
41. Yamaguchi H, Hirai S, Morimatsu M et al. Diffuse type of senile plaques in the cerebellum of Alzheimer-type dementia demonstrated by beta protein immunostain. *Acta Neuropathol* 1989;77:314-319.
42. Soininen H, Helkala E, Kuikka J et al. Regional cerebral blood flow measured by 99mTc-HMPAO SPECT differs in subgroups of Alzheimer's disease. *J Neural Transm Park Dis Dem Sect* 1995;9:95-109.

43. Devanand DP, Mikhno A, Pelton GH et al. Pittsburgh compound-B (11C)PIB and fluorodeoxyglucose (18F-FDG) PET in patients with Alzheimer disease, mild cognitive impairment and healthy controls. *J Geriatr Psychiatry Neurol* 2010;23:185-198.
44. Forster S, Grimmer T, Miederer I et al. Regional expansion of hypometabolism in Alzheimer's disease follows amyloid deposition with temporal delay. Biolog Psychiatry 2012;71:792:297.
45. Hardy JA, Selkoe DJ. The amyloid hypothesis of Alzheimer's disease: progress and problems on the road to therapeutics. *Science* 2002;197:353-356.
46. Choo IH, Lee DY, Kim JW et al. Relationship of amyloid-beta burden with age-at-onset in Alzheimer disease. *Am J Geriatr Psych* 2011;19:627-634.
47. Jack Jr CR, Knopman DS, Jagust WJ et al. Hypothetical model of dynamic biomarkers of the Alzheimer's pathological cascade. *Lancet Neurol* 2010;9:119-128.
48. de Souza LC, Corlier F, Habert MO et al. Similar amyloid-B burden in posterior cortical atrophy and Alzheimer's disease. *Brain* 2011;134:2036-2043.
49. Rosenbloom MH, Alkalay A, Agarwal N et al. Distinct clinical and metabolic deficits in PCA and AD are not related to amyloid distribution. *Neurology* 2011;76:1789-1796.
50. Leyton CE, Villemagne VL, Savage G et al. Subtypes of progressive aphasia: application of the international consensus criteria and validation using B-amyloid imaging. *Brain* 2011;134:3030-3043.
51. Rabinovici GD, Jagust WJ, Furst AJ et al. Abeta amyloid and glucose metabolism in three variants of primary progressive aphasia. *Ann Neurol* 2008;64:388-401.
52. Raichle ME, MacLeod AM, Snyder AZ et al. A default mode of brain function. *Proc Natl Acad Sci* 2001;98:676-682.
53. Buckner RL, Snyder AZ, Shannon BJ et al. Molecular, structural, and functional characterization of Alzheimer's disease: evidence for a relationship between default activity, amyloid and memory. *J Neurosci* 2005;25:7709-7717.
54. Hedden T, Van Dijk KRA, Becker JA et al. Disruption of Functional Connectivity in Clinically Normal Older Adults Harboring Amyloid Burden. *J Neurosci* 2009;29:12686-12694.
55. Corbetta M, Shulman GL. Control of goal-directed and stimulus-driven attention in the brain. *Nat Rev Neurosci* 2002;3:201-215.
56. Vincent JL, Kahn I, Snyder AZ et al. Evidence for a frontoparietal control system revealed by intrinsic functional connectivity. *J Neurophysiol* 2008;100:3328-42.
57. Kloet RW, Berckel BNM, Pouwels PJW et al. Effects of MR scanner type, scanning sequence and segmentation algorithm on MR-based partial volume corrections of [^{11}C](*R*)-PK11195 studies. *NeuroImage* 2006;[Supplement 2]:T83.

Chapter 4.2

Differential Effect of APOE genotype on Amyloid Load and Glucose Metabolism in AD Dementia

Neurology 2013; 80(4): 359-65

Rik Ossenkoppele, Wiesje M. van der Flier, Marissa D. Zwan,
Sofie F. Adriaanse, Ronald Boellaard, Albert D. Windhorst,
Frederik Barkhof, Adriaan A. Lammertsma,
Philip Scheltens and Bart N.M. van Berckel

ABSTRACT

Objective

To examine the relationships between APOE ε4 dose and *in vivo* distributions of both fibrillary amyloid burden and glucose metabolism in the same Alzheimer's disease (AD) dementia patients, selected for abnormal amyloid imaging.

Methods

22 APOE ε4 negative, 40 heterozygous, and 22 homozygous AD dementia patients underwent dynamic (90 minutes) [^{11}C]Pittsburgh compound-B (PIB) and static [^{18}F]-2-fluoro-2-deoxy-D-glucose (FDG) PET scans. Parametric non-displaceable binding potential images of [^{11}C]PIB and standardized uptake value ratio images of [^{18}F]FDG were generated using cerebellar grey matter as reference tissue. Frontal, parietal, temporal, posterior cingulate, and occipital cortices were selected as regions-of-interest.

Results

Multivariate general linear models with adjustment for age, sex and MMSE showed main effects of APOE ε4 dose on distributions of both [^{11}C]PIB (p for trend <0.05) and [^{18}F]FDG (p for trend <0.01). More specifically, univariate GLM of individual regions showed increased [^{11}C]PIB binding in frontal cortex of APOE ε4 non-carriers compared with APOE ε4 carriers ($p<0.05$). In contrast, APOE ε4 carriers had reduced [^{18}F]FDG uptake in occipital cortex ($p<0.05$) and a borderline significant effect in posterior cingulate ($p=0.07$) in a dose dependent fashion.

Conclusion

We found a reversed APOE ε4 dose effect for amyloid deposition in the frontal lobe, while APOE ε4 carriership was associated with more profound metabolic impairment in posterior parts of the cortex. These findings suggest that APOE genotype has a differential effect on the distribution of amyloid plaques and glucose metabolism. This may have important implications for emerging therapies that aim to directly intervene in the disease process.

INTRODUCTION

Apolipoprotein E (APOE) ε4 is the major genetic risk factor for sporadic Alzheimer's disease (AD) dementia [1]. Cognitively normal APOE ε4 carriers consistently show increased amyloid-beta plaque load and subtle metabolic and morphological reductions [2-4]. Once patients progress to clinically manifest AD, however, the effects of APOE ε4 are less clear. Most post-mortem, CSF and MRI studies have reported higher pathological burden and more profound brain atrophy in APOE ε4 carrying AD dementia patients [5,6], but several other studies did not [7,8]. APOE genotype is apparently related to clinical manifestation of the disease. Presence of an ε4 allele predisposes for the amnestic – predominantly hippocampal driven - variant of AD dementia [9.10], while more prominent non-memory deficits such as visuo-spatial disabilities, language problems, and executive dysfunction have been reported in APOE ε4 non-carriers [11,12]. Furthermore, APOE ε4 negative AD dementia patients have been suggested to follow a more aggressive disease course [13,14].

Neuroimaging with [^{11}C]Pittsburgh compound-B ([^{11}C]PIB) enables *in vivo* quantification of distribution of amyloid pathology. An earlier [^{11}C]PIB PET study showed greater amyloid load in APOE ε4 carrying AD dementia patients [15], but this was not confirmed in another study.[16] Both studies did not assess cerebral glucose metabolism. [^{18}F]-2-fluoro-2-deoxy-D-glucose ([^{18}F]FDG) PET studies showed that APOE ε4 carriers display increased metabolic vulnerability in AD specific regions [17], although this has been disputed by others [18,19]. The purpose of the present study was to examine the relationships between APOE genotype and distributions of both fibrillary amyloid deposition and glucose metabolism in the same AD dementia patients.

METHODS

Subjects

92 AD dementia patients and 17 cognitively normal controls with [^{11}C]PIB and [^{18}F]FDG scans and known APOE status were included. All subjects underwent

standard dementia screening that included medical history, informant-based history, physical and neurological examinations, screening laboratory tests, MRI and neuropsychological testing (including Mini-Mental State Examination (MMSE), a Dutch version of the Rey Auditory Verbal Learning Test (RAVLT), Trailmaking Test (TMT) part A and B, and Digit Span forward and backward) [20]. Clinical diagnosis was established by consensus in a multidisciplinary team, without awareness of PET results. Patients were diagnosed according to National Institute of Neurological and Communicative disorders and Stroke and the Alzheimer's Disease and Related Disorders Association (NINCDS-ADRDA) guidelines for probable AD [21]. Furthermore, all patients met criteria proposed by the National Institute on Aging and the Alzheimer's Association (NIA-AA) workgroup for probable AD with at least intermediate likelihood due to abnormal [^{11}C]PIB PET [22].

Exclusion criteria were history of major psychiatric or neurological illness, drug and/or alcohol abuse, major vascular events and known genetic mutations (presenilin-1, presenilin-2 and amyloid-β precursor protein). Furthermore, eight [^{11}C]PIB-negative AD dementia patients were excluded, leaving 84 patients for analysis. Parametric images of [^{11}C]PIB were visually classified by an experienced nuclear medicine physician (BvB). [^{11}C]PIB scans were considered positive if there was cortical binding in more than one brain region (e.g. frontal, parietal, temporal, occipital). Controls were recruited through newspaper advertisements as described elsewhere [20].

Standard Protocol Approvals, Registrations and Patient Consents

Written informed consent was obtained from all subjects after complete written and verbal description of the study. The Medical Ethics Review Committee of the VU University Medical Center approved the study.

APOE

APOE genotyping was performed after DNA isolation from 10 mL ethylenediaminetetraacetic acid (EDTA) blood, using the LightCycler APOE mutation detection method (Roche Diagnostics GmbH, Mannheim, Germany). There

were 22 APOE ε4 negative, 40 heterozygous and 22 homozygous AD dementia patients, and 14 negative and 3 heterozygous controls.

PET

PET scans were obtained on an ECAT EXACT HR+ scanner (Siemens/CTI, Knoxville, TN, USA) equipped with a neuroinsert to reduce the contribution of scattered photons. The properties of this scanner have been reported elsewhere [23]. Subjects received a venous cannula for tracer injection. First, a 10 min transmission scan was obtained, followed by a dynamic emission scan in 3-dimensional acquisition mode that was started simultaneously with the intravenous injection of 367±42 MBq [^{11}C]PIB, using an infusion pump (Med-Rad; Beek, the Netherlands) at a rate of 0.8mL·s^{-1}, followed by a flush of 42 mL of saline at 2.0 mL·s^{-1}. [^{11}C]PIB was synthesized according to a modified procedure [24], yielding a specific activity of 99±27 GBq·μmol^{-1}. The [^{11}C]PIB scan consisted of 23 frames with progressive increase in duration (1x15, 3x5, 3x10, 2x30, 3x60, 2x150, 2x300, 7x600 s) for a total scan duration of 90 min. After an interval of at least two hours to allow decay of [^{11}C]PIB, an intravenous bolus injection of approximately 185 MBq of [^{18}F]FDG was injected. All subjects rested for 15 min before injection and 35 min after injection with eyes closed and ears unplugged in a dimly lit room with minimal background noise. Next, patients underwent a 10 min transmission scan followed by a 15 min emission scan (3x5 min frames). Patient motion was restricted by a head holder and regularly checked using laser beams. Due to tracer synthesis failure, 15 patients did not undergo [^{11}C]PIB and [^{18}F]FDG scans on the same day (interval was at most 4 weeks). Scans were performed within 4±3 months after the clinical diagnosis was made.

MRI

All subjects underwent structural MRI using 1.5T Sonata (Siemens, Erlangen, Germany) (29 patients) or 3T Signa HDxt (General Electric, Milwaukee, USA) scanners (55 patients). The scan protocol included a coronal T1-weighted 3-dimensional magnetization-prepared-acquisition gradient echo (MPRAGE) (1.5T scanner: slice thickness 1.5 mm, 160 slices, matrix size 256x256, voxel size 1x1x1.5

mm, echo time 3.97 ms, repetition time 2700 ms, flip angle, 8°; 3T scanner: slice thickness 1 mm, 180 slices, matrix size 256x256, voxel size 1x1x1.5 mm, echo time 3 ms, repetition time 708 ms, flip angle 12°). The MRI scan was used for co-registration and region-of-interest (ROI) definition.

Image and Data Analysis

All PET sinograms were corrected for dead time, tissue attenuation, decay, scatter and randoms, and were reconstructed using a standard filtered back projection algorithm and a Hanning filter with a cut-off at 0.5 times the Nyquist frequency. A zoom factor of 2 and a matrix size of 256x256x63 were used, resulting in a voxel size of 1.2x1.2x2.4 mm and spatial resolution of approximately 7 mm full width at half-maximum at the center of the field of view.

MR images were aligned to corresponding PET images using a mutual-information algorithm. Data were further analyzed using PVE-lab, a software program that uses a probability map based on 35 previously validated ROIs [25]. ROIs were projected onto [^{11}C]PIB parametric (BP_{ND}) images. These images were generated by applying a 2-step basis-function implementation (RPM2) of the simplified reference tissue model to the full dynamic 90 min PET data [26]. RPM2 has previously been identified as the parametric model of choice [27]. For [^{18}F]FDG, parametric images of standardized uptake value ratio (SUVr) were generated using activity concentrations from the interval between 45 and 60 min after injection. Cerebellar grey matter was used as reference tissue for both PET tracers [28].

The following volume weighted ROIs were used for regional analysis of [^{11}C]PIB and [^{18}F]FDG as they are especially relevant for AD: frontal (orbital, medial inferior, and superior), temporal (superior and medial inferior), parietal, occipital and posterior cingulate cortices. In addition, global cortical BP_{ND} and SUVr were calculated, based on volume-weighted averages of the aforementioned regions. Finally, the 16 unweighted subregions (bilaterally) were analyzed individually.

Statistics

Differences in baseline characteristics between groups were assessed using ANOVA, Kruskal Wallis tests and χ^2 tests, where appropriate. ANOVA was used to compare cognitive test performance (adjusted for age, sex and education) between groups. Differences in global [^{11}C]PIB BP_{ND} and [^{18}F]FDG SUVr were assessed using univariate GLMs with post-hoc Bonferroni tests, adjusted for age, sex and MMSE. Multivariate general linear models (GLMs) were used to assess the relationships between APOE ε4-dose (as continuous variable) and [^{11}C]PIB BP_{ND} and [^{18}F]FDG SUVr in frontal, temporal, parietal, occipital and posterior cingulate cortices. Post hoc, we used univariate GLMs with age and sex as covariates, to assess APOE effects in individual regions. In a second model, MMSE score was entered additionally to adjust for potential confounding of disease severity. Effect sizes were expressed in η^2 (η^2=0.01 indicates a small effect, η^2=0.06 a medium effect and η^2=0.14 a large effect) [30]. Similar analyses were performed with the 16 subregions as dependent variables. Linear regression analyses were performed to assess relationships between 1) [^{11}C]PIB BP_{ND} and [^{18}F]FDG SUVr within ROIs (adjusted for age, sex and MMSE), and 2) [^{11}C]PIB BP_{ND}/[^{18}F]FDG SUVr and cognition (adjusted for age, sex and education). Statistical significance was set at $p<0.05$.

RESULTS

Subject characteristics

Characteristics according to APOE ε4-dose are presented in Table 1. Groups did not differ in age or education. The APOE ε4 negative AD dementia group comprised more males than the APOE ε4 carriers ($p<0.05$). Furthermore, APOE ε4 negative patients had shorter disease durations than APOE ε4 homozygous patients ($p<0.05$).

On average, patients were mildly to moderately demented and MMSE scores did not differ between groups. Adjusted for age, sex and education, APOE ε4 homozygous AD dementia patients showed more severe impairment on the RAVLT delayed recall ($p<0.05$) than APOE ε4 negative patients (Table 1). APOE ε4 heterozygous patients performed worse on TMT B ($p<0.05$) compared with homozygous patients.

Table 1. Demographic and clinical characteristics of AD dementia patients according to APOE genotype

	ε4 negative	ε4 heterozygous	ε4 homozygous	Controls
N	22	40	22	17
Age at PET	61(44-77)	62(49-78)	65(50-80)	67(57-80)
Sex (m/f)	16/6	25/15[a]	13/9[a]	11/6
Education*	5(3-7)	5(3-7)	5 (3-7)	6(2-7)
Disease duration	3±1	4±2	4±1[a]	NA
MMSE (30)	24±4	23±5	24±3	29±1
RAVLT – total learning (75)	24±8	26±10	26±11	38±9
RAVLT – delayed recall (15)	4±3	2±3	1±3[a]	7±2
Trailmaking Test A (240")	73±54	88±61	68±62	71±36
Trailmaking Test B (360")	205±26	250±21	162±25[b]	143±77
Digit Span forward (21)	11±4	11±3	12±3	12±2
Digit Span backward (21)	7±3	7±3	9±3	9±3
Global [^{11}C]PIB BP_{ND}	0.78±0.16	0.72±0.20	0.70±0.18	0.08±0.13
Global [^{18}F]FDG SUVr	0.99±0.08	0.99±0.08	0.98±0.14	1.09±0.08

Data are presented as mean ± SD or mean (range). Maximum attainable neuropsychological test scores are presented in parentheses.
Abbreviations: AD = Alzheimer's disease; m = male; f = female; MMSE = Mini-Mental-State Examination; RAVLT = Rey Auditory Verbal Learning Test (Dutch version); BP_{ND} = non-displaceable binding potential; SUVr = standardized uptake value ratio; NA = not available.
Differences between groups were assessed using ANOVA with post hoc Bonferroni t-tests (age, disease duration, cognition, global [^{11}C]PIB BP_{ND}, and global [^{18}F]FDG SUVr), Kruskal Wallis with post hoc Mann Whitney U tests (education) and χ^2 (sex).
* Education using Verhage's classification
[a] compared to APOE ε4 negative AD dementia patients: $p<0.05$
[b] compared to APOE ε4 heterozygous AD dementia patients: $p<0.05$

Global [^{11}C]PIB BP_{ND} and [^{18}F]FDG SUVr

Univariate GLM, adjusted for age, sex, and MMSE, showed a trend towards higher global [^{11}C]PIB BP_{ND} for APOE ε4 negative patients (0.78±0.16) compared with heterozygous (0.72±0.20), and homozygous (0.70±0.18) AD dementia patients (p

for trend=0.09) (Table 1, Figure 1). There were no differences in global [^{18}F]FDG SUVr between APOE ε4 negative (0.99±0.08), heterozygous (0.99±0.08), and homozygous (0.98±0.14) patients (p=0.74) (Table 1).

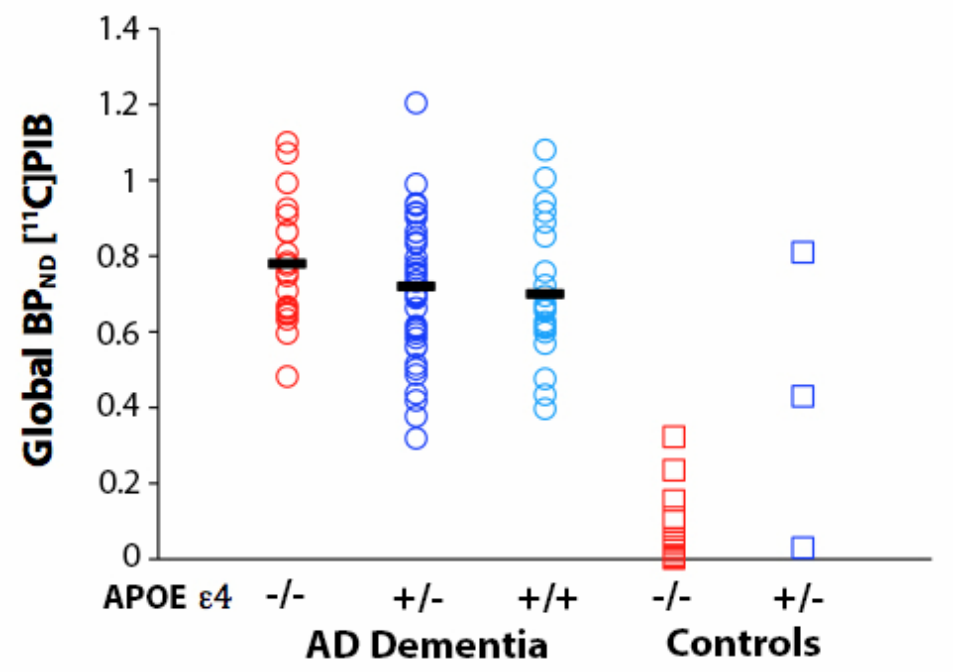

Figure 1. Global cortical [^{11}C]PIB BP$_{ND}$ according to APOE genotype

Regional [^{11}C]PIB BP$_{ND}$

Regional [^{11}C]PIB BP$_{ND}$ according to APOE ε4-dose are presented in Figure 2. Multivariate GLM with APOE ε4 dose as (continuous) independent variable, regional BP$_{ND}$ as dependent variable and age and sex as covariates, showed a main effect for APOE ε4-dose (p for trend <0.05). Post-hoc univariate GLMs showed that APOE ε4 negative patients had higher [^{11}C]PIB BP$_{ND}$ in the frontal cortex compared with APOE ε4 carriers (p for trend =0.01, η^2=0.08) (Figure 2), but not in any of the other regions. These results did not change when additionally adjusting for MMSE. Repeating the latter analysis including unweighted subregions confirmed that APOE ε4 negative patients had higher [^{11}C]PIB BP$_{ND}$ in bilateral medial inferior

frontal, superior frontal and orbitofrontal cortices as well as in left superior temporal cortex compared to APOE ε4 carriers.

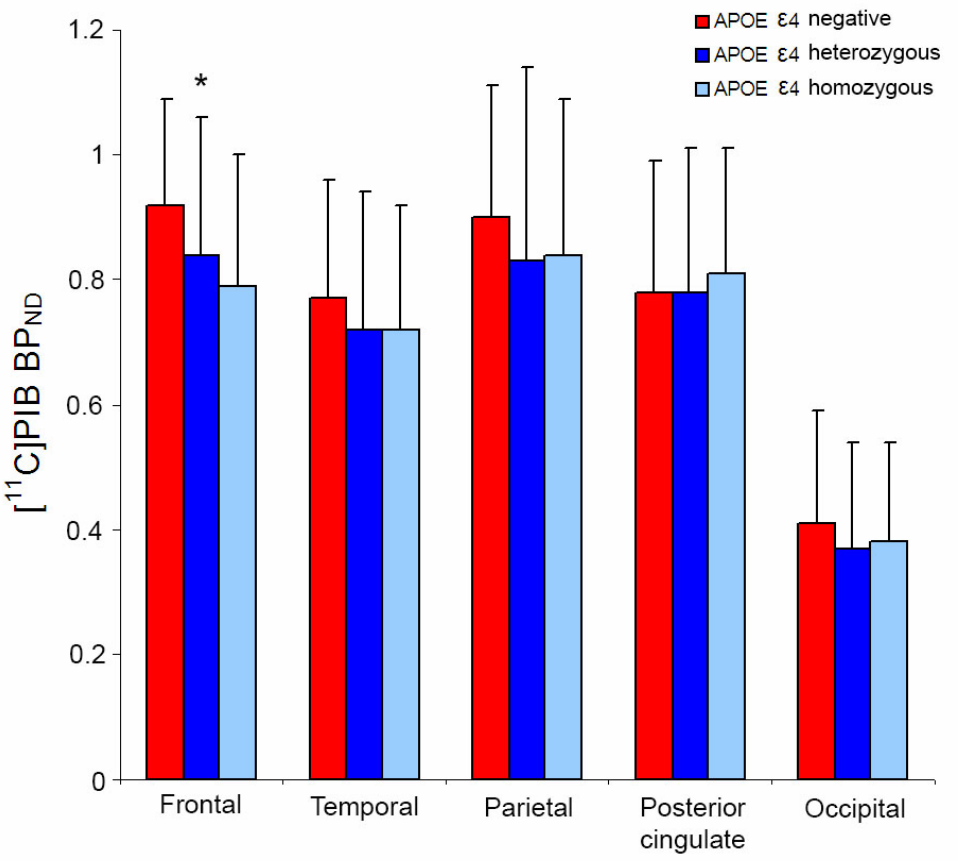

Figure 2. Regional [^{11}C]PIB BP_{ND} in APOE ε4 negative, homozygous, and heterozygous AD dementia patients. Multivariate ANOVA, with APOE dose as independent variable, and age, sex and MMSE as covariates, showed a main effect for APOE dose ($p<0.05$). More specifically, there was a reversed APOE ε4 dose effect for [^{11}C]PIB BP_{ND} in the frontal cortex (* p for trend: <0.05).

Regional [^{18}F]FDG SUVr

Regional [^{18}F]FDG SUVr according to APOE ε4-dose is presented in Figure 3. Multivariate GLM with APOE ε4-dose as (continuous) independent variable, regional SUVr as dependent variable, and age and sex as covariates, showed a main effect for APOE ε4-dose (p for trend <0.01). Post-hoc univariate GLMs of individual brain regions showed lower [^{18}F]FDG uptake in the occipital cortex of APOE ε4

carriers (p for trend =0.05, η^2=0.05) (Figure 3). Additional adjustment for MMSE revealed an even stronger association in occipital (p for trend =0.03, η^2=0.06) and posterior cingulate (p for trend =0.07, η^2=0.05) cortices. Similar analyses including unweighted subregions showed that APOE ε4 carriers had lower FDG uptake in right occipital cortex and posterior cingulate and bilateral orbitofrontal cortex.

There was no interaction between APOE ε4-dose and age for either [^{11}C]PIB BP_{ND} or [^{18}F]FDG SUVr (p>0.05).

[^{11}C]PIB BP_{ND} versus [^{18}F]FDG SUVr

Linear regression analyses in the whole sample, adjusted for age, sex and MMSE, showed no associations between global [^{11}C]PIB and [^{18}F]FDG (St. β=0.07, p=0.54), [^{11}C]PIB and [^{18}F]FDG in the frontal (St. β=0.11, p=0.29) and occipital cortex (St. β=0.03, p=0.78), or frontal [^{11}C]PIB and occipital (St. β=0.15, p=0.17) and posterior cingulate (St. β=-0.09, p=0.44) [^{18}F]FDG.

[^{11}C]PIB BP_{ND}/[^{18}F]FDG SUVr and Cognition

Linear regression analyses, adjusted for age, sex and education, showed a negative association between global [^{11}C]PIB BP_{ND} and RAVLT immediate recall (St. β=-0.25, p=0.043). There were no other correlations between neuroimaging parameters and neuropsychological test results.

DISCUSSION

In this study, we investigated the associations between APOE ε4-dose and regional [^{11}C]PIB binding and [^{18}F]FDG uptake in AD dementia patients selected for abnormal amyloid imaging The main finding was increased frontal amyloid burden in APOE ε4 negative patients, whereas higher APOE ε4-dose was associated with more profound metabolic impairment in occipital and posterior cingulate cortices. These findings suggest that APOE ε4-dose has a differential effect on distribution of amyloid load and glucose metabolism and provide evidence for the notion that AD dementia develops along distinct disease pathways in APOE ε4 carriers and non-carriers. Our approach to subject selection is substantially different than prior studies [15-19], because prior studies did not require amyloid abnormalities.

In the present study, APOE ε4 negative patients displayed increased amyloid pathology in the frontal cortex. It seems rather paradoxical that lack of the major genetic risk factor for AD is associated with increased pathological burden. It should be noted, however, that most studies on the relationships between APOE genotype and amyloid pathology have focused on asymptomatic individuals. In these cognitively normal elderly, APOE ε4 carriership has indeed consistently been associated with increased amyloid load [2]. In the present study all patients had clinically manifest AD and *in vivo* evidence of amyloid pathology. Earlier [^{11}C]PIB studies in AD dementia patients reported conflicting results with either higher amyloid burden in APOE ε4 carriers [15], or no differences according to APOE genotype [16]. Age-at-onset possibly modifies effects of APOE ε4 [30]. Earlier studies showed that absence of APOE ε4 in early-onset AD patients is associated with accelerated shrinkage of the brain and faster cognitive decline [13,14]. Together with the present finding of increased frontal [^{11}C]PIB binding in relatively young APOE ε4 non-carriers, this fits a hypothetical model in which absence of APOE ε4 in conjunction with an early-onset contributes to stronger and differently distributed amyloid pathology. This may ultimately be expressed in clinically distinct and more aggressive manifestation of AD dementia [31].

APOE ε4 carriers showed reduced [^{18}F]FDG uptake in the occipital cortex and, at trend level, the posterior cingulate. The posterior cingulate is a critical structure in AD that shows reduced metabolic activity early in the disease and plays an important role in memory processing through its functional connections with the medial temporal lobe. This finding, in addition to poorer memory performance of APOE ε4 homozygous patients, matches previous observations that APOE ε4 predisposes for the amnestic variant of AD [9,17]. The occipital cortex is a metabolically active region that usually is relatively spared until later stages of AD dementia. There is no obvious explanation as to why this region was more affected

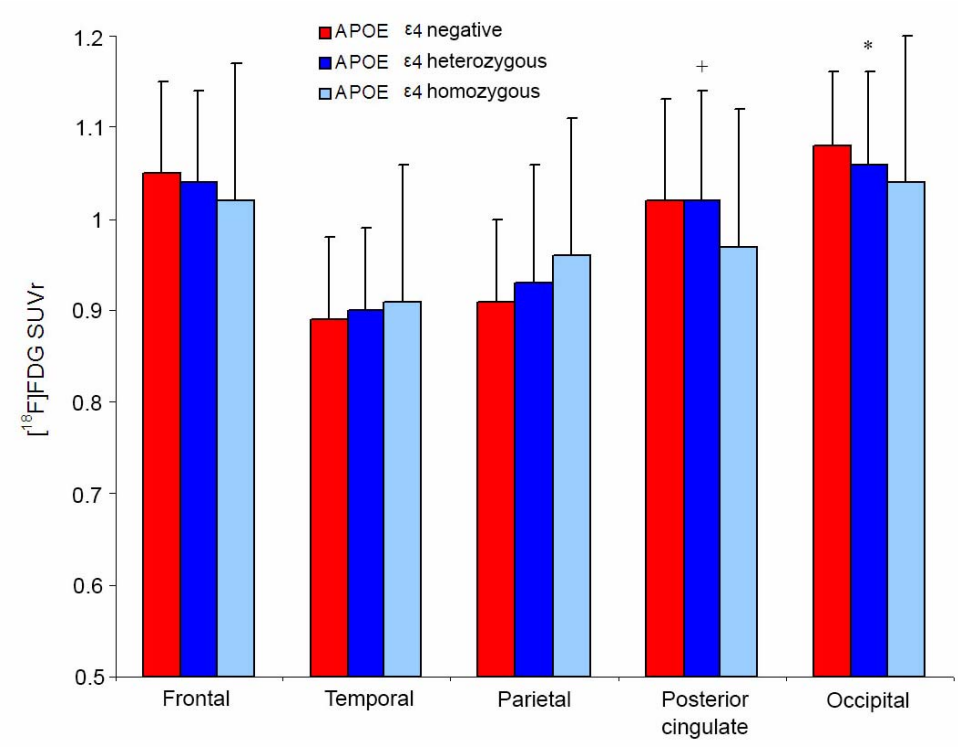

Figure 3. Regional [^{18}F]FDG SUVr in APOE ε4 negative, homozygous, and heterozygous AD dementia patients. Multivariate ANOVA, with APOE-dose as independent variable, and age, sex and MMSE as covariates showed a main effect for APOE ε4 dose ($p<0.01$). APOE ε4 carriers showed reduced [^{18}F]FDG uptake in the occipital cortex (* p for trend: <0.05). Furthermore, there was a borderline significant effect for lower posterior cingulate [^{18}F]FDG uptake in a APOE ε4 dose dependent fashion (+ p for trend =0.07).

in APOE ε4 carrying than in non-carrying patients. More fine-grained exploration of the brain additionally revealed metabolic reductions in the orbitofrontal cortex of APOE ε4 carriers. Previous studies on the effect of APOE genotype on [^{18}F]FDG uptake have not provided consistent results in AD dementia patients, as some found an APOE ε4-dose effect [17], whereas others did not [18,19].
In the present study, APOE ε4 carriers displayed increased regional metabolic vulnerability, but had lower amyloid load than non-carriers. This seemingly paradoxical finding might be explained by the fact that in APOE ε4 carriers, AD dementia likely originates from a multifactorial etiology, as APOE ε4 has also been associated with vascular damage, increased inflammation, and reduced repair mechanisms [32-34]. Potentially, lower amyloid load is required for APOE ε4 carriers to develop dementia as the factors mentioned above all contribute to metabolic dysfunction and cognitive decline.

Marked elevation of amyloid pathology in the frontal lobe of APOE ε4 negative patients did not coincide with more profound metabolic vulnerability in this region. This dissociation has been observed in many studies and remains one of the unresolved questions of molecular imaging in AD [20,35]. Several factors may be involved in this intriguing phenomenon. For instance, [^{11}C]PIB has high affinity for amyloid-beta in its fibrillar content but does not bind to the more soluble, and probably most toxic, species of amyloid-beta (i.e. oligomers). Fibrillarization of amyloid-beta in the frontal cortex may lead to lower levels of oligomers and less neuronal dysfunction, whereas vice versa, lack of fibrillarization may be related to higher levels of oligomers and consequently stronger neuronal dysfunction in other brain regions. Indeed, APOE ε4 has already shown to inhibit fibrillization of soluble amyloid-beta in transgenic mouse models in a dose-dependent manner, and thus may play a role in this process [34]. Another possibility could be that frontal amyloid load causes a disconnection syndrome by disrupting its network function, thereby remotely affecting metabolically vulnerable regions. Furthermore, several studies have shown that asymptomatic individuals with an APOE ε4 allele showed altered functional connectivity in brain networks typically affected in AD dementia

[36,37], even in carriers without amyloid pathology [38,39]. This suggests that APOE ε4 has an effect on brain activity that is independent of amyloid plaque load in the brain.

A possible limitation of this study is that, despite previously reported differences in extent and pattern of brain atrophy according to APOE genotype [12], PET data were not corrected for partial volume effects (PVE). Many uncertainties affect both accuracy and precision of (MR based) PVE correction methods, such as coregistration and segmentation errors. To date, there is no consensus on the best method for PVE correction of [^{11}C]PIB and [^{18}F]FDG data. A point of interest is that patients were relatively young (63 years) at time of PET scanning. Studies including larger samples with broader age ranges are needed to further examine the effect of APOE genotype on amyloid load and glucose metabolism in AD dementia.

In a recently proposed biomarker model [40], it was hypothesized that accumulation of amyloid-beta initiates a cascade of downstream effects, such as neuronal dysfunction and neurodegeneration, which presumably is followed by cognitive decline and ultimately results in dementia. In this study, we performed [^{11}C]PIB and [^{18}F]FDG PET in the same AD dementia patients to measure different aspects of this model. The observed differential effects of APOE genotype, and in an earlier study of age-at-onset [20], on amyloid deposition and neuronal function highlights the difficulty to account for all subgroups of AD dementia in a single biomarker model. Our data suggest that APOE genotype predisposes for regional vulnerability of the brain that may be associated with distinct clinical phenotypes. These findings underline the importance of APOE genotyping for both selection purposes and for monitoring efficacy of disease modifying agents in clinical trials.

REFERENCES

1. Poirier J, Davignon J, Bouthillier D, et al. Apolipoprotein E polymorphism and Alzheimer's disease. *Lancet* 1993;342:697-699.
2. Reiman EM, Chen K, Liu X, et al. Fibrillar amyloid-beta burden in cognitively normal people at 3 levels of genetic risk for Alzheimer's disease. *Proc Natl Acad Sci* 2009;106:6820-6825.
3. Reiman EM, Chen K, Alexander GE, et al. Correlations between apolipoprotein E epsilon4 gene dose and brain-imaging measurements of regional hypometabolism. *Proc Natl Acad Sci* 2005;102:8299-8302.
4. Burggren AC, Zeineh MM, Ekstrom AD, et al. Reduced cortical thickness in hippocampal subregions among cognitively normal apolipoprotein E e4 carriers. *Neuroimage* 2008;41:1177-1183.
5. Polvikoski T, Sulkava R, Haltia M, et al. Apolipoprotein E, dementia, and cortical deposition of beta-amyloid protein. *N Engl J Med* 1995;333:1242-1247.
6. Bennett DA, Wilson RS, Schneider JA, et al. Apolipoprotein E epsilon4 allele, AD pathology, and the clinical expression of Alzheimer's disease. *Neurology* 2003;60:246-252.
7. Motter R, Vigo-Pelfrey C, Kholodenko D, et al. Reduction of beta-amyloid peptide42 in the cerebrospinal fluid of patients with Alzheimer's disease. *Ann Neurol* 1995;38:643-648.
8. Barber R, Gholkar A, Scheltens P, et al. Apolipoprotein E epsilon4 allele, temporal lobe atrophy, and white matter lesions in late-life dementias. *Arch Neurol* 1999;56:961-965.
9. Sluimer JD, Vrenken H, Blankenstein MA, et al. Whole-brain atrophy rate in Alzheimer disease: identifying fast progressors. *Neurology* 2008;70:1836-1841.
10. van der Vlies AE, Koedam EL, Pijnenburg YA, et al. Most rapid cognitive decline in APOE epsilon4 negative Alzheimer's disease with early onset. *Psychol Med* 2009;39:1907-1911.
11. Schott JM, Ridha BH, Crutch SJ, et al. Apolipoprotein e genotype modifies the phenotype of Alzheimer disease. *Arch Neurol* 2006;63:155-156.
12. van der Vlies AE, Pijnenburg YA, Koene T, et al. Cognitive impairment in Alzheimer's disease is modified by APOE genotype. *Dement Geriatr Cogn Disord*;24:98-103.
13. Lehtovirta M, Soininen H, Helisalmi S, et al. Clinical and neuropsychological characteristics in familial and sporadic Alzheimer's disease: relation to apolipoprotein E polymorphism. *Neurology* 1996;46:413-419.
14. Pievani M, Rasser PE, Galluzzi S, et al. Mapping the effect of APOE epsilon4 on gray matter loss in Alzheimer's disease in vivo. *Neuroimage* 2009;45:1090-1098.
15. Drzezga A, Grimmer T, Henriksen G, et al. Effect of APOE genotype on amyloid plaque load and gray matter volume in Alzheimer disease. *Neurology* 2009;72:1487-1494.
16. Villemagne VL, Pike KE, Chételat G, et al. Longitudinal assessment of Aβ and cognition in aging and Alzheimer disease. *Ann Neurol* 2011;69:181-192.
17. Drzezga A, Riemenschneider M, Strassner B, et al. Cerebral glucose metabolism in patients with AD and different APOE genotypes. *Neurology* 2005;64:102-107.
18. Corder EH, Jelic V, Basun H, et al. No difference in cerebral glucose metabolism in patients with AD and differing apolipoprotein E genotypes. *Arch Neurol* 1997;54:273-277.
19. Hirono N, Mori E, Yasuda M, et al. Lack of effect of apolipoprotein E E4 allele on neuropsychiatric manifestations in AD. *J Neuropsychiatry Clin Neurosci* 1999;11:66-70.
20. Ossenkoppele R, Zwan M, Tolboom N, et al. Amyloid burden and metabolic function in early-onset Alzheimer's disease: parietal lobe involvement. *Brain* 2012; 135:2115-2125.
21. McKhann G, Drachman D, Folstein M, et al. Clinical diagnosis of Alzheimer's disease: report of the NINCDS-ADRDA Work Group under the auspices of Department of Health and Human Services Task Force on Alzheimer's Disease. *Neurology* 1984;34:939-944.

22. McKhann GM, Knopman DS, Chertkow H, et al. The diagnosis of dementia due to Alzheimer's disease: recommendations from the National Institute on Aging-Alzheimer's Association workgroups on diagnostic guidelines for Alzheimer's disease. *Alzheimers Dement* 2011;7:263-269.
23. Brix G, Zaers J, Adam LE, et al. Performance evaluation of a whole-body PET scanner using the NEMA protocol. National Electrical Manufacturers Association. *J Nucl Med* 1997;38:1614-1623.
24. Wilson S. A Rapid One-step radiosynthesis of the beta-amyloid imaging radiotracer N-methyl-[C-11]2-('4methylaminophenyl)--hydroxybenzothiazole ([C-11]-6-OH-BTA-1). *J Labelled Comp Radiopharma* 2004;47:47679-47682.
25. Svarer C, Madsen K, Hasselbalch SG, et al. MR-based automatic delineation of volumes of interest in human brain PET images using probability maps. *Neuroimage* 2005;24:969-979.
26. Wu Y, and Carson RE. Noise reduction in the simplified reference tissue model for neuroreceptor functional imaging. *J Cereb Blood Flow Metab* 2002;22:1440-1452.
27. Yaqub M, Tolboom N, Boellaard R, et al. Simplified parametric methods for [11C]PIB studies. *Neuroimage* 2008;42:76-86.
28. Yamaguchi H, Hirai S, Morimatsu M, et al. Diffuse type of senile plaques in the cerebellum of Alzheimer-type dementia demonstrated by beta protein immunostain. *Acta Neuropathol* 1989;77:314-319.
29. Cohen J. A power primer. *Psychological Bulletin* 1992; 112(1):155-159
30. Kester MI, Blankenstein MA, Bouwman FH, et al. CSF biomarkers in Alzheimer's disease and controls: associations with APOE genotype are modified by age. *J Alz Dis* 2009;16:601-607.
31. van der Flier WM, Pijnenburg YA, Fox NC, et al. Early-onset versus late-onset Alzheimer's disease: the case of the missing APOE ε4 allele. *Lancet Neurol* 2011;10:280-288.
32. Haan MN, Shemanski L, Jagust WJ, et al. The role of APOE epsilon4 in modulating effects of other risk factors for cognitive decline in elderly persons. *JAMA* 1999;282:40-46.
33. Akiyama H, Barger S, Barnum S, et al. Inflammation and Alzheimer's disease. *Neurobiol Aging* 2000;21:383-421.
34. Terwel D, Steffensen KR, Verghese PB, et al. Critical role of astroglial apolipoprotein E and liver X receptor-α expression for microglial Aβ phagocytosis. *J Neurosci* 2011;31:7049-7059.
35. Förster S, Grimmer T, Miederer I, et al. Regional Expansion of Hypometabolism in Alzheimer's Disease Follows Amyloid Deposition with Temporal Delay. *Biol Psychiatry* 2012;71:792-797
36. Hedden T, Van Dijk KR, Becker JA, et al. Disruption of functional connectivity in clinically normal older adults harboring amyloid burden. *J Neurosci* 2009;29:12686-12694.
37. Sheline YI, Raichle ME, Snyder AZ, et al. Amyloid plaques disrupt resting state default mode network connectivity in cognitively normal elderly. *Biol Psychiatry* 2010;67:584-587.
38. Filippini N, MacIntosh BJ, Hough MG, et al. Distinct patterns of brain activity in young carriers of the APOE-epsilon4 allele. *Proc Natl Acad Sci* 2009;106:7209-7214.
39. Sheline YI, Morris JC, Snyder AZ, et al. APOE4 allele disrupts resting state fMRI connectivity in the absence of amyloid plaques or decreased CSF Aβ42. *J Neurosci* 2010;30:17035-17040.
40. Jack CR, Knopman DS, Jagust WJ, et al. Hypothetical model of dynamic biomarkers of the Alzheimer's pathological cascade. *Lancet Neurol* 2010;9:119-128.

Chapter 5

Clinical application of molecular imaging

Chapter 5.1

Impact of Molecular Imaging on the Diagnostic Process in a Memory Clinic

Alzheimer's & Dementia [Epub ahead of print]

Rik Ossenkoppele, Niels D. Prins, Yolande A.L. Pijnenburg, Afina W. Lemstra, Wiesje M. van der Flier, Sofie F. Adriaanse, Albert D. Windhorst, Ron L.H. Handels, Claire A.G. Wolfs, Pauline Aalten, Frans R.J. Verhey, Marcel M. Verbeek, Mark A. van Buchem, Otto S. Hoekstra, Adriaan A. Lammertsma, Philip Scheltens & Bart N.M. van Berckel

ABSTRACT

Introduction

[^{11}C]Pittsburgh compound-B ([^{11}C]PIB) and [^{18}F]-2-fluoro-2-deoxy-D-glucose ([^{18}F]FDG) PET measure fibrillar amyloid-beta load and glucose metabolism, respectively. We evaluated the impact of these tracers on the diagnostic process in a memory clinic population.

Methods

154 patients underwent paired dynamic [^{11}C]PIB and static [^{18}F]FDG PET scans shortly after completing a standard dementia screening. Two-year clinical follow-up data were available for 39 patients. Parametric PET images were assessed visually and results were reported to the neurologists who were responsible for the initial diagnosis. Outcome measures were (change in) clinical diagnosis and confidence in that diagnosis before and after disclosing PET results.

Results

[^{11}C]PIB scans were positive in 40/66 (61%) patients with a clinical diagnosis of Alzheimer's disease (AD), 5/18 (28%) patients with frontotemporal dementia (FTD), 4/5 (80%) patients with Lewy body dementia, and 3/10 (30%) patients with other dementias. [^{18}F]FDG uptake patterns matched the clinical diagnosis in 38/66 (58%) of AD patients, and in 6/18 (33%) of FTD patients. PET results led to a change in diagnosis in 35 (23%) patients. This only occurred when prior diagnostic certainty was lower than 90%. Diagnostic confidence increased from 71±17% before to 87±16% after PET ($p<0.001$). Two-year clinical follow-up (n=39) showed that [^{11}C]PIB and [^{18}F]FDG predicted progression to AD for patients with mild cognitive impairment, and that the diagnosis of dementia established after PET remained unchanged in 96% of patients.

Conclusions

In a memory clinic setting, combined [^{11}C]PIB and [^{18}F]FDG PET are of additional value on top of the standard diagnostic work-up, especially when prior diagnostic confidence is low.

INTRODUCTION

The diagnosis of patients with cognitive and/or behavioural symptoms can be complicated as different types of neurodegenerative disorders show overlap in clinical presentation, particularly in patients with an early onset (<65 years) [1]. Furthermore, it is difficult to identify patients in a prodromal stage of Alzheimer's disease (AD) or other forms of dementia based on clinical symptoms alone. Improvement of early and differential diagnosis is desirable, especially in view of emerging disease modifying agents. Over the past decades, several biomarkers have been developed to increase diagnostic accuracy in neurodegenerative diseases. These biomarkers have caused a major paradigm shift and have been incorporated in recently revised criteria that aim for more accurate and earlier diagnosis of AD, frontotemporal dementia (FTD) and dementia with Lewy bodies (DLB) [2-6].

Molecular imaging biomarkers most frequently used in the diagnosis of dementia are [^{18}F]-2-fluoro-2-deoxy-D-glucose ([^{18}F]FDG) and [^{11}C]Pittsburgh compound-B ([^{11}C]PIB), which can be imaged using positron emission tomography (PET). [^{18}F]FDG is the more established tracer and provides a measure of metabolic activity of the brain. [^{18}F]FDG does not directly measure pathology, but the extent of metabolic impairment predicts cognitive decline and is closely related to disease severity [7-9]. Mapping the pattern of glucose hypometabolism has high sensitivity (94%) for diagnosing AD, but specificity is lower (73%), as other neurodegenerative diseases can induce a decrease in glucose metabolism resembling the pattern seen in AD [10-12]. Reading [^{18}F]FDG images requires a well trained eye, and even then only moderate interrater reliability is accomplished [13,14].

More recently, [^{11}C]PIB [15] became available for *in vivo* detection of fibrillary amyloid plaques, a neuropathological hallmark of AD. Probing the underlying neuropathological substrate may be helpful in identifying the correct type of dementia, particularly in patients with an atypical presentation [16]. [^{11}C]PIB discriminates AD patients from cognitively normal elderly [15,17,18], is a strong predictor of progression of mild cognitive impairment (MCI) to AD [19-21], and

distinguishes AD reasonably well from other forms of dementia such as FTD [16,22] and vascular dementia (VaD) [23]. Patients with DLB, however, show positive [^{11}C]PIB scans in up to 89% of cases [24], which corresponds to increased amyloid burden found at post-mortem examination in the majority of DLB patients [25]. Visual assessment of parametric [^{11}C]PIB images is straightforward and shows high agreement between readers [14].

Current literature on [^{18}F]FDG and especially [^{11}C]PIB PET typically comprise comparisons of highly selected diagnostic groups. In general, these studies show good correspondence between clinical diagnosis and neuroimaging results. The potential lack of variation in pre-test diagnostic certainty, however, possibly overestimates this concordance and may actually be lower in a more representative sample of a memory clinic population. The aim of the present study was therefore to assess the impact of [^{11}C]PIB and [^{18}F]FDG PET on the diagnostic process in a large sample of patients from a memory clinic, encompassing a wide spectrum of cognitive and/or behavioural symptoms.

METHODS

Subjects and diagnostic procedure

Between March 2009 and September 2011, 154 patients were included from the outpatient memory clinic of the VU University Medical Center. All patients underwent standard diagnostic work-up for dementia consisting of medical history, informant based history, physical and neurological examinations, screening laboratory tests, brain magnetic resonance imaging (MRI) and neuropsychological testing [26]. This was followed by paired [^{11}C]PIB and [^{18}F]FDG PET scans. To ensure substantial variation in pre-test diagnostic certainty, patients were recruited from two cohorts. 109 patients were enrolled in the Center for Translational Molecular Medicine (CTMM) LeARN (Leiden Alzheimer Research Netherlands) project. The aim of this project is to evaluate the cost-effectiveness of ancillary investigations in a memory clinic setting, encompassing a wide spectrum of cognitive and/or behavioural symptoms. Patients with a mini-mental state

examination (MMSE) score of at least 20 and a maximum clinical dementia rating (CDR) of 1, without major neurological and psychiatric disorders, recent vascular events and excessive substance abuse could participate in LeARN. In a second group of 45 patients, [^{11}C]PIB and [^{18}F]FDG PET scans were performed in case of substantial uncertainty about the diagnosis after the standard diagnostic work-up. Aforementioned inclusion criteria did not apply to the latter group of patients. A clinical diagnosis was made by consensus in a multidisciplinary team using established clinical criteria [27-31]. Diagnostic categories were AD, FTD, VaD, DLB, dementia-other (i.e. corticobasal degeneration (CBD), progressive supranuclear palsy (PSP)), MCI, subjective memory complaints (SMC), psychiatry, and neurology-other (i.e. normal pressure hydrocephalus). In December 2011, two-year clinical follow-up data (consisting of neurological and neuropsychological re-evaluation, without neuroimaging) were available for 39 patients. All patients gave written informed consent after they had received a complete written and verbal description of the study. The Medical Ethics Review Committee of the VU University Medical Center approved the study.

PET imaging and analysis

PET procedures have been reported elsewhere [26]. Briefly, PET scanning was performed on an ECAT EXACT HR+ scanner (Siemens/CTI, Knoxville, TN, USA). After a 10 minutes transmission scan, a dynamic 90 minutes emission scan was started simultaneously with an intravenous injection of 367±43 MBq [^{11}C]PIB. After co-registration of the MR images to the corresponding PET images, data were further analyzed using PVE-lab [32]. Regions of interest (ROI) were projected onto non-displaceable binding potential (BP_{ND}) images of [^{11}C]PIB. These images were generated by applying a 2-step basis-function implementation of the simplified reference tissue model (RPM2) [33]. For 12 patients, standardized uptake value ratio (SUVr) images of [^{11}C]PIB for the interval between 60 and 90 minutes (34), rather than BP_{ND} images, were generated because of patient movement and/or technical issues. Cerebellar grey matter was chosen as reference tissue.

After an interval of at least two hours to allow for decay of [^{11}C]PIB, an intravenous bolus of approximately 185 MBq of [^{18}F]FDG was administered. All subjects rested for 15 minutes before and for 35 minutes after injection with eyes closed and ears unplugged in a dimly lit room with minimal background noise. Next, patients underwent a 10 minute transmission scan followed by a 15 minute emission scan. Parametric SUVr images were extracted from the interval between 45 and 60 minutes after injection. In addition, [^{18}F]FDG scans were analyzed using the PMOD Alzheimer's discrimination (PALZ) tool [35]. Briefly, the PALZ tool compares age corrected [^{18}F]FDG uptake with predicted uptake. The t-values of all abnormal voxels within a predefined AD mask are summed, yielding an AD t-sum that automatically classifies the scan into either normal or abnormal.

For both tracers, T1-weighted MRI (3T Signa HDxt, General Electric, Milwaukee, USA) scans were used for co-registration and segmentation. Due to tracer synthesis failure, 21 patients did not undergo [^{11}C]PIB and [^{18}F]FDG PET scans on the same day but within an interval of at most 4 weeks. [^{11}C]PIB and [^{18}F]FDG PET scans were performed 2±1 months after dementia screening.

Visual assessment of parametric [^{11}C]PIB and [^{18}F]FDG images

BP_{ND} (n=142) and SUVr (n=12) images of [^{11}C]PIB and SUVr images of [^{18}F]FDG were assessed visually by an experienced nuclear medicine physician (BvB). [^{11}C]PIB PET scans were rated as either PIB-positive (PIB+, binding in more than one cortical brain region, i.e. frontal, parietal, temporal or occipital) or PIB-negative (PIB−, predominantly white matter binding). For [^{18}F]FDG PET scans, the reader had access to both the original images and the results of the PALZ tool. The nuclear medicine physician made the final decision. [^{18}F]FDG PET scans were interpreted as either normal or deviant and suggestive for AD (posterior cingulate and parietotemporal hypometabolism), FTD (frontotemporal metabolic impairment), DLB (occipital hypometabolism with relatively intact posterior cingulate gyrus) or dementia-other (PSP: mesenchepalon, prefrontal, caudate nucleus and thalamus hypometabolism, CBD: asymmetric hypometabolism with involvement of the basal

ganglia). [^{11}C]PIB and [^{18}F]FDG scans were assessed together and the reader had access to the clinical differential diagnosis.

Assessment of impact PET on the diagnostic process

After clinical assessment, i.e. prior to PET, one of the neurologists (NDP, AWL, YALP or PS) indicated the most probable (consensus) diagnosis on a questionnaire (Supplementary material). It was mandatory for the neurologists to select a diagnosis. In addition, the level of diagnostic certainty was estimated on a scale ranging from 0 to 100%. Next, PET scanning and subsequent rating was performed and the scans were discussed in a monthly meeting in the presence of the neurologists. Subsequently, the most probable diagnosis and corresponding diagnostic certainty were indicated again by the neurologist responsible for the initial diagnosis, now taking into account the findings on PET in addition to the clinical information. Furthermore, it was indicated whether both tracers, [^{11}C]PIB alone, [^{18}F]FDG alone or none contributed to the diagnostic process. To specify the utility of the individual tracers, the neurologists were asked whether [^{11}C]PIB and [^{18}F]FDG improved, confused or had only little or no effect on their understanding of a patient's disease.

Statistics

Differences in baseline values between groups were assessed using ANOVA, Kruskal-Wallis tests and χ^2 tests, where appropriate. Paired-samples t-tests were used to assess change of diagnostic certainty after PET. Independent-samples t-tests were used to assess differences in diagnostic certainty prior to PET between AD patients with PIB+ and PIB− PET scans, and between patients with and without diagnostic alteration after PET.

RESULTS

Subject characteristics

After the initial standard dementia work-up, patients received the following clinical diagnoses: AD (n=66), MCI (n=30), SMC (n=15), FTD (n=18), DLB (n=5), dementia-

other (n=10), psychiatry (n=6), and neurology-other (n=4). Characteristics according to diagnostic group are presented in Table 1. Diagnostic certainty did not differ between groups prior to PET.

Visual PET ratings

Table 1 also provides visual ratings of [^{11}C]PIB and [^{18}F]FDG PET scans. Most AD patients had PIB+ scans (61%) and most patients with non-Alzheimer dementia had [^{11}C]PIB− scans (67%). Consequently, still relatively high number of PIB− scans were seen in patients with a clinical AD diagnosis (39%), and PIB+ scans in patients with a clinical diagnosis of FTD (28%), DLB (80%), "dementia-other" (30%), MCI (57%) and SMC (20%). Furthermore, [^{18}F]FDG uptake patterns matched the clinical diagnosis of AD in 58% and of FTD in 33% of cases. [^{18}F]FDG scans were normal in 93% of SMC patients.

Change of diagnosis

The clinical diagnosis changed in 35 out of the 154 patients (23%) after disclosing PET results. Figure 1 shows an overview of clinical diagnoses and corresponding diagnostic certainty before and after PET for all dementia patients. In patients with a clinical diagnosis of AD (n=66), the diagnosis remained AD in 67% and was changed in 33% into either FTD (17%), "dementia-other" (6%), psychiatry (5%), DLB (3%), neurology-other (2%) or vascular dementia (2%). Figure 2 shows an illustrative patient whose clinical diagnosis changed from AD to CBD after revelation of a [^{11}C]PIB scan and a [^{18}F]FDG pattern suggestive of CBD.

A clinical diagnosis of FTD (n=18) remained FTD in 61% of cases, with the remaining 39% changing into AD (22%), SMC (6%), DLB (6%) or psychiatry (6%) after PET. The diagnosis of patients in the "dementia-other" category (n=10) changed to AD in two patients (20%), and a clinical diagnosis of DLB (n=5) was changed to AD in one case (20%) after PET. Two patients initially diagnosed as psychiatric or "neurology-other" were classified as FTD patients after PET. All clinical diagnoses of SMC or MCI, by definition remained unchanged after PET.

Table 1. Demographic and clinical characteristics according to clinical diagnosis prior to PET

	AD (n=66)	MCI (n=30)	SMC (n=15)	FTD (n=18)	DEM-other (n=10)	DLB (n=5)	Psychiatry (n=6)	NEU-other (n=4)
Age	64±7	64±9	64±6	67±6	65±10	65±7	56±7	59±9
Gender (M,F)	44,22	23,7[a]	7,8	12,6	5,5	3,2	4,2	2,2
MMSE	21±5[b]	27±2	28±2	23±5[c]	25±3	22±2	26±4	26±4
CDR	0.9±0.4[d]	0.5±0.1	0.4±0.3	0.8±0.7	1.2±0.7	1.0±0	0.3±0.3	0.9±0.3
% Pre-PET certainty	71±19	69±15	79±16	71±16	62±12	66±11	73±13	73±10
% [^{11}C]PIB+	61	57	20	28	30	80	0	50
[^{18}F]FDG pattern	10 normal 38 AD 8 FTD 2 DLB 7 Dem-other	15 normal 14 AD 1 DLB	14 normal 1 FTD	4 normal 4 AD 6 FTD 3 DLB 1 Dem-other	1 normal 3 AD 2 FTD 4 Dem-other	4 AD 1 DLB	4 normal 1 FTD 1 Dem-other	2 normal 2 AD

Data are presented as mean ± SD unless indicated otherwise.
Differences between groups were assessed using ANOVA with post hoc Bonferroni tests (age and MMSE), χ^2 (gender), and Kruskal Wallis with post hoc Mann Whitney U tests (CDR).
[a] MCI > SMC: $p<0.05$; [b] AD < MCI, SMC and psychiatry: $p<0.05$; [c] FTD < SMC: $p<0.05$; [d] AD > MCI, SMC and psychiatry: $p<0.05$

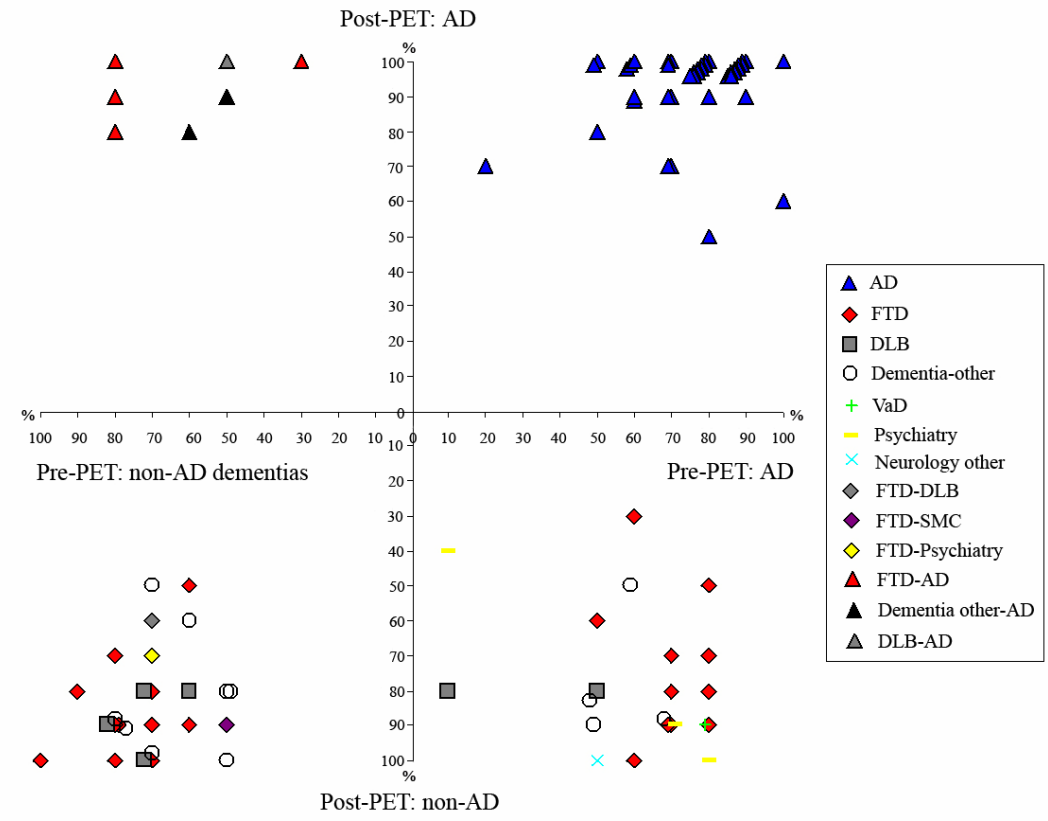

Figure 1. The scatter plot shows the diagnosis before and after PET of all demented patients (n=99). Patients in the upper right quadrant were diagnosed with AD at both baseline and after disclosure of PET results. Patients in the lower left quadrant were consistently diagnosed with a non-AD type of dementia. Patients in the left upper quadrant had a clinical diagnosis of a non-AD type of dementia prior to PET but their diagnoses changed to AD after PET. In the right lower quadrant, clinically diagnosed AD patients are presented whose diagnoses were changed after PET. The legend specifies the direction of diagnostic changes. The X- and Y-axis represent the confidence of the clinicians in the diagnosis before and after PET, respectively.
AD, Alzheimer's disease; FTD, frontotemporal dementia; DLB, dementia with Lewy bodies; VaD, vascular dementia; SMC, subjective memory complaints.

Diagnostic certainty

For all patients together, diagnostic certainty increased from 71±17% before to 87±16% after PET ($p<0.001$). Diagnostic confidence prior to PET was lower for diagnoses that changed after PET (62±18%) than for those that remained unchanged (73±15%, $p<0.05$). Also, diagnostic confidence prior to PET was higher in patients with a clinical AD diagnosis who showed PIB+ PET scans (75±16%) compared to those that showed PIB− scans (64±20%, $p<0.05$). A change in clinical diagnosis only occurred

when diagnostic confidence prior to PET was lower than 90% (Figure 1). Percent change in diagnosis after PET increased with lower pre-PET diagnostic confidence of the clinician (Figure 3).

Contribution of [^{11}C]PIB and [^{18}F]FDG to the diagnostic process

In patients whose diagnosis changed after PET, 7 were PIB+ and 28 patients were PIB−. Corresponding patterns of [^{18}F]FDG uptake fitted best to AD (12 cases), FTD (9 cases), DLB (2 cases) and dementia-other (2 cases), or were considered normal (10 cases). As illustrated in Table 2, combined [^{11}C]PIB and [^{18}F]FDG contributed most often to the diagnosis (104 cases), followed by [^{11}C]PIB only (29 cases), [^{18}F]FDG only (11 cases).

Utility of [^{11}C]PIB and [^{18}F]FDG

[^{11}C]PIB provided information that improved the clinicians understanding of a patient's disease in 125 (81%) patients, whilst for [^{18}F]FDG this was the case in 98 (64%) patients. [^{11}C]PIB and [^{18}F]FDG each confused the clinician in 8 (6%) and 12 (10%) cases respectively. [^{18}F]FDG more often (43 cases, 34%) had only little or no effect on the clinician's comprehension of a patient's disease than [^{11}C]PIB (20 cases, 16%).

Clinical follow-up

Two year clinical follow-up data were available for 39 patients. Six out of 7 patients with MCI and [^{11}C]PIB+ PET scans progressed to AD during follow-up, of whom five had a baseline [^{18}F]FDG scan suggestive of AD (Table 3). None of the five MCI patients with [^{11}C]PIB− and normal [^{18}F]FDG PET scans converted to AD. SMC patients did not convert during follow-up. Post-PET diagnosis changed in only 1 out of 23 demented patients (4%).

DISCUSSION

In this study we investigated the added value of combined [^{11}C]PIB and [^{18}F]FDG PET in the diagnostic process in a large sample of patients from a specialized memory clinic. The main result was that molecular imaging is indeed of additional value over standard diagnostic work-up, given that 23% of the initial clinical diagnoses changed and that diagnostic confidence increased after PET. The lower the diagnostic certainty prior to

PET, the larger was the percent change in diagnosis after PET. Two year clinical follow-up in a small subset of patients (n=39) showed that PET predicted progression to AD in MCI patients and that the clinical dementia diagnoses established after PET remained unchanged in 96% of cases. Application of [^{11}C]PIB and [^{18}F]FDG PET seems therefore most useful when confidence in a dementia diagnosis is low, and to increase prognostic certainty in patients with MCI.

Table 2. Contribution of [^{11}C]PIB and [^{18}F]FDG to diagnosis

Diagnosis prior to PET	**[^{11}C]PIB+[^{18}F]FDG**	**[^{11}C]PIB only**	**[^{18}F]FDG only**	**None of both**
Whole group	104/68%	29/28%	11/7%	10/6%
AD	45/68%	15/23%	3/5%	3/5%
MCI	19/63%	8/27%	1/3%	2/7%
SMC	7/47%	5/33%	1/7%	2/13%
FTD	14/78%	0/0%	3/17%	1/6%
Dementia-other	8/80%	0/0%	1/10%	1/10%
DLB	4/80%	0/0%	1/20%	0/0%
Psychiatry	4/67%	1/17%	1/17%	0/0%
Neurology-other	3/75%	0/0%	0/0%	1/25%

Data are presented as number/percentage.
Neurologists indicated whether both tracers, [^{11}C]PIB alone, [^{18}F]FDG alone or none contributed to the diagnostic process.

There was a frequent mismatch between clinical diagnosis and PET findings in this study. Absence of [^{11}C]PIB binding in clinically diagnosed AD patients is a common finding, but in general this is less than the 39% observed in the present study [15]. False negative findings can not be ruled out, as [^{11}C]PIB PET may not be able to detect more soluble species of Aβ-42 or atypical amyloid deposits [36]. This, however, is rare and it is more likely that these patients present with an AD-like phenotype that originates from non-amyloidogenic neuropathology. On the other hand, [^{11}C]PIB positive scans are regularly observed in patients with non-AD dementias, particularly in FTD and in DLB [16,22,24]. Autopsy studies in DLB patients have proven that these

are not false positive findings but truly reflect AD pathology, next to the presence of Lewy bodies [25]. With respect to FTD, it is known from post-mortem studies that about 15-20% of clinical FTD patients actually have AD [37]. These patients potentially mimic an FTD clinical syndrome that is actually driven by AD pathology, also known as "the frontal variant of AD" [38]. Alternatively, comorbid FTD and AD pathology may be present, with FTD pathology as the force driving the clinical presentation and amyloid pathology as by-product of aging. In the present study, clinicians tended to use [^{11}C]PIB PET mostly to rule out AD, which seems justified according to aforementioned neuropathological findings.

Table 3. Two year clinical follow-up of SMC and MCI patients

N	Dx prior to PET	[^{11}C]PIB	[^{18}F]FDG	Dx after 2 year FU
5	MCI	+	AD	AD
1	MCI	+	normal	AD
1	MCI	+	normal	MCI
2	MCI	-	normal	MCI
1	MCI	-	normal	FTD
1	MCI	-	normal	SMC
1	MCI	-	normal	Psychiatry
3	SMC	-	normal	SMC
1	SMC	+	normal	SMC

Dx, diagnosis; FU, follow-up; MCI, mild cognitive impairment; AD, Alzheimer's disease; SMC, subjective memory complaints; FTD, frontotemporal dementia.

Unlike [^{11}C]PIB, [^{18}F]FDG does not provide dichotomous information, as metabolic impairment occurs in many brain disorders that cause cognitive deterioration [10]. [^{18}F]FDG PET, however, can be used to identify patterns of cerebral glucose hypometabolism that characterize several neurodegenerative diseases. Due to its close relation with neuronal function and therefore cognitive status, [^{18}F]FDG PET can be helpful in diagnostic dilemmas [10]. In the present study, discrepancies between clinical diagnosis and [^{18}F]FDG PET findings were common. This may be explained by

diagnostic misclassification or by patients with atypical clinical presentations and equivalent patterns of glucose hypometabolism or by patients with an typical clinical presentation but atypical [^{18}F]FDG uptake.

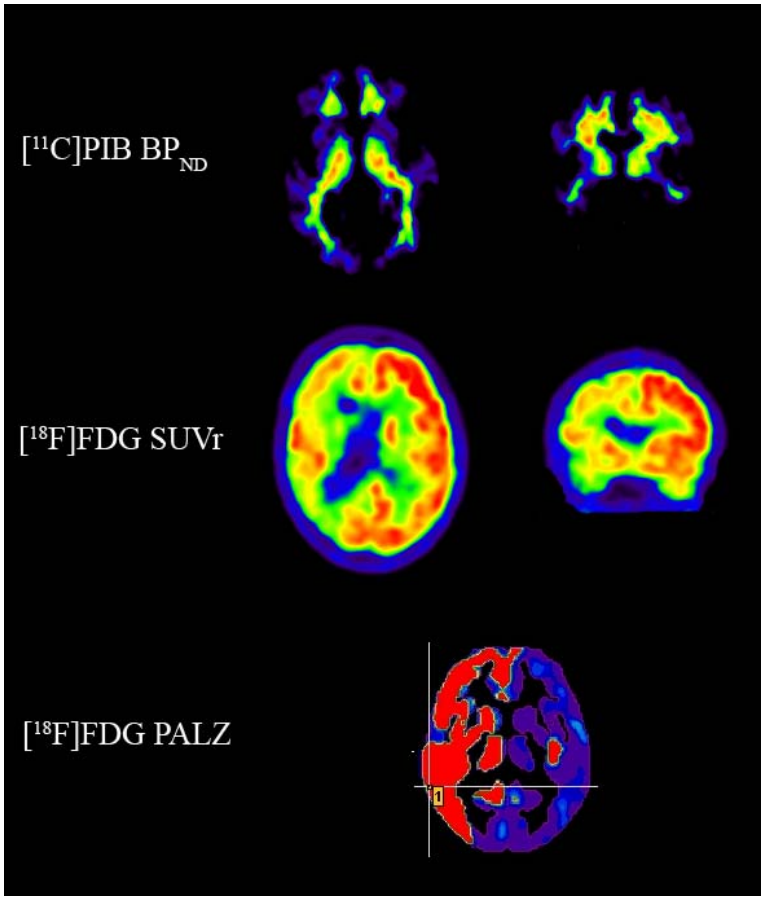

Figure 2. Example of a 59 year old male who visited the memory clinic for a second opinion. He presented with memory problems and spatial disorientation. This was confirmed by his spouse who also mentioned several behavioural problems like aggression and apathy. Neuropsychological testing revealed visuo-spatial disturbances, memory deficits and low MMSE (22) and CAMCOG (80) scores. Fronto-temporo-parietal brain atrophy was observed on MRI, most pronounced in the right hemisphere. Differential diagnosis after the multidisciplinary consensus meeting consisted of 1) atypical Alzheimer's disease (AD), 2) corticobasal degeneration (CBD), or 3) behavioural variant frontotemporal dementia. For this study, the probability diagnosis was set to AD with a diagnostic certainty of 50%. [^{11}C]PIB PET showed predominantly white matter binding and the diagnosis of AD is therefore highly unlikely. [^{18}F]FDG PET displayed extremely asymmetric metabolic impairment in the right hemisphere with involvement of the basal ganglia. This pattern is suggestive for CBD. According to these PET findings, the clinician changed the diagnosis to CBD with a diagnostic certainty of 90%. Two-year follow-up revealed cognitive deterioration (MMSE declined to 12), further progression of brain atrophy and a disease course that fits the diagnosis of CBD.

The case presented in Figure 2 illustrates the synergistic effect of using both pathophysiological and metabolic tracers. Indeed, clinicians indicated that the combination of [^{11}C]PIB and [^{18}F]FDG most often contributed to the diagnosis, followed by [^{11}C]PIB alone and [^{18}F]FDG alone. Cases in which [^{11}C]PIB was decisive were mainly initial clinical diagnoses of SMC, MCI or AD, whilst [^{18}F]FDG was essential in some cases with a clinical diagnosis of FTD, DLB or psychiatry. Based on the present study, combining [^{11}C]PIB and [^{18}F]FDG PET seems most useful in patients with low diagnostic certainty after standard diagnostic work-up. Cost-effectiveness of both [^{11}C]PIB and [^{18}F]FDG in a memory clinic setting have to be proven yet but, assuming that PET improves diagnostic accuracy, this will be greatly enhanced by the availability of disease modifying agents in the next future.

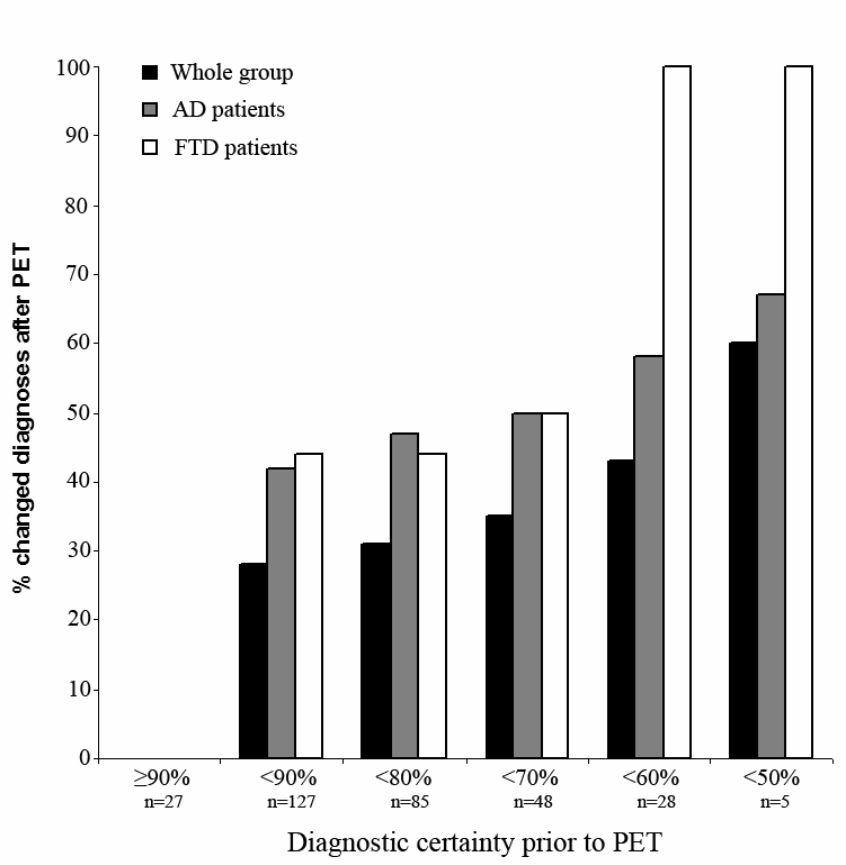

Figure 3. Bar diagrams indicating the percentage of diagnoses that changed after disclosing PET results as a function of diagnostic certainty prior to PET. Black bars represent the entire group, grey bars Alzheimer's disease (AD) patients alone, and white bars patients with frontotemporal dementia (FTD) alone.

The results of present study cannot simply be generalized to a general memory clinic population. Patients in this study visited a last resort memory clinic, most of them for a second or third opinion. The relatively young age of the patients (64 years on average) make an initial diagnosis more difficult as clinical presentations tend to overlap between diagnostic categories and this may not be representative for an older sample [1]. Furthermore, a subset of this sample underwent PET for diagnostic purposes because standard diagnostic work-up was not sufficient. All these factors together complicate the interpretation of the present results. In addition, the study design may have affected the outcome as it was mandatory for the neurologists to select a probability diagnosis, even in complex cases that would usually be postponed, awaiting for clinical follow-up and/or additional investigations. Another potential limitation of this study is the lack of post-mortem verification as no autopsy data were available. Alternatively, a subset of patients underwent two-year clinical follow-up and in these patients the post-PET diagnoses remained stable in demented patients. Finally, [^{11}C]PIB and [^{18}F]FDG were always assessed together and the nuclear medicine physician was provided with the clinical differential diagnosis, which may have affected the interpretation of both scans.

In conclusion, in a memory clinic [^{11}C]PIB and [^{18}F]FDG PET have additional value above standard diagnostic work-up. Molecular imaging in this setting is most useful for early diagnosis of AD and in case of high diagnostic uncertainty after standard work-up.

REFERENCES

1. Galton CJ, Patterson K, Xuereb JH et al. Atypical and typical presentations of Alzheimer's disease: a clinical, neuropsychological, neuroimaging and pathological study of 13 cases. *Brain* 2000;123:3484-3498.
2. Dubois B, Feldman HH, Jacova C et al. Research criteria for the diagnosis of AD: revising the NINCDS-ADRDA criteria. *Lancet Neurol* 2009;6:734-746.
3. Albert MS, DeKosky ST, Dickson D et al. The diagnosis of mild cognitive impairment due to Alzheimer's disease: recommendations from the National Institute on Aging-Alzheimer's Association workgroups on diagnostic guidelines for AD. *Alzheimers Dement* 2011;7:270-279.
4. McKhann GM, Knopman DS, Chertkow H et al. The diagnosis of dementia due to Alzheimer's disease: recommendations from the National Institute on Aging-Alzheimer's Association workgroups on diagnostic guidelines for AD. *Alzheimers Dement* 2011;7:263-269.
5. Rascovsky K, Hodges JR, Knopman D et al. Sensitivity of revised diagnostic criteria for the behavioural variant of frontotemporal dementia. *Brain* 2011;134:2456-2477.
6. McKeith IG, Dickson DW, Lowe J et al. Diagnosis and management of dementia with Lewy bodies: third report of the DLB Consortium. *Neurology* 2005;65:1863-1872.
7. Chételat G, Desgranges B, de la Sayette V et al. Mild cognitive impairment: Can FDG-PET predict who is to rapidly convert to Alzheimer's disease? *Neurology* 2003;60:1374-1377.
8. Landau SM, Harvey D, Madison CM et al. Comparing predictors of conversion and decline in mild cognitive impairment. *Neurology* 2010;75:230-238.
9. Drzezga A, Lautenschlager N, Siebner H et al. Cerebral metabolic changes accompanying conversion of MCI into Alzheimer's disease: a PET follow-up study. *Eur J Nucl Med Mol Imaging* 2003;30:1104-1113.
10. Silverman DH, Small GW, Chang CY et al. PET in evaluation of dementia: Regional brain metabolism and long-term outcome. *JAMA* 2001;286:2120-27.
11. Ishii K, Sakamoto S, Sasaki M et al. Cerebral glucose metabolism in patients with frontotemporal dementia. *J Nucl Med* 1998;39:1875-1878.
12. Ishii K, Imamura T, Sasaki M et al. Regional cerebral glucose metabolism in dementia with DLB and AD. *Neurology* 1998;51:125-130.
13. Ng S, Villemagne VL, Berlangieri S et al. Visual assessment versus quantitative assessment of 11C-PIB PET and 18F-FDG PET for detection of AD. *J Nucl Med* 2007;48:547-552.
14. Tolboom N, van der Flier WM, Boverhoff J et al. Molecular imaging in the diagnosis of Alzheimer's disease: visual assessment of [^{11}C]PIB and [^{18}F]FDDNP PET images. *J Neurol Neurosurg Psychiatry* 2010;81:882-884.
15. Klunk WE, Engler H, Nordberg A et al. Imaging brain amyloid in Alzheimer's disease with Pittsburgh Compound-B. *Ann Neurol* 2004;55:306-319.
16. Leyton CE, Villemagne VL, Savage S et al. Subtypes of progressive aphasia: application of the International Consensus Criteria and validation using β-amyloid imaging. *Brain* 2011;134:3030-3043.
17. Tolboom N, Yaqub M, van der Flier WM et al. Detection of Alzheimer pathology in vivo using both 11C-PIB and 18F-FDDNP PET. *J Nucl Med* 2009;50:191-197.
18. Morris JC, Roe CM, Grant EA et al. Pittsburgh compound B imaging and prediction of progression from cognitive normality to symptomatic Alzheimer disease. *Arch Neurol* 2009;66:1469-1475.
19. Okello A, Koivunen J, Edison P et al. Conversion of amyloid + and - MCI to AD over 3 years: an 11C-PIB PET study. *Neurology* 2009;73:754-760.
20. Forsberg A, Engler H, Almkvist O et al. PET imaging of amyloid deposition in patients with mild cognitive impairment. *Neurobiol Aging* 2008;29:1456-1465.
21. Koivunen J, Scheinin N, Virta JR et al. Amyloid PET imaging in patients with MCI: a 2-year follow-up study. *Neurology* 2011;76:1085-1090.
22. Rabinovici GD, Rosen HJ, Alkalay A et al. Amyloid vs FDG-PET in the differential diagnosis of AD and FTLD. *Neurology* 2011;77:2034-2042.

23. Lee JH, Kim SH, Kim GH et al. Identification of pure subcortical vascular dementia using 11C-Pittsburgh compound B. *Neurology* 2011;77:18-25.
24. Gomperts SN, Rentz DM, Moran E et al. Imaging amyloid deposition in Lewy body diseases. *Neurology* 2008;71:903-910.
25. Harding AJ, Halliday GM. Cortical Lewy body pathology in the diagnosis of dementia. *Acta Neuropathol* 2001;102:355-363.
26. Ossenkoppele R, Tolboom N, Foster-Dingley JC et al. Longitudinal imaging of Alzheimer pathology using [11C]PIB, [18F]FDDNP and [18F]FDG PET. *Eur J Nucl Med Mol Imaging* 2012;39:990-1000
27. McKhann G, Drachman D, Folstein M et al. Clinical diagnosis of Alzheimer's disease: report of the NINCDS-ADRDA Work Group on Alzheimer's Disease. *Neurology* 1984;34:939-944.
28. Litvan I, Agid Y, Calne D et al. Clinical research criteria for the diagnosis of progressive supranuclear palsy (Steele-Richardson-Olszewski syndrome): report of the NINDS-SPSP international workshop. *Neurology* 1996;47:1-9.
29. Neary D, Snowden JS, Gustafson L et al. Frontotemporal lobar degeneration: a consensus on clinical diagnostic criteria. *Neurology* 1998;51:1546-1554.
30. Riley D, Lang A. Clinical diagnostic criteria: Corticobasal degeneration and related disorders. *Advances in Neurology* 2000;8229-8234.
31. Petersen RC, Doody R, Kurz A et al. Current concepts in mild cognitive impairment. *Arch* Neurol 2001;58:1985-1992.
32. Svarer C, Madsen K, Hasselbalch SG, Pinborg LH, Haugbøl S, Frøkjaer VG, et al. MR-based automatic delineation of volumes of interest in human brain PET images using probability maps. *Neuroimage* 2005;24:969-979.
33. Wu Y, Carson RE. Noise reduction in the simplified reference tissue model for neuroreceptor functional imaging. *J Cereb Blood Flow Metab* 2002;22:1440-52.
34. Yaqub M, Tolboom N, Boellaard R et al. Simplified parametric methods for [11C]PIB studies. *Neuroimage* 2008;42:76-86.
35. Herholz K, Salmon E, Perani D et al. Discrimination between AD and controls by automated analysis of multicenter FDG PET. *Neuroimage* 2002;17:302-316.
36. Leinonen V, Alafuzoff I, Aalto S et al. Assessment of beta-amyloid in a frontal cortical brain biopsy specimen and by positron emission tomography with carbon 11-labeled Pittsburgh Compound B. *Arch Neurol* 2008;65:1304-1309.
37. Forman MS, Farmer J, Johnson JK et al. Frontotemporal dementia: clinicopathological correlations. *Ann Neurol* 2006;59:952-962.
38. Johnson JK, Head E, Kim R et al. Clinical and pathological evidence for a frontal variant of Alzheimer disease. *Arch Neurol* 1999;56:1233-1239.

Chapter 5.2

Amyloid Imaging in Prodromal Alzheimer's Disease

Alzheimers Research & Therapy 2011 3(5):26

Rik Ossenkoppele, Bart N.M. van Berckel & Niels D. Prins

ABSTRACT

Patients with mild cognitive impairment are at an increased risk of progression to Alzheimer's disease. However, not all patients with mild cognitive impairment progress, and it is difficult to accurately identify those patients who are in the prodromal stage of Alzheimer's disease. In a recent paper, Koivunen et al. report that Pittsburgh compound-B, an amyloid-beta positron emission tomography ligand, predicts the progression of patients with mild cognitive impairment to Alzheimer's disease. Twenty-one of 29 (72%) subjects with mild cognitive impairment had a positive Pittsburgh compound-B positron emission tomography scan. In their study, 15 of the 21 (71%) Pittsburgh compound-B-positive mild cognitive impairment patients progressed to Alzheimer's disease, whilst this was only the case in one out of eight (12.5%) Pittsburgh compound-B-negative mild cognitive impairment patients. Moreover, in these mild cognitive impairment patients, the overall amyloid burden increased with approximately 2.5% during the follow-up period. This seems to be in contrast with current theories that propose a flattening of the increase of brain amyloid deposition already in the preclinical stage of Alzheimer's disease. These findings may have important implications for the design of future clinical trials aimed at preventing progression to Alzheimer's disease by lowering the brain amyloid-beta burden in patients with mild cognitive impairment.

INTRODUCTION

Mild cognitive impairment (MCI) is considered a transitional stage between normal aging and dementia, in particular Alzheimer's disease (AD) [1]. The rate of conversion from MCI to AD is approximately 15% per year [2]. However, a substantial number of MCI patients have cognitive complaints caused by other conditions such as depression, stress, or sleeping disorders. It is therefore important for clinicians to identify individuals who are in the prodromal stage of AD, in particular because these patients may be a target for future disease modifying treatments. Advanced neuroimaging techniques may improve diagnostic accuracy in this patient group. The positron emission tomography (PET) ligand ^{11}C labeled Pittsburgh compound-B ([^{11}C]PIB) [3] detects fibrillary amyloid-beta (Aβ) *in vivo,* and may be used for this purpose. [^{11}C]PIB PET discriminates well between AD and controls [3,4] and between AD and other types of dementia [5], with the exception of dementia with Lewy bodies [6]. In patients with MCI, little is known about the predictive value of [^{11}C]PIB PET for progression to AD, or about the temporal changes in [^{11}C]PIB binding.

Recently, Koivunen et al. [7] reported the results of a prospective 2 year follow-up study, in which they assessed the predictive value of [^{11}C]PIB PET for progression to AD as well as the temporal changes in amyloid deposition in MCI patients. In the present commentary, we discuss the findings of this study and its potential implications for future clinical trials with disease modifying agents in prodromal AD.

Identifying prodromal AD with [^{11}C]PIB PET

Koivunen et al. performed amyloid imaging with [^{11}C]PIB PET at baseline and after 2 years of follow-up in a sample of 29 MCI patients. They divided MCI patients into converters and non-converters, based on clinical diagnosis at follow-up. At baseline, MCI converters had substantially higher mean [^{11}C]PIB levels as compared to MCI non-converters in the posterior cingulate, lateral frontal and temporal cortices and in putamen and caudate nucleus. After classifying [^{11}C]PIB PET scans into either positive or negative, using a cut-off point of 1.5 standardized uptake value ratio (SUVr), 21 of 29 (72%) subjects with MCI had a positive [^{11}C]PIB PET scan. In their study, 15 of the 21 (71%) PIB-positive MCI patients progressed to AD whilst this was only the case in one

out of eight (12.5%) PIB-negative MCI patients. These results are in accordance with several previous studies [8,9] and indicate that [^{11}C]PIB PET predicts progression to AD in MCI patients.

Temporal changes in amyloid burden in MCI

Recently, Jack et al. proposed a hypothetical model which positioned established and novel biomarkers in the continuum of AD [10]. This model elaborates on the amyloid-cascade hypothesis [11], which states that accumulation of Aβ initiates a cascade of neuropathological events, such as the formation of neurofibrillary tangles and neuroinflammation. This may in turn lead to neurodegeneration that presumably is followed by cognitive deterioration and finally results in dementia. Accumulation of Aβ is thought to set in decades before the first cognitive complaints arise, starts to accelerate already in the preclinical stage of AD, and reaches a relative plateau at the time symptoms emerge [12].

In the study by Koivunen et al., the overall amyloid burden in MCI patients increased with approximately 2.5% in 2 years. This increase was most prominent for those MCI patients who did not convert to AD. However, the overall increase in amyloid deposition was only modest, whilst hippocampal volumes decreased more strongly. This is in line with the idea that Aβ starts off the cascade and may uncouple at a later time point from neurodegenerative processes. Previous studies that related the presence of amyloid plaques with the course of brain atrophy [13] and glucose hypometabolism [14] also found this dissociation between amyloid deposition and structural and functional changes. The findings of Koivunen et al. suggest that the time span between deposition of amyloid and actual neurodegeneration, may perhaps be shorter than previously assumed, given the dynamic Aβ changes in MCI patients in this study.

A limitation of the study by Koivunen et al, especially given its longitudinal design, is the use of SUVr which overestimates [^{11}C]PIB binding in comparison with fully quantitative kinetic models [15]. Furthermore, SUVr does not correct for factors that are inherently associated with disease progression, such as heterogeneous flow effects in the region of interest compared to the reference region. We therefore argue that

quantitative modeling, and thus dynamic PET scanning, is essential for longitudinal amyloid imaging studies.

Amyloid imaging in clinical trials

The finding that [^{11}C]PIB PET can help identifying prodromal AD patients and that most MCI patients show an increased amyloid burden over time may have implications for the design of future clinical trials. First of all, amyloid imaging may be used as an enrichment strategy by enabling the selection of subjects at risk for AD, in order to administer disease modifying agents to the right patients. Secondly, Aβ PET ligands may be used as a secondary outcome measure to provide biological insight in cognitive primary outcome measures. Finally, amyloid imaging can be applied as surrogate outcome measure to test whether anti-amyloid therapies are efficacious by measuring the amount of fibrillary Aβ prior and after the time window of the intervention. In this respect one should note that patients with prodromal AD may still show an increase in amyloid plaque formation, instead of the previously assumed plateau due to an equilibrium between production and clearance of Aβ. This will affect power calculations for such trials. Current development of several fluor-18 labeled amyloid PET tracers (which have a longer half-life time compared to carbon-11) will further increase the availability and applicability of amyloid imaging in both clinical practice and for scientific purposes.

CONCLUSION

Koivunen et al. showed that amyloid imaging may be used to predict clinical progression to AD in patients with MCI and that, contrary to current hypothetical biomarker models, amyloid deposition increases over time in patients with MCI. These findings are relevant for the design of future clinical trials aimed at the prevention of progression to AD by lowering the Aβ burden in the brains of patients with MCI.

REFERENCES

1. Petersen RC, Smith GE, Waring SC et al. Mild Cognitive Impairment: Clinical Characterization and Outcome. *Arch Neurol* 1999:56:303-308.DeCarli C. Mild cognitive impairment: prevelance, prognosis, aetiology, and treatment. *Lancet Neurol* 2003;2:15-21.
2. Klunk WE, Engler H, Nordberg A et al. Imaging Brain Amyloid in Alzheimer's Disease with Pittsburgh Compound-B. *Ann Neurol* 2004;55:306-319.
3. Tolboom N, Yaqub M, van der Flier WM et al. Detection of Alzheimer Pathology In Vivo Using Both 11C-PIB and 18F-FDDNP PET. *J Nucl Med* 2009;50:191-197.
4. Rabinovici GD, Furst AJ, O'Neill JP et al. 11C-PIB PET imaging in Alzheimer disease and frontotemporal lobar degeneration. *Neurology* 2007;68:1205-1212.
5. Gomperts SN, Rentz DM, Moran E et al. Imaging amyloid deposition in Lewy body diseases. *Neurology* 2008;71:903-910.
6. Koivunen J, Scheinin M, Virta JR et al. Amyloid PET imaging in patients with mild cognitive impairment: a 2-year follow-up study. *Neurology* 2011;76:1085-1090.
7. Forsberg A, Engler H, Almkvist O et al. PET imaging of amyloid deposition in patients with mild cognitive impairment. *Neurobiol Aging* 2008;29:1456-1465.
8. Okello A, Koivunen J, Edison P et al. Conversion of amyloid positive and negative MCI to AD over 3 years: An 11C-PIB PET study. *Neurology* 2009;73:754-760.
9. Jack Jr CR, Knopman DS, Jagust WJ et al. Hypothetical model of dynamic biomarkers of the Alzheimer's pathological cascade. *Lancet Neurol* 2010;9:119-128.
10. Hardy JA, Selkoe DJ. The amyloid hypothesis of Alzheimer's disease: progress and problems on the road to therapeutics. *Science* 2002;197:353-356.
11. Engler H, Forsberg A, Almkvist O et al. Two-year follow-up of amyloid deposition in patients with Alzheimer's disease. *Brain* 2006;129:2856-2866.
12. Tosun D, Schuff N, Mathis CA et al. Spatial patterns of brain amyloid-beta burden and atrophy rate associations in mild cognitive impairment. *Brain* 2011;134:1077-1088.
13. Forster S, Grimmer T., Miederer I et al. Regional expansion of hypometabolism in Alzheimer's disease follows amyloid deposition with temporal delay. *Biol Psychiatry* 2012;71:792:797.
14. Yaqub M, Tolboom N, Boellaard R et al. Simplified parametric methods for [11C]PIB studies. *NeuroImage* 2008;42:76-86.

Chapter 6

Summary

General discussion

Future perspectives

SUMMARY

The aims of the studies described in this thesis were (1) to describe longitudinal patterns of [^{11}C]PIB and [^{18}F]FDDNP binding and [^{18}F]FDG uptake, (2) to investigate the inter-relationships between amyloid burden, glucose metabolism and cognition in cognitively normal elderly, (3) to explore distributions of amyloid pathology and glucose metabolism according to age-at-onset and APOE genotype in order to find plausible mechanisms underlying clinical heterogeneity in AD, and (4) to determine the additional value of [^{11}C]PIB and [^{18}F]FDG PET in the diagnostic work-up in a memory clinic.

In this chapter, the main findings of these studies are summarized and discussed. In addition, possibilities and directions for future research are given.

Main findings

First, longitudinal aspects of Alzheimer pathology were assessed. In **chapter 2.1** several models for analyzing [^{11}C]PIB data were evaluated in order to identify the method of choice for measuring longitudinal changes in amyloid deposition. Repeat [^{11}C]PIB scans, with on average an interval of 2.5 years, were analyzed using receptor parametric mapping (RPM2), reference Logan and standardized uptake value ratios (SUVr). SUVr values overestimated [^{11}C]PIB binding with approximately 13%, whereas reference Logan values were on average 6% lower than RPM2. Furthermore, tracer delivery to the cortex relative to reference cerebellar grey matter (R_1) decreased over time in AD patients, but not in MCI patients and controls. Simulations showed that SUVr highly fluctuate as a function of uptake period and of heterogeneous changes in blood flow. It was therefore concluded that for reliable assessment of [^{11}C]PIB binding over time, for example in drug intervention studies or when studying pathophysiological changes associated with progression of disease, quantitative methods for data analysis are essential.

In **chapter 2.2** temporal changes in [^{11}C]PIB and [^{18}F]FDDNP binding and [^{18}F]FDG uptake were assessed. A significant increase in global cortical [^{11}C]PIB binding was found in MCI patients, but not in AD patients or controls. No changes were observed in specific [^{18}F]FDDNP binding. [^{18}F]FDG uptake was reduced at follow-up in the AD group only, especially in frontal, parietal and temporal cortices. These findings indicate that

[^{11}C]PIB and [^{18}F]FDG track molecular changes in different stages of AD and thus provide complementary information. It was also established that [^{18}F]FDDNP is not useful for tracking progression of AD.

Chapter 3 describes the inter-relationships between amyloid deposition, glucose metabolism and cognition in cognitively normal elderly. A longstanding debate in the field of cognitive aging is centred on how some individuals maintain cognitive function despite molecular evidence of amyloid pathology, whereas others show less brain resilience. Higher [^{11}C]PIB retention in the precuneus was associated with higher metabolic activity in AD specific regions and with worse visual episodic memory performance. [^{18}F]FDG uptake did not correlate with cognitive function across groups. Within individuals with elevated [^{11}C]PIB retention, however, increased metabolic activity related to better performance on verbal episodic memory tasks. These findings suggest that asymptomatic elderly with cerebral amyloidosis are, at least temporarily, able to preserve cognitive function through enhanced neuronal function.

Chapter 4 aims to characterize variability in disease pathways that may account for clinical heterogeneity often observed in AD patients. For instance, early-onset AD patients often present with a distinct (non-memory) cognitive profile. In **chapter 4.1** 100 AD patients were divided into younger and older groups (by median split at age 62) in order to investigate the role of age-at-onset on extent and distribution of amyloid deposition and glucose metabolism. Younger patients showed increased [^{11}C]PIB binding and decreased [^{18}F]FDG uptake in the parietal cortex. Furthermore, parietal amyloid pathology and metabolic activity were directly related to visuo-spatial functioning (for both [^{11}C]PIB and [^{18}F]FDG) and executive functions and attention ([^{18}F]FDG only) in younger AD patients. This led to the conclusion that increased amyloid burden, together with metabolic dysfunction, in the parietal cortex of younger AD patients may contribute to the distinct cognitive profile frequently observed in these patients.

The same data set was used to investigate the relationships between APOE genotype and distributions of amyloid load and glucose metabolism (**chapter 4.2**). AD patients without an APOE ε4 allele showed greater amyloid pathology than APOE ε4 carriers, whereas carrying APOE ε4 was associated with more profound metabolic impairment

in posterior parts of the brain in a dose-dependent fashion. This differential impact of APOE genotype provides evidence for the notion that AD develops along distinct disease pathways in APOE ε4 carriers and non-carriers. In addition, this may partially explain differences in clinical presentation according to APOE status.

Chapter 5 focuses on the application of molecular imaging using PET in a clinical setting. **Chapter 5.1** describes the diagnostic performance of [^{11}C]PIB and [^{18}F]FDG PET in 154 memory clinic patients with a wide variety of cognitive and behavioural deficits. Outcome measures were (change in) clinical diagnosis and confidence in that diagnosis before and after disclosing PET results. PET results led to a diagnostic change in 23% of the patients and diagnostic confidence increased from 71 to 87% after PET. Diagnostic change only occurred in cases of low diagnostic confidence (≤80%) prior to PET. It was concluded that combined [^{11}C]PIB and [^{18}F]FDG PET is of additional value in the diagnostic work-up in a memory clinic. In **chapter 5.2** the potential of [^{11}C]PIB PET to identify AD in a prodromal phase is discussed. Review of the literature shows that MCI patients who progress to AD have cerebral amyloidosis in the vast majority of cases, whereas [^{11}C]PIB negative patients rarely convert. [^{11}C]PIB PET is thus a strong predictor for clinical progression in prodromal AD patients.

GENERAL DISCUSSION

The amyloid cascade hypothesis

Development of the PET tracer [^{11}C]PIB enabled for the first time *in vivo* testing of the amyloid cascade hypothesis [1]. This leading hypothesis for the pathogenesis of AD states that deposition of Aβ initiates a cascade of neuropathological events (e.g. neurofibrillary tangle formation, inflammation of the brain or vascular pathology) that lead to neuronal damage and cell death and ultimately result in the onset of dementia [2,3]. Aβ starts to accumulate approximately 15 years before the first clinical signs of AD and is present in 20-40% of asymptomatic elderly [4-9]. There is increasing evidence that this is not benign, as individuals with cerebral amyloidosis are at risk for future cognitive decline [8,10-12] and already show subtle morphological changes in AD specific regions [13-17]. At a functional level, amyloid pathology in cognitively normal individuals is often associated with increased brain activity [18-21]. This may

be explained by at least two mechanisms. First, a recent study showed that unilateral whisker stimulation leads to amyloid plaque growth in transgenic mice, suggesting that synaptic activity causes Aβ accumulation [22]. Second, heightened brain activity may be a compensatory response to neurotoxic effects of Aβ [23-25]. Data in this thesis support the "compensation" hypothesis, as increased metabolic activity was associated with better verbal episodic memory performance in elderly who harboured amyloid pathology (**chapter 3**).

In a recently proposed hypothetical biomarker model [26], amyloid deposition follows a sigmoid-shaped trajectory [27]. Amyloid deposition supposedly starts to rise in the asymptomatic phase, flattens when clinical symptoms emerge and reaches a relative plateau when AD dementia is diagnosed. In this thesis, it was shown that, contrary to this biomarker model, [^{11}C]PIB binding increases over time in MCI patients. This occurred in both converters and non-converters (**chapter 2.2 and 5.2**). Furthermore, in accordance with the biomarker model a plateau effect was found in the small series of AD patients. Some recent studies, however, reported a slight increase in [^{11}C]PIB SUVr, suggesting that Aβ accumulation is a more dynamic process than initially thought [8,28,29].

The clinico-pathological correlation for amyloid deposition is modest, particularly in comparison with biomarkers of "downstream" processes such as glucose metabolism or brain atrophy. A possible explanation is that Aβ starts to accumulate long before cognitive deficits manifest [4,5]. One may hypothesize that Aβ initiates a cascade of events in an early disease stage and gets detached from neurodegeneration and cognitive decline in later stages. This idea is further supported by brain regions that show high [^{11}C]PIB binding but relatively mild brain atrophy (e.g. frontal cortex) or the other way around (e.g. medial temporal lobe) in AD patients [30]. The missing link between amyloid burden and brain damage further down the cascade could be neurofibrillary tangle pathology [31]. Results in **chapter 2.2** show that [^{18}F]FDDNP PET does not seem to have the potential to fill this gap. As such, there is great interest for a suitable PET tracer for visualisation and quantification of tangle pathology to further investigate this hypothesis.

Longitudinal amyloid imaging

Amyloid imaging is a promising tool for monitoring the efficacy of disease modifying agents that target amyloid pathology. In a recent phase 2 clinical trial with bapineuzumab, a monoclonal Aβ antibody, [^{11}C]PIB PET was used to quantify changes in amyloid burden [28]. Unfortunately, bapineuzumab had no effect on cognitive outcome. In contrast with this outcome, however, the treatment arm showed significantly reduced amyloid load compared with placebo patients and this "biological" effect contributed to the decision to proceed with a phase 3 trial. Recently, the phase 3 study was terminated prematurely due to a lack of clinical effect, despite stable Aβ levels in the treatment arm compared with increased Aβ deposition in the placebo group. In this longitudinal bapineuzumab study, [^{11}C]PIB data were analysed using SUVr, a method that is often used because of its computational simplicity and relatively short scan duration (10-30 minutes) [32]. In **Chapter 2.1**, it was shown that, for repeated imaging, this method is inferior to fully quantitative methods such as RPM2 or reference Logan [33,34]. SUVr overestimates specific binding in an inconsistent manner and is vulnerable to heterogeneous flow effects that potentially occur during disease progression or due to treatment effects. The majority of longitudinal studies have been performed using SUVr, making results of these studies hard to interpret. Given the enormous financial costs and human efforts involved in clinical trials, these studies should not be performed using suboptimal methods such as SUVr, which carry the inherent risk that ineffective drugs are not identified appropriately or, more importantly, that potential effective drugs are dismissed. Longitudinal amyloid imaging should therefore be performed using quantitative methods.

Clinical heterogeneity

The core clinical symptom of AD is memory disturbance, but especially young patients often present with other cognitive deficits such as agnosia, apraxia or aphasia [35,36]. This clinical heterogeneity led to the recognition of posterior cortical atrophy (visual), logopenic aphasia (language) and frontal (executive/behavioural) variants of AD [37-39]. These subtypes are characterized by reduced grey matter density and metabolic dysfunction in brain regions responsible for their clinical features [40-43]. Amyloid imaging provides a unique opportunity to study the distribution of neuropathology underlying these subtypes of AD *in vivo*. Results in **chapter 4.1** showed that younger

AD patients have most prominent deficits in non-memory domains and are relatively more vulnerable for metabolic dysfunction and amyloid deposition in the parietal cortex. Furthermore, the magnitude of [^{11}C]PIB binding was directly related to visuo-spatial functioning in young AD patients. This suggests that clinical heterogeneity does not only result from topographical differences in neuronal dysfunction, but likely originates from distinct distributions of amyloid pathology. Another factor that potentially contributes to clinical manifestation of AD is APOE genotype [44]. The APOE ε4 allele is strongly associated with AD-like cognitive, functional and structural changes in asymptomatic and prodromal AD patients [45-48], but its effect on patients who have already been diagnosed with AD dementia is unclear [49-52]. Previous studies suggest that AD patients without an APOE ε4 allele are more likely to present in an atypical manner [44,53]. In **chapter 4.2** it was shown that these patients have higher amyloid load, specifically in the frontal cortex, compared with APOE ε4 carriers, possibly related to this clinical presentation.

Pioneering [^{11}C]PIB studies showed that subjects had either high or low tracer retention throughout the cortex. Due to this bimodal distribution, [^{11}C]PIB PET was initially considered a typical "on/off" marker that only indicated the presence or absence of amyloid pathology. To date, this is the main diagnostic purpose in the use of amyloid imaging. More recent studies have shown that quantification of both extent and distribution of amyloid in the brain could also be relevant. For instance, the degree of cortical amyloid load was associated with disease severity [54], and especially [^{11}C]PIB retention in the temporal cortex was related to memory function [55]. Data in this thesis show that regional amyloid burden differs according to age-at-onset and genetic predisposition and is related to cognitive function in AD patients who had molecular evidence for cerebral amyloidosis. Elaborate exploration of regional amyloid load is most likely not useful in a memory clinic, but seems to be worthwhile for research purposes to evaluate its impact on clinical heterogeneity.

The nuclear medicine physician as in vivo neuropathologist?

FDA approval of Amyvid (also known as [^{18}F]florbetapir [56]) in April 2012 made amyloid imaging available for widespread clinical use. **Chapter 5.1** gives an impression what can be expected when amyloid imaging (in conjunction with [^{18}F]FDG PET) is

used as an add-on to standard diagnostic work-up in a memory clinic. Molecular imaging had a substantial impact on the diagnostic process due to frequently conflicting PET results, which led to a change in diagnosis in almost a quarter of all patients. Two factors had a major impact on diagnostic change: 1) low diagnostic confidence prior to PET, and 2) a negative [^{11}C]PIB scan. This seems justified as patients with a negative amyloid scan rarely have cerebral amyloid plaques at autopsy [57,58]. On the other hand, amyloid positive scans may be less informative due to the possibility of comorbid pathologies in patients with DLB or vascular dementia [59,60], particularly in older patients. Amyloid imaging can be misleading and it is important to recognize that amyloid PET measures presence of fibrillary amyloid plaques, but it is not a surrogate for a clinical diagnosis of AD dementia. It should also be emphasized that amyloid imaging is only valuable in conjunction with thorough clinical evaluation of the patient. The most optimal use of the technique is probably in young patients (<70 years) with low pre-PET diagnostic confidence for 1) an early diagnosis of AD or 2) a differential diagnosis that includes AD with an atypical presentation.

The development of [^{18}F]-labeled amyloid tracers (e.g. florbetapir, flutemetamol, florbetaben [56,61,62]) will increase future use of amyloid imaging in the memory clinics. The longer half-life of ^{18}F compared to ^{11}C (110 versus 20 min) enables tracer transportation to medical centres with a PET camera but without synthesis facilities. It also reduces costs as multiple patients can be scanned using a single production. Nevertheless, amyloid imaging is an expensive technique and, with Aβ measurements in CSF, a cheaper alternative is available. Measurements in CSF have the advantage that multiple measures are obtained at the same time (e.g. Aβ-42, Aβ-40, p-tau, t-tau). In addition, patients are not exposed to radiation [63]. Disadvantages are its invasive character and the fact that analyses are hindered by standardization problems [64]. Amyloid PET and CSF-Aβ tend to correlate well (between -0.48 and -0.72) but concordance ranges from only 54% to 100% [65-68], indicating that they possibly measure different aspects of amyloid pathology. Amyloid PET maps fibrillary amyloid deposits whereas in CSF the more soluble species of Aβ are detected. This discrepancy is nicely illustrated in patients with a rare Arctic APP mutation that obstructs fibrillization of Aβ. These patients show an AD-like pattern in CSF whereas there is no

[^{11}C]PIB retention when imaged with PET [69]. Head-to-head comparisons in a memory clinic population are needed to determine test characteristics for these biomarkers.

Amyloid imaging in 2020

The development of [^{11}C]PIB caused a major paradigm shift in diagnostic thinking and led to new criteria to diagnose AD in an earlier stage. These (research) criteria state that individuals with a positive amyloid scan have AD, even when their cognitive functions are intact [70]. Furthermore, patients with a clinical diagnosis of AD but a negative amyloid scan suffer from "dementia unlikely due to AD", according to new McKhann criteria [71]. This implies that 1) clinical symptoms are no longer a prerequisite for AD, and 2) a textbook AD patient without cerebral amyloid pathology does not have AD. This illustrates a shift from a primarily clinically oriented diagnosis towards a process with an inclusive role of pathophysiological markers. This raises the question whether AD is a clinical syndrome or an abbreviation for "amyloid disease". The field is moving towards the latter and, consequently, it is expected that the use of amyloid imaging in the memory clinic will increase rapidly. Other future applications of amyloid imaging could be patient selection (confirming that AD dementia patients have amyloid pathology and to identify individuals at risk) and monitoring clinical trials or approved interventions.

The availability of a tool that possibly detects AD 15 years before onset of cognitive symptoms brings up several ethical issues [4,5]. To date, there is no cure available, so there is no direct benefit from disclosing amyloid imaging results. Nevertheless, should cognitively normal persons be informed about their amyloid status? If so, what to tell them if the scan is abnormal? What would be the prognosis for such an individual? To answer these questions, more knowledge should be acquired about the significance and consequences of amyloid pathology in asymptomatic individuals. Current literature indicates that these individuals are at risk for deterioration of cognitive functions in the next years [8,10-12]. If this association between amyloid pathology and future cognitive decline proves to be robust, it could be argued that the Prime Minister, CEO's of large multinationals and the head coach of the national soccer team should undergo amyloid imaging prior to their assignment. For example, Ronald Reagan (born in 1911 and president of the USA between 1981 and 1989) was diagnosed with AD in 1994. His

family, colleagues and journalists noted memory problems, spatial disorientation and subtle problems of speech already during his second administration [72]. If an amyloid PET scan had been made at the time of his re-election in 1985 (9 years before he was diagnosed with AD dementia), it would probably have shown widespread amyloid pathology throughout the presidential brain. This may foreshadow subtle cognitive decline, which may, in turn, negatively affect high-level decision making and lead to suboptimal governmental policy. On the contrary, if an amyloid PET scan is negative, it is highly unlikely that within the next decade cognitive problems will emerge that can be attributed to AD. Many questions are still unanswered but it is likely that future application of amyloid imaging will go beyond memory clinic patients in that it will be open to asymptomatic elderly as well, particularly if disease modifying agents become available.

Methodological considerations

Patient selection

The data presented in **chapters 2.1** and **2.2** were obtained in a relatively small sample. Outliers could thus have influenced results. Multiple quality checks of the PET data were performed, however, and aberrant values due to technical issues were excluded. Consequently, conclusions drawn from these data are likely to be valid.

Due to the focus of the Alzheimer center VUmc on early-onset dementia, in addition to demanding PET protocols, AD patients that participated in the studies were relatively young. This minimizes age-related brain damage such as vascular pathology and provides the unique opportunity to study a "purer" form of AD. On the other hand, it may not be entirely valid to generalise results to an average AD patient, who on average is 10 years older.

Data acquisition and analysis

PET data were analysed without applying motion correction. This could potentially have affected accuracy of the measurements. During the 90 minutes scanning period, however, patients were continuously checked for motion using laser beams. Subjects with severe motion were excluded from analysis.

PET data were not corrected for partial volume effects. This was a deliberate choice because of the inherent risk of overcorrection that may lead to an artificially high signal

[73]. This approach guarantees that any increase observed in [^{11}C]PIB or [^{18}F]FDDNP binding is true, although underestimation may conceal potential associations. The opposite effect is true for [^{18}F]FDG. At present, there is no reliable partial volume correction method available for brain PET scans so this needs further elaboration before standard application.

FUTURE PERSPECTIVES

A common phenomenon in science is that studies raise more questions than they answer. To start, amyloid pathology and neuronal function are weakly correlated in several brain regions. Possibly some brain structures are more sensitive to neurotoxic effects of amyloid pathology than others. More likely, however, other factors mediate the effects of amyloid pathology on the distribution of neuronal dysfunction and brain atrophy. Potential candidates are tau pathology, neuroinflammation, oligomeric Aβ and functional connectivity. The first three are awaiting suitable (PET) markers but functional connectivity can already be measured using functional MRI or MEG. These techniques in conjunction with amyloid imaging are of particular interest for further investigation of clinical heterogeneity in AD.

Other unresolved questions further down the amyloid cascade are why some individuals are resilient to brain pathology and maintain normal cognitive function and why the relationships between imaging markers and cognitive performance are far from perfect. Answers may rely on the same concept: cognitive reserve. Individuals with higher education, greater pre-morbid IQ, more life-long engagement in physical and cognitive activities, no APOE ε4 allele and a healthy lifestyle are capable of better cognitive performance under equivalent conditions of brain damage. Studies including a combination of these cognitive reserve factors in conjunction with molecular and structural brain imaging and longitudinal cognitive testing may help to more accurately predict onset and progression of the disease.

Another important point of attention for future research is further validation of the most widely used pathophysiological (amyloid imaging and CSF-Aβ) and topographical ([^{18}F]FDG PET, CSF-tau and structural MRI) markers in the memory clinic. The best

biomarker (or combination of markers) for diagnosing AD dementia or prodromal AD/MCI-due-to-AD has yet to be determined. This can only be accomplished by head-to-head comparisons in large samples, with extended clinical follow-up, preferentially followed by neuropathological examination. The concept of preclinical or asymptomatic AD needs further elaboration as well, which requires even longer follow-up studies given the estimated time of 15 years between Aβ deposition and cognitive symptoms. Better understanding of both preclinical and symptomatic stages is crucial for the development of disease modifying agents to eventually prevent full blown AD.

REFERENCES

1. Klunk W, Engler H, Nordberg A, et al. Imaging brain amyloid in Alzheimer disease with Pittsburgh compound-B. Ann Neurol 2004;55:306-19.
2. Hardy JA, Higgins GA. Alzheimer's disease: The amyloid cascade hypothesis. Science 1992;256:184-5.
3. Hardy J, Selkoe DJ. The amyloid hypothesis of Alzheimer's disease: Progress and problems on the road to therapeutics. Science 2002;297:353-6.
4. Rowe C, Ellis K, Rimajova M, et al. Amyloid imaging results from the Australian imaging, biomarkers and lifestyle study of aging. Neurobiol Aging 2010;31:1275-83.
5. Bateman RJ, Xiong C, Benzinger TL, et al. Clinical and biomarker changes in dominantly inherited Alzheimer's disease. N Engl J Med 2012;367:795-804.
6. Price JL, Morris JC. Tangles and plaques in nondemented aging and "preclinical" Alzheimer's disease. Ann Neurol 1999;45:358-68.
7. Bennett DA, Schneider JA, Arvanitakis Z, et al. Neuropathology of older persons without cognitive impairment from two community-based studies. Neurology 2006;66:1837-44.
8. Villemagne VL, Pike KE, Chételat G, et al. Longitudinal assessment of aβ and cognition in aging and Alzheimer disease. Ann Neurol 2011;69:181-92.
9. Fleisher AS, Chen K, Liu X, et al. Apolipoprotein E ε4 and age effects on florbetapir positron emission tomography in healthy aging and AD. Neurobiol Aging 2013;34:1-12.
10. Morris J, Roe C, Grant E, et al. Pittsburgh compound B imaging and prediction of progression from cognitive normality to symptomatic AD. Arch Neurol 2009;6612:1469-75.
11. Storandt M, Mintun MA, Head D, et al. Cognitive decline and brain volume loss as signatures of cerebral amyloid-beta peptide deposition identified with [^{11}C]PIB: Cognitive decline associated with abeta deposition. Arch Neurol 2009;66:1476-81.
12. Resnick SM, Sojkova J, Zhou Y, et al. Longitudinal cognitive decline is associated with fibrillar amyloid-beta measured by [^{11}C]PIB. Neurology 2010;74:807-15.
13. Dickerson BC, Bakkour A, Salat DH, et al. The cortical signature of AD: Regionally specific cortical thinning relates to symptom severity in very mild to mild AD dementia and is detectable in asymptomatic amyloid-positive individuals. Cereb Cortex 2009;19:497-510.
14. Mormino EC, Kluth JT, Madison CM, et al. Episodic memory loss is related to hippocampal-mediated beta-amyloid deposition in elderly subjects. Brain 2009;132:1310-23.
15. Chételat G, Villemagne VL, Bourgeat P, et al. Relationship between atrophy and beta-amyloid deposition in Alzheimer disease. Ann Neurol 2010;67:317-24.
16. Oh H, Mormino EC, Madison C, et al. B-Amyloid affects frontal and posterior brain networks in normal aging. Neuroimage 2011;54:1887-95.
17. Becker JA, Hedden T, Carmasin J, et al. Amyloid-β associated cortical thinning in clinically normal elderly. Ann Neurol 2011;69:1032-42.
18. Cabeza R, Anderson ND, Locantore JK, et al. Aging gracefully: Compensatory brain activity in high-performing older adults. Neuroimage 2002;17:1394-402.
19. Rosen AC, Prull MW, O'Hara R, et al. Variable effects of aging on frontal lobe contributions to memory. Neuroreport 2002;13:2425-8.
20. Park DC, Reuter-Lorenz P. The adaptive brain: Aging and neurocognitive scaffolding. Annu Rev Psychol 2009;60:173-96.
21. Mormino EC, Brandel MG, Madison CM, et al. Aβ deposition in aging is associated with increases in brain activation during successful memory encoding. Cereb Cortex 2012;22:1813-23.
22. Bero A, Yan P, Roh J, et al. Neuronal activity regulates the regional vulnerability to amyloid-β deposition. Nat Neurosci 2011;14:750-6.
23. Buckner R, Snyder A, Shannon B, et al. Molecular, structural, and functional characterization of Alzheimer disease: Evidence for a relationship between default activity, amyloid, and memory. J Neurosci 2005;25:7709-17.
24. Cohen A, Price J, Weissfeld L, et al. Basal cerebral metabolism may modulate the cognitive effects of Aβ in MCI: An example of brain reserve. J Neurosci 2009;29:14770-8.

25. Stern Y. Cognitive reserve in ageing and Alzheimer's disease. Lancet Neurol 2012;11:1006-12.
26. Jack CR, Knopman DS, Jagust WJ, et al. Hypothetical model of dynamic biomarkers of the Alzheimer's pathological cascade. Lancet Neurol 2010;9:119-28.
27. Jack CR, Vemuri P, Wiste HJ, et al. Shapes of the trajectories of 5 major biomarkers of Alzheimer disease. Arch Neurol 2012;69:856-67.
28. Rinne JO, Brooks DJ, Rossor MN, et al. ^{11}C-PIB PET assessment of change in fibrillar amyloid-beta load in patients with AD treated with bapineuzumab: A phase 2, double-blind, placebo-controlled, ascending-dose study. Lancet Neurol 2010;9:363-72.
29. Villain N, Chételat G, Grassiot B, et al. Regional dynamics of amyloid-β deposition in healthy elderly, mild cognitive impairment and Alzheimer's disease: A voxelwise PIB-PET longitudinal study. Brain 2012;135:2126-39.
30. Förster S, Grimmer T, Miederer I, et al. Regional expansion of hypometabolism in AD follows amyloid deposition with temporal delay. Biol Psychiatry 2011;71:792-797.
31. Desikan RS, McEvoy LK, Thompson WK, et al. Amyloid-β--associated clinical decline occurs only in the presence of elevated p-tau. Arch Neurol 2012;69:709-13.
32. Lopresti BJ, Klunk WE, Mathis CA, et al. Simplified quantification of [^{11}C]PIB amyloid imaging PET studies: A comparative analysis. J Nucl Med 2005;46:1959-72.
33. Wu Y, Carson RE. Noise reduction in the simplified reference tissue model for neuroreceptor functional imaging. J Cereb Blood Flow Metab (2002);22:1440-52.
34. Logan J, Fowler J, Volkow N, et al. Distribution volume ratios without blood sampling from graphical analysis of PET data. J Cereb Blood Flow Metab 1996;16:834-40.
35. van der Flier WM, Pijnenburg YA, Fox NC, et al. Early-onset versus late-onset AD: The case of the missing APOE ε4 allele. Lancet Neurol 2011;10:280-8.
36. Smits LL, Pijnenburg YA, Koedam EL, et al. Early onset Alzheimer's disease is associated with a distinct neuropsychological profile. J Alzheimers Dis 2012;30:101-8.
37. Johnson JK, Head E, Kim R, et al. Clinical and pathological evidence for a frontal variant of Alzheimer disease. Arch Neurol 1999;56:1233-9.
38. Gorno-Tempini ML, Dronkers NF, Rankin KP, et al. Cognition and anatomy in three variants of primary progressive aphasia. Ann Neurol 2004;55:335-46.
39. Benson DF, Davis RJ, Snyder BD. Posterior cortical atrophy. Arch Neurol 1988;45:789-93.
40. Rogalski E, Cobia D, Harrison TM, et al. Anatomy of language impairments in primary progressive aphasia. J Neurosci 2011;31:3344-50.
41. Crutch SJ, Lehmann M, Schott JM, et al. Posterior cortical atrophy. Lancet Neurol 2012;11:170-8.
42. Rabinovici GD, Jagust WJ, Furst AJ, et al. Abeta amyloid and glucose metabolism in three variants of primary progressive aphasia. Ann Neurol 2008;64:388-401.
43. Rosenbloom MH, Alkalay A, Agarwal N, et al. Distinct clinical and metabolic deficits in PCA and AD are not related to amyloid distribution. Neurology 2011;76:1789-96.
44. van der Vlies AE, Pijnenburg YA, Koene T, et al. Cognitive impairment in Alzheimer's disease is modified by APOE genotype. Dement Geriatr Cogn Disord 2007;24:98-103.
45. Poirier J, Davignon J, Bouthillier D, et al. Apolipoprotein E polymorphism and Alzheimer's disease. Lancet 1993;342:697-9.
46. Reiman EM, Chen K, Alexander GE, et al. Correlations between APOE ε4 gene dose and brain-imaging measurements of regional hypometabolism. Proc Natl Acad Sci USA 2005;102:8299-302.
47. Reiman EM, Chen K, Liu X, et al. Fibrillar amyloid-beta burden in cognitively normal people at 3 levels of genetic risk for AD. Proc Natl Acad Sci USA 2009;106:6820-5.
48. Machulda M, Jones D, Vemuri P, et al. Effect of APOE ε4 status on intrinsic network connectivity in cognitively normal elderly subjects. Arch Neurol 2011;68:1131-6.
49. Drzezga A, Grimmer T, Henriksen G, et al. Effect of APOE genotype on amyloid plaque load and gray matter volume in Alzheimer disease. Neurology 2009;72:1487-94.
50. Drzezga A, Riemenschneider M, Strassner B, et al. Cerebral glucose metabolism in patients with AD and different APOE genotypes. Neurology 2005;64:102-7.

51. Sluimer JD, Vrenken H, Blankenstein MA, et al. Whole-brain atrophy rate in Alzheimer disease: Identifying fast progressors. Neurology 2008;70:1836-41.
52. van der Vlies AE, Koedam EL, Pijnenburg YA, et al. Most rapid cognitive decline in APOE ε4 negative Alzheimer's disease with early onset. Psychol Med 2009;39:1907-11.
53. Schott JM, Ridha BH, Crutch SJ, et al. Apolipoprotein e genotype modifies the phenotype of Alzheimer disease. Arch Neurol 2006;63:155-6.
54. Grimmer T, Henriksen G, Wester HJ, et al. Clinical severity of Alzheimer's disease is associated with PIB uptake in PET. Neurobiol Aging 2009;30:1902-9.
55. Chételat G, Villemagne VL, Pike KE, et al. Relationship between memory performance and β-amyloid deposition at different stages of Alzheimer's disease. Neurodegener Dis 2012;10:141-4.
56. Clark CM, Schneider JA, Bedell BJ, et al. Use of florbetapir-PET for imaging beta-amyloid pathology. JAMA 2011;305:275-83.
57. Ikonomovic MD, Klunk WE, Abrahamson EE, et al. Post-mortem correlates of in vivo PIB-PET amyloid imaging in a typical case of AD. Brain 2008;131:1630-45.
58. Clark CM, Pontecorvo MJ, Beach TG, et al. Cerebral PET with florbetapir compared with neuropathology at autopsy for detection of neuritic amyloid-β plaques: A prospective cohort study. Lancet Neurol 2012;11:669-78.
59. Gomperts SN, Rentz DM, Moran E, et al. Imaging amyloid deposition in lewy body diseases. Neurology 2008;71:903-10.
60. Lee JH, Kim SH, Kim GH, et al. Identification of pure subcortical vascular dementia using ^{11}C-Pittsburgh compound B. Neurology 2011;77:18-25.
61. Vandenberghe R, Van Laere K, et al. ^{18}F-flutemetamol amyloid imaging in Alzheimer disease and mild cognitive impairment: A phase 2 trial. Ann Neurol 2010;68:319-29.
62. Barthel H, Gertz HJ, Dresel S, et al. Cerebral amyloid-β PET with florbetaben (^{18}F) in patients with AD and healthy controls: A multicentre phase 2 diagnostic study. Lancet Neurol 2011;10:424-35.
63. Blennow K, Hampel H. CSF markers for incipient Alzheimer's disease. Lancet Neurol 2003;2:605-13. Verwey NA, van der Flier WM, Blennow K, et al. A worldwide multicentre comparison of assays for cerebrospinal fluid biomarkers in AD. Ann Clin Biochem 2009;46:235-40.
64. Fagan AM, Mintun MA, Mach RH, et al. Inverse relation between in vivo amyloid imaging load and cerebrospinal fluid abeta42 in humans. Ann Neurol 2006;59:512-9.
65. Koivunen J, Pirttilä T, Kemppainen N, et al. PET amyloid ligand [11C]PIB uptake and cerebrospinal fluid beta-amyloid in MCI. Dement Geriatr Cogn Disord 2008;26:378-83.
66. Jagust WJ, Landau SM, Shaw LM, et al. Relationships between biomarkers in aging and dementia. Neurology 2009;73:1193-9.
67. Tolboom N, van der Flier WM, Yaqub M, et al. Relationship of cerebrospinal fluid markers to 11c-PIB and 18F-FDDNP binding. J Nucl Med 2009;50:1464-70.
68. Schöll M, Wall A, Thordardottir S, et al. Low PIB PET retention in presence of pathologic CSF biomarkers in arctic APP mutation carriers. Neurology 2012;79:229-36.
69. Sperling R, Aisen P, Beckett L, et al. Toward defining the preclinical stages of Alzheimer's disease: Recommendations from the national institute on aging-Alzheimer's association workgroups on diagnostic guidelines for AD. Alzheimers Dement 2011;7:280-92.
70. McKhann GM, Knopman DS, Chertkow H, et al. The diagnosis of dementia due to Alzheimer's disease: Recommendations from the national institute on aging-Alzheimer's association workgroups on diagnostic guidelines for AD. Alzheimers Dement 2011;7:263-9.
71. Reagan R. My father at 100. first ed. Viking Adult; 2011.
72. Kloet A. Effects of MR scanner type, scanning sequence and segmentation algorithm on MR-based partial volume corrections of [^{11}C]*(R)*-PK11195 studies. Neuroimage 2006;32:Suppl 2:T83.

Addendum

Nederlandse samenvatting

List of publications

Hall of fame Alzheimer center

Curriculum vitea

Dankwoord

NEDERLANDSE SAMENVATTING

"ALZHEIMER **PET**HOLOGIE"

Achtergrond

De ziekte van Alzheimer

De ziekte van Alzheimer is een progressieve neurodegeneratieve aandoening waaraan circa 250.000 Nederlanders lijden. De ziekte is momenteel niet te behandelen en door de vergrijzing zal de hoeveelheid Alzheimer patiënten verdrievoudigd zijn in 2050. De klachten starten meestal met geheugenstoornissen en later in de ziekte komen daar problemen met taal, handelen, oriëntatie en neuropsychiatrische symptomen bij. Bij mensen die de ziekte van Alzheimer op jonge leeftijd krijgen (<65 jaar) en/of de grootste genetische risicofactor (apolipoprotein E ε4) niet bij zich dragen presenteert de ziekte zich vaker op een atypische manier. Bij deze patiënten is in eerste instantie het geheugen relatief gespaard en staan problemen in taal, handelen en de motoriek voorop. De onderliggende mechanismen die dit zouden kunnen verklaren zijn nog onbekend.

De ziekte van Alzheimer wordt vooraf gegaan door milde cognitieve stoornissen (MCI), meestal in het geheugen. Jaarlijks converteren 10-15% van deze MCI patiënten naar de ziekte van Alzheimer. Echter, niet alle MCI patiënten krijgen de ziekte van Alzheimer aangezien er soms andere oorzaken kunnen zijn voor de klachten, bijvoorbeeld somberheid of slaapproblemen. Deze groep patiënten is zeer interessant omdat we de ziekte van Alzheimer mogelijk in een vroeg stadium vast kunnen stellen mits we over de juiste diagnostische hulpmiddelen beschikken. Wellicht is het in de toekomst zelfs mogelijk om bij ouderen zonder klachten te voorspellen wie wel en niet de ziekte van Alzheimer gaat krijgen.

Neuropathologie

Door het bestuderen van de hersenen van overleden Alzheimer patiënten is er veel kennis opgedaan over processen die betrokken zijn bij het ontstaan de ziekte. De ziekte van Alzheimer kenmerkt zich neuropathologisch door ophopingen van het eiwit amyloid-beta (Aβ) in plaques en neurofibrillaire kluwens bestaande uit het tau eiwit. De neerslag van Aβ vindt waarschijnlijk plaats ruim 15 jaar voordat men klachten

krijgt. Dit giftige eiwit zorgt ervoor dat hersencellen stikken en hun functie en structuur verliezen. Als er voldoende hersencellen afgestorven zijn leidt dit tot cognitieve klachten en uiteindelijk tot dementie. De vroege verschijning van Alzheimer eiwitten biedt grote mogelijkheden om de ziekte vroeg op te sporen. Dit kan nu tijdens het leven met behulp van positron emissie tomografie (PET) hersenscans.

Positron emissie tomografie

PET is een beeldvormende techniek die het mogelijk maakt fysiologische processen in het lichaam zichtbaar te maken en te kwantificeren door injectie van een licht radioactieve stof (ook wel tracer genoemd). Bij het PET onderzoek beschreven in dit proefschrift is gebruik gemaakt van drie verschillende tracers. De eerste tracer, [^{11}C]PIB, bindt aan amyloid plaques en geeft een goede afspiegeling van de hoeveelheid en verdeling amyloid deposities in de hersenen. De tweede tracer, [^{18}]FDDNP, bindt zowel aan amyloid plaques als aan neurofibrillaire kluwens. Uit eerder onderzoek kwam naar voren dat [^{11}C]PIB een betere tracer is voor diagnostisch gebruik vanwege het scherpere contrast tussen patiënten en gezonde vrijwilligers. Aangezien neurofibrillaire kluwens, meer dan amyloid plaques, samenhangen met progressie van de ziekte is [^{18}]FDDNP mogelijk een geschikte tracer om het beloop van de ziekte te meten. De derde tracer, [^{18}F]FDG, kijkt naar het gebruik van glucose door de hersenen. De hersenen omvangen 2% van het totale lichaamsgewicht maar gebruiken 20% van de totale glucose huishouding. Bij de ziekte van Alzheimer neemt dit gebruik af in hersengebieden die cruciaal zijn voor ons functioneren.

Doel

Het doel van dit proefschrift was om meer inzicht te krijgen in de rol van amyloid pathologie bij de ziekte van Alzheimer door de samenhang tussen amyloid deposities met glucose metabolisme en cognitie te bestuderen. Nog specifieker is gekeken naar:

1. veranderingen over de tijd in [^{11}C]PIB en [^{18}F]FDDNP binding en [^{18}F]FDG opname;
2. de relaties tussen amyloid, glucose metabolisme en cognitie bij gezonde ouderen;
3. onderliggende mechanismen die verschillen in klinische presentatie kunnen verklaren bij jonge en/of niet-APOE ε4 dragende Alzheimer patiënten;
4. de diagnostische waarde van [^{11}C]PIB en [^{18}F]FDG PET in de geheugenpolikliniek.

Opzet

In de afgelopen jaren is een grote hoeveelheid gegevens verzameld. Ongeveer 200 patiënten met de ziekte van Alzheimer, andere vormen van dementie of MCI en gezonde vrijwilligers hebben eerst ons standaard diagnostisch protocol doorlopen, o.a. bestaande uit neurologisch en neuropsychologisch onderzoek, afname van bloed en hersenvocht en een MRI hersenscan. Daarnaast ondergingen zij in het kader van wetenschappelijk onderzoek [^{11}C]PIB en [^{18}F]FDG (allen) en [^{18}F]FDDNP (een kleinere groep) PET scans. Deze dataset staat aan de basis van dit proefschrift.

Resultaten

Allereerst werden veranderingen over de tijd van amyloid pathologie onderzocht. In **hoofdstuk 2.1** werden diverse analytische modellen geëvalueerd om deze veranderingen nauwkeurig te kwantificeren. Hiervoor werden [^{11}C]PIB PET scans gedaan tijdens een nulmeting en na gemiddeld 2,5 jaar. Hieruit kwam naar voren dat receptor parametric mapping (RPM2) en Logan superieur waren aan zogenaamde "SUVr's". RPM2 en Logan vereisen een beduidend langere scanduur dan SUVr (90 minuten versus 10-30 minuten) maar voor accurate metingen, bijvoorbeeld bij interventiestudies, zijn kwantitatieve PET scans essentieel. In **hoofdstuk 2.2** keken we naar temporele veranderingen in [^{11}C]PIB en [^{18}F]FDDNP binding en [^{18}F]FDG opname. Er was een significante toename zien van amyloid deposities (gemeten met [^{11}C]PIB) bij MCI patiënten, maar niet bij Alzheimer patiënten en controles. Er werden geen veranderingen geobserveerd in [^{18}F]FDDNP binding. De opname van [^{18}F]FDG nam af over de tijd bij Alzheimer patiënten, vooral in de frontale, pariëtale en temporale schorsen. Dit toont aan dat [^{11}C]PIB en [^{18}F]FDG moleculaire veranderingen meten tijdens verschillende stadia van de ziekte en dat ze dus complementaire informatie leveren. [^{18}F]FDDNP bleek niet geschikt voor het van het meten van ziekte progressie.

In **hoofdstuk 3** werd gekeken naar de relaties tussen amyloid, glucose metabolisme en cognitie bij cognitief normale ouderen. Het is bekend dat circa 30% van de ouderen boven de 70 jaar amyloid pathologie in hun hersenen hebben terwijl ze goed functioneren. In deze studie was er binnen de ouderen met verhoogde [^{11}C]PIB binding een sterke relatie tussen verhoogd glucose metabolisme en betere geheugenprestaties. Dit suggereert dat asymptomatische ouderen met het Alzheimer eiwit, in ieder geval

tijdelijk, in staat zijn om hun cognitief functioneren op peil te houden door verhoogde metabole activiteit.

Het doel van **hoofdstuk 4** was om te kijken naar onderliggende mechanismen die de verschillen in klinische presentatie tussen patiënten zouden kunnen verklaren. Jonge Alzheimer patiënten (<65 jaar) presenteren zich vaker atypisch dan oudere patiënten. In **hoofdstuk 4.1** wordt beschreven dat jonge patiënten meer amyloid pathologie en lager metabolisme hebben in de pariëtale cortex. Dit hersengebied wordt frequent geassocieerd met functies die vaker eerder aangedaan zijn bij jonge Alzheimer patiënten zoals ruimtelijk inzicht en rekenvaardigheden. Patiënten zonder het grootste risicogen (APOE ε4) maar die toch de ziekte krijgen presenteren lijken een agressievere vorm van Alzheimer te hebben. In **hoofdstuk 4.2** komt naar voren dat Alzheimer patiënten zonder APOE ε4 meer amyloid pathologie in de voorste hersendelen hebben. Patiënten met APOE ε4 hadden echter minder metabole activiteit in de posterieure hersengebieden. Mogelijk volgen Alzheimer patiënten met en zonder APOE ε4 verschillende pathologische trajecten. Verschillen in amyloid pathologie en glucose metabolisme vormen dus mogelijk een verklaring voor de klinische heterogeniteit binnen Alzheimer patiënten.

In **hoofdstuk 5** staat de klinische toepassing van PET centraal. **Hoofdstuk 5.1** bevat data van 154 patiënten die het standaard protocol van het Alzheimercentrum VUmc ondergingen, resulterend in een breed scala aan diagnoses. Aanvullend werden [^{11}C]PIB en [^{18}F]FDG PET scans verricht. Deze PET scans leiden tot een verandering van de initiële diagnose in 23% van de gevallen. Daarnaast steeg het vertrouwen van de arts in de juistheid van de diagnose van 71% voor de scans tot 87% na PET. [^{11}C]PIB en [^{18}F]FDG PET hebben dus een toegevoegde waarde bovenop de standaard diagnostische hulpmiddelen. In **hoofdstuk 5.2** wordt de potentie van [^{11}C]PIB PET bediscussieerd. Een literatuuroverzicht laat zien dat MCI patiënten die na twee jaar de diagnose Alzheimer krijgen vaak een afwijkende [^{11}C]PIB scan hebben, terwijl patiënten met een normale [^{11}C]PIB scan zelden converteren. [^{11}C]PIB PET lijkt dus een goede voorspeller voor klinische achteruitgang bij MCI patiënten.

Conclusies

Bovenstaande resultaten laten zien dat amyloid pathologie een belangrijke rol speelt bij de ziekte van Alzheimer. Amyloid kan al in een heel vroeg stadium van de ziekte aangetoond worden. In het vroegste stadium van amyloid stapeling treedt er mogelijk een compensatie mechanisme in werking waardoor het glucose metabolisme omhoog gaat en de cognitie (tijdelijk) intact blijft. Bij MCI patiënten is de aanwezigheid van amyloid deposities sterk voorspellend voor het wel of niet converteren naar Alzheimer dementie. Regionale deposities van amyloid spelen mogelijk een rol bij de klinische manifestatie van de ziekte. Tot slot zijn [^{11}C]PIB en [^{18}F]FDG PET nuttige technieken voor het eerder en nauwkeuriger stellen van de diagnose in een geheugenpolikliniek.

LIST OF PUBLICATIONS

International (peer-reviewed) journals

1. **R. Ossenkoppele**, C.M. Madison, H. Oh, M. Wirth, B.N.M. van Berckel & W.J. Jagust. 'Is verbal episodic memory in elderly with amyloid deposits preserved through altered neuronal function?' *Cerebral Cortex* [in press].

2. **R. Ossenkoppele**, W.M. van der Flier, M.D. Zwan, S. Adriaanse, R. Boellaard, A.D. Windhorst, F. Barkhof, A.A. Lammertsma, P. Scheltens & B.N.M. van Berckel. 'Differential effect of APOE genotype on amyloid load and glucose metabolism in AD dementia'. *Neurology* 2013;80(4):359-65.

3. B. van Berckel, **R. Ossenkoppele**, N. Tolboom, M. Yaqub, J. Foster-Dingley, A. Windhorst, P. Scheltens, A. Lammertsma, R. Boellaard. 'Longitudinal amyloid imaging using [^{11}C]PIB: Methodological considerations'. *Journal of Nuclear Medicine*[in press].

4. S. Morbelli, R. Perneczky, A. Drzezga, G. Frisoni, A. Caroli, B. van Berckel, **R. Ossenkoppele**, E. Guedj, M. Didic, A. Brugnolo, M. Naseri, G. Sambuceti, M. Pagani, F. Nobili. 'Metabolic networks underlying cognitive reserve in prodromal Alzheimer's disease: A EADC project'. *Journal of Nuclear Medicine* 2013 [in press].

5. Prestia, A. Caroli, W.M. van der Flier, **R. Ossenkoppele**, B.N.M. van Berckel, F. Barkhof, C.E. Theunissen, A.E. Wall, S. Carter, M. Scholl, I.H. Choo, A. Nordberg, P. Scheltens & G.B. Frisoni. 'Prediction of dementia in MCI patients base don core diagnostic markers for Alzheimer's disease'. *Neurology* 2013;80(11):1048-56..

6. **R. Ossenkoppele**, M.D. Zwan, N. Tolboom, D.M. van Assema, S.F. Adriaanse, R.W. Kloet, R. Boellaard, A.D. Windhorst, F. Barkhof, A.A. Lammertsma, P. Scheltens, W.M. van der Flier & B.N.M. van Berckel. 'Amyloid burden and metabolic function in early-onset Alzheimer's disease: parietal lobe involvement'. *Brain* 2012:135(Pt 7);2115-2125.

7. **R. Ossenkoppele**, N. Tolboom, J.C. Foster-Dingley, R. Boellaard, M. Yaqub, A.D. Windhorst, W.M. van der Flier, F. Barkhof, A.A. Lammertsma, P. Scheltens & B.N.M. van Berckel. 'Longitudinal imaging of Alzheimer pathology using [^{11}C]PIB, [^{18}F]FDDNP and [^{18}F]FDG PET'. *European Journal of Nuclear Medicine and Molecular Imaging* 2012:39(6);990-1000.

8. S. Morbelli, A. Drzezga, R. Perneczky, G.B. Frisoni, A. Caroli, B.N.M. van Berckel, **R. Ossenkoppele**, E. Guedj, M. Didic, A. Brugnolo, G. Sambuceti, M. Pagani, E. Salmon & F. Nobili. 'Resting metabolic connectivity in prodromal Alzheimer's disease. A European Alzheimer disease consortium (EADC) project'. *Neurobiology of Aging* 2012:33(11);2533-50.

9. Caroli, A. Prestia, K. Chen, N. Ayutyanont, S.M. Landau, C.M. Madison, C. Haense, K. Herholz, F. Nobili, E.M. Reiman, W.J. Jagust, G.B. Frisoni, **EADC-PET consortium**, Nest-DD, and Alzheimer's disease initiative. 'Summary metrics to assess Alzheimer disease-related hypometabolic pattern with [^{18}F]FDG PET: head-to-head comparison'. *Journal of Nuclear Medicine* 2012:53(4);592-600.

10. **R. Ossenkoppele**, N.D. Prins, Y.A.L. Pijnenburg, A.W. Lemstra, W.M. van der Flier, S.F. Adriaanse, A.D. Windhorst, R.L.H. Handels, C.A.G. Wolfs, P. Aalten, F.R.J. Verheij, M.M. Verbeek, M.A. van Buchem, O.S. Hoekstra, A.A. Lammertsma, P. Scheltens & B.N.M. van Berckel. 'Impact of molecular imaging on the diagnostic process in a memory clinic'. *Alzheimer's & Dementia* 2012[Epub ahead of print].

11. S. Adriaanse, E.J. Sanz-Arigita, M.A. Binnewijzend, **R. Ossenkoppele**, N. Tolboom, D.M.E. van Assema, A.M. Wink, R. Boellaard, M. Yaqub, A.D. Windhorst, W.M. van der Flier, P. Scheltens, A.A. Lammertsma, S.A. Rombouts, F. Barkhof & B.N.M. van Berckel. 'Amyloid and its association with default mode network integrity in Alzheimer's disease'. *Human Brain Mapping* 2012[Epub ahead of print].

12. **R. Ossenkoppele**, B.N.M. van Berckel & N.D. Prins. 'Amyloid imaging in prodromal Alzheimer disease'. *Alzheimer's Research & Therapy* 2011:3(5);26.

National (peer reviewed) journals

1. **R. Ossenkoppele**, N. Tolboom, Y.A.L. Pijnenburg, A.A. Lammertsma, P.Scheltens & B.N.M. van Berckel. 'Amyloid-plaque imaging of the brain using PET'. *Nederlands Tijdschrift voor Geneeskunde* 2011:155(18).

2. **R. Ossenkoppele**, B.N.M. van Berckel, N. Tolboom, Y.A. Pijnenburg, N.D. Prins, A.W. Lemstra, A.A. Lammertsma & P. Scheltens. 'Molecular imaging in Alzheimer's disease'. *Tijdschrift voor Neurologie en Neurochirurgie* 2011:112;201-208.

3. N. Tolboom, **R. Ossenkoppele** & B.N.M. van Berckel. 'Amyloid imaging in Alzheimer's disease'. *Tijdschrift voor Nucleaire Geneeskunde* 2011:33(4);816-820.

4. **R. Ossenkoppele** & B.N.M. van Berckel. 'Prediction of Alzheimer's disease with PET'. *Neurology News International* 2011:2(2):5.

Bookchapters

1. **R. Ossenkoppele**, J. Booij, P. Scheltens & B.N.M. van Berckel. Bookchapter 'Dementia due to neurodegenerative disease – Molecular imaging findings' in 'SPECT and PET in Neurology'. Springer Verlag 2013[in press].

2. **R. Ossenkoppele** & B.N.M. van Berckel. Bookchapter 'Hersenen en veroudering' ('The aging brain') in 'Handboek beeldvorming van het brein: Imaging voor psychiaters en psychologen' ('Manual Imaging the brain: Imaging for psychiatrists and psychologists'). De Tijdstroom uitgeverij 2013[in press].

HALL OF FAME ALZHEIMER CENTER

1. L. Gootjes: Hemispheric connectivity and laterality of language processing (14-9-2004)
2. R. Goekoop: Pharmacological fMRI: a clinical exploration (16-1-2005) (Cum Laude)
3. K. van Dijk: Peripheral electrical nerve stimulation in AD (6-9-2005)
4. N.S.M. Schoonenboom: Cerebrospinal fluid markers for the early and differential diagnosis of Alzheimer's disease (10-11-2006)
5. E.S.C. Korf: Medial Temporal Lobe atrophy on MRI: vascular risk factors and predictive value in dementia (29-11-2006)
6. B. van Harten: Aspects of subcortical vascular ischemic disease (22-12-2006).
7. B. F. Jones: Cingular cortex networks (23-3-2007)
8. L. van de Pol: Hippocampal atrophy from aging to dementia: a clinical perspective (11-5-2007)
9. Y. Pijnenburg: Frontotemporal dementia: towards an early diagnosis (5-7-2007)
10. A. J. Bastos Leite: Pathological ageing of the Brain (16-11-2007)
11. E.C.W. van Straaten: MRI correlates of vascular cerebral lesions and cognitive impairment (11-1-2008)
12. R.L.C. Vogels: Cognitive impairment in heart failure (11-4-2008)
13. J. Damoiseaux: The brain at rest (20-5-2008)
14. G.B. Karas: MRI patterns of cerebral atrophy in dementia (19-6-2008)
15. F.H. Bouwman: Biomarkers in dementia: longitudinal aspects and combination with MRI (20-6-2008)
16. A.A. Gouw: Cerebral small vessel disease on MRI (20-3-2009)
17. H. van der Roest: Care needs in dementia and interactive digital information provisioning (12-10-2009)
18. C. Mulder: Biomarkers in Alzheimer's disease (11-11-2009)
19. W. Henneman. Advances in hippocampal atrophy measurement in dementia: beyond diagnostics (27-11-2009)
20. S.S. Staekenborg: Risk factors and clinical findings in relation to vascular changes on brain MRI (23-12-2009)
21. N. Tolboom: Imaging Alzheimer's disease pathology in vivo: towards an early diagnosis (12-2-2010)
22. E. Altena: Mapping insomnia: brain structure, function and sleep intervention (17-3-2010).
23. N.A. Verwey: Biochemical markers in dementia: from mice to men (15-4-2010)
24. M.I. Kester: Biomarkers for Alzheimer's pathology; monitoring, predicting and understanding the disease (14-01-2011)
25. J.D. Sluimer: Visualizing the shrinking brain (28-4-2011).
26. S.D Mulder: amyloid associated proteins in Alzheimer's disease (07-10-2011)
27. S.A.M. Sikkes: measuring IADL in dementia (14-10-2011)
28. A. Schuitemaker: Inflamation in Alzheimer's Disease: in vivo quantification (27-1-2012)
29. K. Joling: Depression and anxiety in family caregivers of persons with dementia (2-4-2012)
30. W. De Haan: In a network state of mind (02-11-2012) (Cum Laude)
31. D. Van Assema: Blood-brain barrier P-glycoprotein function in aging and Alzheimer's disease (07-12-12)
32. J. D.C. Goos: Microbleed in dementia: connecting the dots (6-2-2013)
33. R. Ossenkoppele: Alzheimer PEThology (8-5-2013)

CURRICULUM VITEA

Rik Ossenkoppele was born on December 1st, 1981 in Uithoorn, the Netherlands. In 1998, he graduated from the Alkwin College in Uithoorn thanks to Mr. Antonini and Mr. Bax. After a well-deserved sabbatical year, Rik started to study physical education at the Amsterdam University of Applied Sciences. This is where he developed a particular interest in people who somewhat deviate from the norm, reflected by him teaching sports at a school for children with chronic disease and at an institution for mentally disabled people. In the meanwhile, he fully enjoyed his student life in Amsterdam, as well as his internship at the University of Örebro in Sweden. After obtaining his degree in 2004, Rik started to study psychology, a decision partly based on a short-lived fascination with the work of Sigmund Freud. His interest quickly shifted towards the more biological mechanisms driving human behaviour and cognition and in the summer of 2008 he fulfilled a master in clinical neuropsychology. After exploring Southern Africa, Rik started his PhD trajectory in 2009 at the Alzheimer center and the department of Radiology & Nuclear Medicine of the VU University medical center, which eventually resulted in this thesis. A few highlights amongst many during this period were scientific conferences held in exotic places like Hawaii, Miami and Amstelveen, and a 6 months fellowship at the University of California in Berkeley. At the time of writing, he is a “post doc” researcher at the VU University medical center.

DANKWOORD

Dit proefschrift is mogelijk gemaakt door talloze personen. Allen heel hartelijk dank daarvoor!! Een aantal verdienen het om eens extra in de schijnwerpers gezet te worden. Daar gaan we…

Allereerst alle patiënten, mantelzorgers en vrijwilligers vanwege hun geweldige inzet bij het ondergaan van ellenlange hersenscans, slopende neuropsychologische onderzoeken en het invullen van diverse vragenlijsten. Daarbij heb ik veel geleerd van uw bijzondere verhalen tijdens de scandagen. Dank!

Vervolgens dank ik mijn "dreamteam" van promotoren en co-promotoren, bestaande uit prof. dr. Ph Scheltens, prof. dr. A.A. Lammertsma, dr. W.M. van der Flier en dr. B.N.M. van Berckel.

Beste Philip, pragmatisme, netwerker, humor, joi de vive, Daarnaast zijn we beide groot sportliefhebber en dat schept een band,

Beste Adriaan, taalpurist, erudiet, goede verhalen verteller

Beste Wiesje,

Beste Bart, loyaal, continue stroom aan nieuwe ideeen, vasthoudendheid, staan voor principes,

Next, I would like to thank the members of the reading committee: prof. dr. W.J. Jagust, prof. dr. R. Vandenberghe, dr. N.D. Prins, prof. dr. J. Booij, prof. dr. P.R. Luijten and prof. dr. E.J.A. Scherder. Thanks a lot for reading my thesis and I look forward to discuss the content in May! Dear Bill, … Beste Niels, … Beste Erik, …

Zijn er nu echt te veel om iedereen persoonlijk te noemen. Excuus daarvoor + namen.

Frederik, Otto, Ronald, Hugo

Thalia, Paul, Nikkie, Judith, Femke, Suzette, Robin, Maqsood, Robert, Kevin, Henri,
Pieter, Human, Adriaan, Ronald,
De oude garde Fransje, Wouter, Alida, Salka, Niek,
Last men standing Willem en Dr. Goose,
Argonde, Welmoed, Daniela, Floor, Anne-Catrien, Marije,
Marian, Karlijn, Elisabeth, Eddy, Evan, Els,
Yolande, Evelien, Femke, PJ,
Annefloor, Nicole, Astrid, Annebet,
Bunker genoten Smitsie, Möllert, Maja, Eva,
Aquarium bewoners Maartje, Elle-Marije
Villa grootgrondbezitters Hannie, van Rossum,
PET collega's Nelleke, Danielle, Alie, Sofie, Marissa
Ted, Martin, Ilona,
+ iedereen die ik onverhoopt vergeten ben…

Reina, Sander, Jessica, jullie zijn toppers!

CTMM Ron, Petra, Lies, Stefanie, Paulien, Claire,

Berkeley

Vrienden

Gert, Lenie, Fieke, Otje, Thijs, Thomas

Jo